UPPSALA
UNIVERSITET

*Digital Comprehensive Summaries of Uppsala Dissertations from the Faculty of Science and Technology* 698

# Integrated Antenna Solutions for Wireless Sensor and Millimeter-Wave Systems

SHI CHENG

ACTA
UNIVERSITATIS
UPSALIENSIS
UPPSALA
2009

ISSN 1651-6214
ISBN 978-91-554-7681-6
urn:nbn:se:uu:diva-111197

Dissertation presented at Uppsala University to be publicly examined in Siegbhansalen, Lägerhyddsvägen 1, The Ångström Laboratory, Uppsala, Friday, January 29, 2010 at 13:30 for the degree of Doctor of Philosophy. The examination will be conducted in English.

**Abstract**
Cheng, S. 2009. Integrated Antenna Solutions for Wireless Sensor and Millimeter-Wave Systems. Acta Universitatis Upsaliensis. *Digital Comprehensive Summaries of Uppsala Dissertations from the Faculty of Science and Technology* 698. 114 pp. Uppsala. ISBN 978-91-554-7681-6.

This thesis presents various integrated antenna solutions for different types of systems and applications, e.g. wireless sensors, broadband handsets, advanced base stations, MEMS-based reconfigurable front-ends, automotive anti-collision radars, and large area electronics.

For wireless sensor applications, a T-matched dipole is proposed and integrated in an electrically small body-worn sensor node. Measurement techniques are developed to characterize the port impedance and radiation properties. Possibilities and limitations of the planar inverted cone antenna (PICA) for small handsets are studied experimentally. Printed slot-type and folded PICAs are demonstrated for UWB handheld terminals.

Both monolithic and hybrid integration are applied for electrically steerable array antennas. Compact phase shifters within a traveling wave array antenna architecture, on single layer substrate, is investigated for the first time. Radio frequency MEMS switches are utilized to improve the performance of reconfigurable antennas at higher frequencies. Using monolithic integration, a 20 GHz switched beam antenna based on MEMS switches is implemented and evaluated. Compared to similar work published previously, complete experimental results are here for the first time reported. Moreover, a hybrid approach is used for a 24 GHz switched beam traveling wave array antenna. A MEMS router is fabricated on silicon substrate for switching two array antennas on a LTCC chip.

A concept of nano-wire based substrate integrated waveguides (SIW) is proposed for millimeter-wave applications. Antenna prototypes based on this concept are successfully demonstrated for automotive radar applications.

W-band body-worn nonlinear harmonic radar reflectors are proposed as a means to improve automotive radar functionality. Passive, semi-passive and active nonlinear reflectors consisting of array antennas and nonlinear circuitry on flex foils are investigated.

A new stretchable RF electronics concept for large area electronics is demonstrated. It incorporates liquid metal into microstructured elastic channels. The prototypes exhibit high stretchability, foldability, and twistability, with maintained electrical properties.

*Keywords:* harmonic radar (HR), liquid alloy, millimeter-wave, micromachining, phase shifters, planar inverted cone antennas (PICA), printed circuit boards (PCB), quasi-Yagi antennas, radio frequency microelectromechanical system (RF MEMS), stretchable antennas, substrate integrate waveguides (SIW), T-matched dipole antennas, tapered slot antennas, traveling wave array antennas, ultrawideband (UWB), wireless sensor networks.

*Shi Cheng, Department of Engineering Sciences, Microwave and Terahertz Technology, Box 534, Uppsala University, SE-75121 Uppsala, Sweden*



ISSN 1651-6214
ISBN 978-91-554-7681-6
urn:nbn:se:uu:diva-111197 (http://urn.kb.se/resolve?urn=urn:nbn:se:uu:diva-111197)

*To Yiwen*

# List of Papers

The following scientific papers that are included in this thesis are referred to in the text by their Roman numerals.

I. **S. Cheng**, E. Öjefors, P. Hallbjörner and A. Rydberg, "Compact reflective microstrip phase shifter for traveling wave antenna applications," *IEEE Microwave and Wireless Components Letters*, 16(7): 431-433, 2006.

II. E. Öjefors, **S. Cheng**, K. From, I. Skarin, P. Hallbjörner and A. Rydberg, "Electrically steerable single-layer microstrip traveling wave antenna with varactor diode based phase shifters," *IEEE Transactions on Antennas and Propagation*, 55(9): 2451-2460, 2007.

III. P. Hallbjörner, **S. Cheng**, A. Rydberg and K. Karlsson, "Modified planar inverted cone antenna for mobile communication handsets," *IEEE Antennas and Wireless Propagation Letters*, 6: 472-475, 2007.

IV. **S. Cheng**, P. Hallbjörner and A. Rydberg, "Printed slot planar inverted cone antenna for ultrawideband applications," *IEEE Antennas and Wireless Propagation Letters*, 7: 18-21, 2008.

V. H. Yousef, **S. Cheng** and H. Kratz, "Substrate integrated waveguides (SIWs) in a flexible printed circuit board for millimeter wave applications," *Journal of Micro-electromechanical Systems*, 18(1): 154-162, 2009.

VI. **S. Cheng**, H. Yousef and H. Kratz, "79 GHz slot antennas based on substrate integrated waveguides (SIW) in a flexible printed circuit board," *IEEE Transactions on Antennas and Propagation*, 57(1): 64-71, 2009.

VII. **S. Cheng**, P. Hallbjörner, A. Rydberg, D. Vanotterdijk and P. van Engen, "T-matched dipole antenna integrated in electrically small body-worn wireless sensor node," *IEE Proceedings IET Microwaves*, *Antennas & Propagation*, 3(5): 774-781, 2009.

VIII. **S. Cheng**, A. Rydberg, K. Hjort and Z.G. Wu, "Liquid metal stretchable unbalanced loop antenna," *Applied Physics Letters*, 94(14): 144103(1)-(3), 2009.

IX. **S. Cheng**, P. Rantakari, R. Malmqvist, C. Samuelsson, T. Vähä-Heikkilä, A. Rydberg and J. Varis, "Switched beam antenna based on RF MEMS SPDT switch on quartz substrate," *IEEE Antennas and Wireless Propagation Letters*, 8: 383-386, 2009.

X. **S. Cheng**, Z.G. Wu, P. Hallbjörner, K. Hjort and A. Rydberg, "Foldable and stretchable liquid metal planar inverted cone antenna," *IEEE Transactions on Antennas and Propagation*, 57(12): 3765-3771, 2009.

XI. **S. Cheng**, A. Rydberg, P. Hallbjörner, L. Pettersson, M. Salter and D. Platt, "Millimeter-wave tapered slot antenna for integration on micromachined low resistivity silicon substrates," *Proc. of IEEE International Workshop on Antenna Technology (IWAT'09),* pp. 1-4, Santa Monica, USA, Mar. 2009. (Invited)

XII. **S. Cheng**, P. Hallbjörner and A. Rydberg, "Array antenna for body-worn automotive harmonic radar tag," *Proc. of the 3rd European Conference on Antennas and Propagation (EuCAP)*, pp. 2823-2827, Berlin, Germany, Mar. 2009. (Invited)

XIII. L. Pettersson, **S. Cheng**, M. Salter, A. Rydberg and D. Platt, "Compact integrated slot array antennas for the 79 GHz automotive band," *Proc. of the 39th European Microwave Conference*, pp. 228-231, Rome, Italy, Sept.-Oct. 2009.

Reprints were made with permission from the respective publishers.

## Comments on the author's contributions to the papers

I. Design, manufacturing, measurements, and part of manuscript writing.

II. Part of the followings: design, manufacturing, measurements, and manuscript writing.

III. Simulations, part of measurements and manuscript writing.

IV. Idea, planning, design, manufacturing, measurements, and manuscript writing.

V. Invention of nanowire-based SIWs. Part of planning, all design and measurements, and part of manuscript writing.

VI. Invention of nanowire-based SIWs. Part of planning, all design, measurements and manuscript writing.

VII. Design, measurements, and part of manuscript writing.

VIII. Invention of liquid metal based stretchable RF electronics. Part of planning, all design, measurements and manuscript writing.

IX. Design of the antenna, measurements of the complete module, and manuscript writing.

X. Invention of liquid metal based stretchable RF electronics. Part of planning, all design and measurements, and part of manuscript writing.

XI. Idea, planning, design, measurements, and manuscript writing.

XII. Part of the followings: planning, design, measurements, and manuscript writing.

XIII. Part of the followings: design, measurements, and manuscript writing.

# Related Work

The following scientific papers and patents by the author have not been included as they are either out of the scope of the thesis or overlap with some attached papers.

XIV. **S. Cheng**, H. Kratz and H. Yousef, "Substrate integrated waveguides," *International Patent*, No. PCT/SE2009/050271, Mar. 2009.

XV. **S. Cheng** and Z.G. Wu, "Stretchable devices," *US Provisional Patent,* No. 61/122,875, Dec. 2008.

XVI. **S. Cheng**, A. Ferrari, M. Johnson, A. Rydberg, V. Ziemann and E. Öjefors, "Reduction of the coupling to external sources and modes of propagation by a nearly confocal resonator," *IEEE Transactions on Microwave Theory and Techniques*, 55(10): 2257-2261, 2007.

XVII. T. Bartnitzek, W. Gautier, G.W. Qu, **S. Cheng** and A. Ziaei, "RF and microwave microelectronics packaging," *ed. K. Kuang, F. Kim and S. Cahill*, Springer, 2009.

XVIII. **S. Cheng**, E. Öjefors, P. Hallbjörner and A. Rydberg, "Varactor diode phase shifters for electrically steerable microstrip travelling wave antennas" *Proc. of Antenna 2006,* Linköping, Sweden, May 2006.

XIX. M. Andersson, B. Göransson, K. From, I. Skarin, **S. Cheng**, E. Öjefors, P. Hallbjörner, L. Manholm and A. Rydberg, "Antennas with fast beam steering for high spectral efficiency in broadband cellular systems," *Proc. of the 9$^{th}$ European Conference on Wireless Technology*, pp. 12-15, Manchester, UK, Sept. 2006.

XX. **S. Cheng**, E. Öjefors, J. Magrell, K. Hjort and A. Rydberg, "Inverted-F antenna for 3D integrated wireless sensor applications," *Proc. of IEEE International Workshop on Antenna*

*Technology (IWAT'07)* pp. 447-450, Cambridge, UK, Mar. 2007.

XXI. **S. Cheng**, A. Ferrari, E. Öjefors and A. Rydberg, "Analysis of a nearly-confocal resonator for parasitic external modes rejection," *Proc. of the 4th Swedish Conference on Computational Electromagnetics-Methods and Applications (EMB07)*, pp. 61-68, Lund, Sweden, Oct. 2007.

XXII. **S. Cheng**, E. Öjefors, P. Hallbjörner, S. Ogden, J. Margell, K. Hjort and A. Rydberg, "Body surface backed flexible antennas for 17 GHz wireless body area networks sensor applications," *Proc. of the 10th European Conference on Wireless Technology*, pp. 55-58, Munich, Germany, Oct. 2007.

XXIII. P. Hallbjörner, **S. Cheng** and A. Rydberg, "Reverberation chamber for accurate antenna measurements within 2-30 GHz," *Proc. of the 37th European Microwave Conference*, pp. 79-82, Munich, Germany, Oct. 2007.

XXIV. **S. Cheng**, E. Öjefors, S. Ogden, K. Hjort and A. Rydberg, "Gain and efficiency enhanced flip-up antennas for 3D integrated wireless sensor applications," *Proc. of the 2nd European Conference on Antennas and Propagation (EuCAP)*, pp. 1-5, Edinburg, UK, Nov. 2007.

XXV. A. Rydberg, **S. Cheng**, P. Hallbjörner, S. Ogden and K. Hjort, "Integrated antennas for RF MEMS routers," *Proc. of GigaHertz 2008*, Gothenburg, Sweden, Mar. 2008.

XXVI. H. Yousef, **S. Cheng**, H. Kratz, A. Rydberg and K. Hjort, "Substrate integrated waveguides in flexible PCB," *Proc. of Microstructure Workshop* (*MSW'8*), Gothenburg, Sweden, May 2008.

XXVII. T. Bartnitzek, B. Schönlinner, W. Gautier, **S. Cheng**, A. Rydberg, T. Purtova, T. Vähä-Veikkilä and A. Ziaei, "Ceramic systems in package for RF and microwave," *Proc. of Advanced Technology Workshop on RF and Microwave Packaging(IMAPS)*, San Diego, USA, Sept., 20008

XXVIII. P. van Engen, R. van Doremalen, W. Jochems, A. Rommers, **S. Cheng**, A. Rydberg, T. Fritzsch, J. Wolf, W. De Raedt and P. Muller, "3D Si-level integration in wireless sensor node," *Proc.*

*of Smart System Integration Conference 2009*, Brussels, Belgium, Mar. 2009.

XXIX. R. Malmqvist, C. Samuelsson, B. Carlegrim, **S. Cheng**, A. Rydberg, U. Hanke, B. Holter, H. Sagberg, P. Rantakari, T. Vähä-Heikkilä and J. Varis, "A 20 GHz antenna integrated RF MEMS based router and switching networks made on quartz," *Proc. of Smart System Integration Conference 2009*, Brussels, Belgium, Mar. 2009.

XXX. R. van Doremalen, P. van Engen, W. Jochems, A. Rommers, G. Maas, **S. Cheng**, A. Rydberg, T. Fritzsch, J. Wolf, W. De Raedt, R. Jansen, P. Muller, E. Alarcon and M. Sanduleanu, "Wireless activity monitor using 3D integration," *Proc. of Symposium on Design, Test, Integration and Package of MEMS/MOEMS (DTIP 2009)*, Rome, Italy, Apr. 2009.

XXXI. V. Viikari, J. Saebboe, **S. Cheng**, M. Kantanen, M. Al-Nuaimi, T. Varpula, A. Lamminen, P. Hallbjörner, A. Alastalo, T. Mattila, H. Seppä, P. Pursula and A. Rydberg, "Technical solutions for automotive intermodulation radar for detecting vulnerable road users," *Proc. of IEEE Vehicular Technology Conference 2009 (VTC 2009)*, pp. 1-5, Barcelona, Spain, Apr. 2009.

XXXII. A. Rydberg, P. van Engen, **S. Cheng**, R. van Doremalen, M. Sanduleanu and K. Hjort, "Body surface backed flexible antennas and 3D Si-level integrated wireless sensor nodes for 17 GHz wireless body area networks," *Proc. of the 2nd IET Seminar on Body-Centric Wireless Communications 2009*, pp. 1-4, London, UK, Apr. 2009.

XXXIII. P. Hallbjörner, **S. Cheng**, A. Rydberg, D. Vanotterdijk and P. van Engen, "Design and characterization methods for a balanced antenna integrated in a small sensor node," *Proc. of the 2nd IET Seminar on Body-Centric Wireless Communications 2009*, pp. 1-4, London, UK, Apr. 2009.

XXXIV. R. van Doremalen, P. van Engen, W. Jochems, **S. Cheng**, T. Fritzsch and W. De Raedt, "Miniature wireless activity monitor using 3D integration," *Proc. of IEEE International 3D Systems Integration Conference 2009*, San Francisco, USA, Sept. 2009.

XXXV. J. Saebboe, V. Viikari, T. Varpula, H. Seppä, **S. Cheng**, M. Al-Nuaimi, P. Hallbjörner, and A. Rydberg, "Harmonic automotive

radar for VRU classification," *Proc. of International Radar Conference 2009*, Bordeaux, France, Oct. 2009.

XXXVI. **S. Cheng**, Z.G. Wu, A. Rydberg, and K. Hjort, "A highly stretchable microfluidic meandered monopole antenna," *Proc. of International Conference on Miniaturized Systems for Chemistry and Life Sciences (MicroTAS'09)*, Jeju, Korea, Nov. 2009.

XXXVII. R. Malmqvist, P. Rantakari, C. Samuelsson, M. Lahti, **S. Cheng**, J. Saijets, T. Vaha-Heikkila, A. Rydberg, and J. Varis, "RF MEMS based impedance matching networks for tunable multi-band microwave low noise amplifiers," published in *Proc. of International Semiconductor Conference 2009 (CAS2009)*, Volume 1, pp.303-306, Sinaia, Romania, Oct. 2009.

# Contents

# 1 Introduction

## 1.1 Background

Nowadays electronics with wireless communication and remote sensing functions are seen everywhere, with numerous systems in use, for different purposes and markets. Wireless links are extensively replacing cables in many conventional systems. Meanwhile the advances of wireless communication and remote sensing techniques also drive a large number of new applications, e.g. radio frequency identification (RFID), wireless sensor networks, millimeter-wave passive imaging, and THz medical diagnostic tools.

### 1.1.1 Wireless Sensor Networks

Wireless sensor networks (WSN) are one of the fastest growing technologies in industry sector, and the market of WSNs is foreseen to skyrocket in the coming years [1],[2]. Besides saving large mounts of Dollars or Euros on labor for installation, the merits of wireless links are that users can install sensor networking and monitoring capabilities in places where they could not before, and perform measurements that would be extremely expensive with hardwiring. Moreover, wireless links also allow faster network reconfiguration to adapt to varying applications. In addition, WSNs can be configured as autonomous systems for ambient intelligence with low power consumption and self-contained energy scavenging, and maintenance-free in a long term, i. e. a few months or even years. Owing to these attractive features, many new opportunities of WSNs are seen in a variety of applications.

The first research activities in the field of autonomous systems for ambient intelligence were Smart Dust launched by a group in the University of California at Berkeley in 1998 [3]. The goal of this project was to implement a self-contained, millimeter-scale sensing and communication platform for a massively distributed sensor network. This device was approximately in the size of a grain of sand, consisting of sensors, computational capabilities, bidirectional communications, and a power supply, while being cost-effective enough to deploy by hundreds. The successful demonstrations of the Smart Dust project exhibit unimaginable potentials of autonomous WSNs in vari-

ous applications, i. e. remote monitoring of personal health, equipment, contamination, pipelines, and so on. Since then, numerous research and development activities have been conducted both in industry and academia, all the way from hardware to network level.

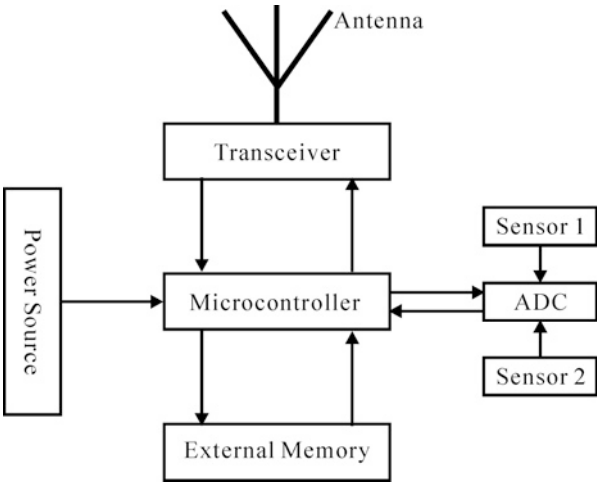


*Figure 1.1: General architecture of a wireless sensor node.*

From hardwire perspective, wireless sensor nodes are often built with simple architectures at affordable price, lightweight, low power consumption, and miniaturized size. Nevertheless, even a simple node is comprised of dozens of subcomponents, e.g. microcontroller, power supply, power management, sensor, memory, radio chip, and antenna, as illustrated in Fig. 1.1. For more advanced or multi-functional nodes, more electronics are certainly needed, and system complexity significantly increases. Implementation of cost-effective miniaturized wireless sensor nodes necessitates high-level integration of various electronic modules. Integration concepts like system-on-chip (SoC) or system-in-package (SiP) are promising solutions. Yet any of these integration approaches require miniaturized subcomponents. The advances of modern semiconductor and MEMS technologies enable miniaturization of most subcomponents, e.g. radio chips, sensors, microcontrollers, power management units and so on. But, due to the fundamental limitations imposed by the physics, miniaturization of some other subcomponents like antennas, batteries and energy scavenging can only be achieved at the expense of poor performance. To maintain reasonable performance, these subcomponents must be made relatively larger than the others, and hence dominate the overall size of sensor nodes.

Integrating antennas into miniaturized sensor nodes is a dedicated task for antenna designers. Traditionally, integration and co-design of antennas with RF front-end circuitry are done with a conservative approach, where anten-

nas are usually designed and fabricated separately, and standardized connectors and system impedances are utilized for interfacing antennas to RF circuitry afterwards. Apparently, this kind of design approach does not suit highly miniaturized wireless sensor nodes anymore. A tiny node connected to a protruding antenna via a standard connector or cable is certainly not a good option. Instead, small and inconspicuous antennas directly integrated onto a chip or into a package together with other electronics are desired. This approach, requiring new design consideration, brings new challenges to antenna designers. Other than stand-alone antennas, system aspects including physical size, production cost, bandwidth, link budget, antenna coverage area and interference have to be taken into account. Although intensive R&D activities have been carried out in this field, many technical issues still remain.

Large area electronics in lightweight, stretchable, foldable, and twistable formats are favored in various applications, e. g. wearable or bio-compatible medical systems, interactive gaming, and conformal electronics for aeronautic remote sensing [4]-[6]. In large area electronics that are in contact with the skin of the user, stretchability and foldability may significantly enhance the comfort of the user. In an application with a curved mechanical interface, flexible, even stretchable electronics can remove the need for mechanical designs with an exact shape. Instead, flat electronics can be built and easily shaped to conform to any surface at installation. Conventional electrics containing a variety of solid metals and dielectrics are however rigid. Flexible electronics, using very thin soft dielectric and metal layers, are implemented, but their flexibility is very limited, and certainly not intended to be stretched or twisted. Stretchable and foldable electronics are not seen on the market yet. Research activities in this area have been recently launched. Stretchable and foldable silicon integrated circuits (ICs) have been demonstrated by Rogers *et al*. where active ICs were fabricated on thin "wavy" silicon films embedded in elastics substrates [7]-[9]. Using meandered line configuration, stretchable interconnects at various frequency ranges were shown [10], cf Fig. 1.2. Moreover, liquid metal filled elastomeric micro-structured channels have recently been employed for stretchable interconnects with enhanced multi-axial stretchability as well as low resistance [11]. However, the previous studies deal with either low-frequency ICs or relatively simple interconnects. Experimental studies on stretchable and twistable antennas are not reported so far. Such studies are certainly of importance to stretchable large area electronics, as integrated antennas are usually larger than other electronics, and thus often determine the mechanical properties of the entire devices.

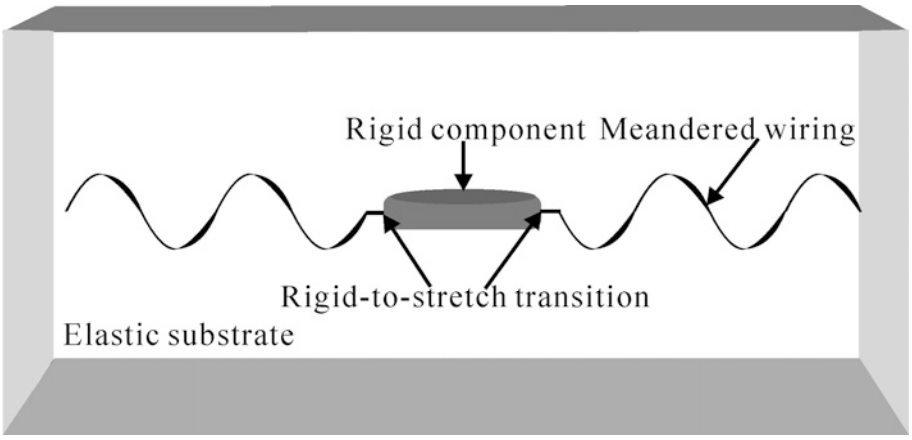


*Figure 1.2: Stretchable electronics based on meandered wiring.*

### 1.1.2 Millimeter-Wave Systems

Millimeter-wave technologies in the frequency range of 30-300 GHz have been traditionally used in scientific and military applications, i. e. radio astronomy [12]-[14] and battleplane radar systems, but during the last decade millimeter-wave technologies have been applied also to commercial applications. For example, automotive anti-collision radars around 77 GHz [15]-[17], mobile broadband telecommunication systems operating in the 62-63 GHz and 65-66 GHz bands, wireless personal area networks in the 59-62 GHz band in Europe, and radio links at 38, 42, 58 and 94 GHz [18]-[21]. Millimeter-wave imaging systems have also been developed both for commercial and defense applications, and they operate around 94 GHz e.g. [22],[23].

It is well known that power is the key issue at millimeter-wave frequencies. Thereby, from the antenna design point of view, how to implement highly efficient antennas is of primary significance to millimeter-wave systems. First of all, conductive, dielectric, and leakage losses should be reduced. Secondly, a main design target should be to simplify the manufacturing, and especially to avoid transitions. Furthermore, mechanical reliability also needs to be considered while physical sizes of the antennas shrink at very high frequencies.

Rectangular waveguides for transmitting RF power from one point to another are widely used at millimeter-wave frequencies due to their advantages of low losses, excellent isolation, and high power handling. But, applications of waveguides at millimeter-wave frequencies are still limited by high manufacturing cost, relatively large volumes, and difficulties of integration with

other components. Recently, the substrate integrated waveguide (SIW) technique has been demonstrated with maintained advantages of rectangular waveguides as well as additional merits, i. e. ease of integration, low cost implementation, and reduced size [24]. SIWs can be seen as low-profile dielectrically filled rectangular waveguides that are enclosed between two metallic walls. When fabricated by PCB processes, each of the walls is built in the form of a row of a number of metalized through-hole vias, as shown in Fig. 1.3. Using conventional PCB technologies, various SIW-based microwave devices such as filters, couplers and antennas have been successfully demonstrated up to 30 GHz [25]. SIWs operating at higher frequencies necessitate more densely placed vias to reduce the leakage losses. This challenges the traditional PCB processes, and also degrades the mechanical performance of the finished samples. Hence, new technologies are desired to overcome the increasing radiative waveguide losses of SIWs at higher frequencies and improve their mechanical properties [26],[27].

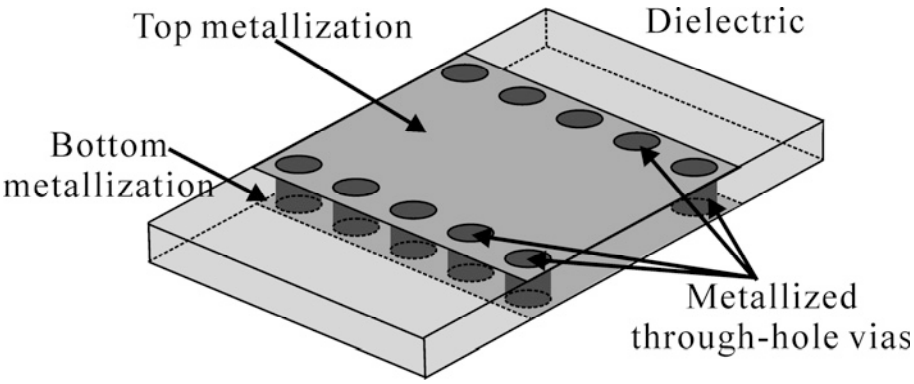


*Figure 1.3: General architecture of conventional SIWs.*

Advanced micro- and nano-technologies have been successfully employed in fabricating a variety of microwave devices at millimeter-wave frequencies. One of the most successful examples is radio frequency microelectromechanical system (RF MEMS). RF MEMS switches are well accepted as a promising technology for future advanced reconfigurable RF front-ends [28]. Numerous MEMS-based tunable passive and active microwave devices at millimeter-wave frequencies with excellent performance have been recently demonstrated [29]. Owing to decreasing manufacturing cost and enhanced reliability, RF MEMS technologies are anticipated to penetrate various electronics markets, evolving from costly military systems to cost-effective consumer electronics in the near future. Integration of antennas with MEMS components enables high performance reconfigurable antenna systems at millimeter-wave frequencies, which are not possible be-

fore, and thus are finding more and more potential application scenarios in a broad range of areas.

Automotive radar systems have been identified as a significant technology for the improvement of road safety. Short and long range radars are under development for features such as anti-collision, lane change assistance, and blind spot monitoring. The demand on automotive radar systems with enhanced resolution and functionalities to further improve the road safety is rising. Electrical beam forming is regarded as one of the promising technologies to increase the radar resolution. Instead of switching among a few broad fix antenna beams in existing automotive radar systems, an electrical scanning of a very sharp beam will be implemented to combine the high resolution with a broad sensing range. Furthermore, existing automotive radar systems can only detect reflective objects in the scanning areas, but they are not capable to single out pedestrians among "dead" objects. An added functionality of distinguishing pedestrians from "dead" targets and clutter can definitely enhance the intelligence of the existing automotive radar systems and further improve the road safety.

## 1.2 Outline of the Thesis

This thesis is mainly based on experimental studies of integrated antennas solutions for various systems operating from a few hundred megahertz up to millimeter-wave frequencies. It is comprised of thirteen previously published *Papers I-XIII* and a summary. Integrating antennas to portable devices is studied in *Papers III*, *IV*, *VII*, *VIII*, and *X*. *Papers I*, *II*, and *IX* present electrically steerable array antennas based on either varactor diodes or MEMS switches at different frequencies. Antennas at higher millimeter-wave frequencies, with enhanced electrical performance using silicon micromachining or nano-wire based SIW technology, are demonstrated in *Papers V*, *VI*, *XI*, *XII*, and *XIII*.

The summary part of the thesis is organized so that Chapter 2 briefly presents integrated antennas for wireless sensor nodes and handheld terminals. Chapter 3 and 4 describe electrically tunable array antennas and millimeter-wave integrated antennas, respectively. The conclusions and potential future work of the presented studies are discussed in Chapter 5. All the papers appended in this thesis are summarized in Chapter 6.

# 2 Wireless Sensor Node and Handheld Terminal Antennas

The available volume for antennas integrated in portable devices is often very restricted. Hence, these antennas can sometimes be defined as electrically small antennas. A common definition for an electrically small antenna is that its greatest dimension is limited to be smaller than $\lambda_0/4$ including any image due to ground plane [30]-[32]. Here, $\lambda_0$ is the free space wavelength. Resonator theory can be applied to small antennas near the fundamental resonance. Since a small antenna stores a large amount of energy, its input impedance has a large reactive component in addition to a small radiation resistance. To efficiently deliver power to (and from) the antenna, it should preferably be tuned to resonance, i.e. the input reactance should be cancelled. Sufficient reactance cancellation can only occur within a narrow bandwidth.

The fundamental limitations of electrically small antennas were first studied by Wheeler in 1947 [33]. A year later, Chu derived an approximate limit for the achievable radiation $Q$ [34], which was reprised by McLean in 1996 [35] as

$$Q = \frac{1}{k^3 a^3} + \frac{1}{ka} \tag{2.1}$$

for the lowest achievable radiation quality factor $Q$ of a linearly polarized antenna which fits in a sphere with radius $a$. The quality factor sets a limit on the maximum achievable relative bandwidth, assuming 100 % radiation efficiency of the radiator. Small antennas, exhibiting low quality factors, often suffer from low radiation efficiency that can result in apparently larger bandwidths than the limit suggested by (2.1). However, it should be noted that (2.1) is based on the assumption of a single $TM_{01}$ spherical mode, equivalent to a linear current element. When the lowest *TE* and lowest *TM* modes are excited (circular polarization) simultaneously, a different expression of $Q$ is obtained [35].

For both linearly and circularly polarized cases, the surrounding radiation sphere should be defined to encompass the entire antenna, including the commonly encountered finite ground planes, because the flowing current in

other structures than the intended radiator will contribute to the stored energy and radiation, and thus affect the quality factor. In addition to the Wheeler-Chu-McLean limitations, the effect of antenna size on gain was investigated by Harrington in 1960 [36], which explains why electrically small antennas feature low gain and omnidirectional radiation patterns.

Impedance matching is one of the crucial technical issues for electrically small antennas. The input impedance of an antenna should be transformed to match the characteristic impedance of the feed line or the optimal load impedance of a radio circuit. Several techniques, i.e. lumped elements, tuning stubs, and single-section quarter-wave transformers, can be employed to match an arbitrary antenna input impedance to any system impedance at a single frequency. For broader bandwidths, multi-section matching transformers and tapered lines can be utilized to obtain various pass-band characteristics. The performance of an impedance matching network is constricted by the fundamental limitations. For a certain load impedance, a theoretical limit on the reflection coefficient over frequency that can be obtained with an arbitrary matching network is expressed by Bode-Fano [37],[38]. It represents the optimum case that can be ideally achieved, even though such a result may only be approximated in practice. Such optimal results are always of great importance, because they give us the upper limit of performance, and provide a benchmark against which a practical design can be compared.

Fig. 2.1 illustrates a lossless network used to match an arbitrary load impedance, which can be modeled as parallel and series *RC* and *RL* circuits.

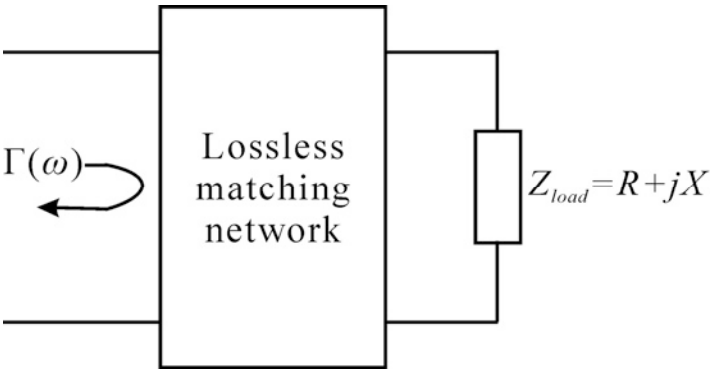


*Figure 2.1: An arbitrary load matched with passive and lossless networks.*

In the case of a parallel *RC* circuit, the expression can be written as

$$\int_0^\infty \ln\frac{1}{|\Gamma(\omega)|}d\omega \le \frac{\pi}{RC}=\frac{\pi}{\tau} \tag{2.2}$$

where $\Gamma(\omega)$ is the reflection coefficient seen looking into the arbitrary lossless matching network and $\tau=RC$ is the time constant of a parallel $RC$ load. The Bode-Fano limit states that a broader bandwidth can be achieved only at the expense of a higher reflection coefficient in the pass-band. Moreover, high-$Q$ circuits result in long time constant and small value of $\pi/\tau$. This implies that, for an electrically small antenna with high-$Q$, a tradeoff between a lower reflection coefficient and a wider bandwidth has sometimes to be made. Although impedance bandwidth can be enhanced using external matching network, the fundamental limitations of an electrically small antenna in terms of size and bandwidth are still valid. Furthermore, an external matching network, with high-$Q$ lumped components or distributed elements, will obviously add some additional cost to the antenna manufacturing.

Apart from the fundamental theoretical restrictions, a designer working on integrated antennas for wireless sensor nodes or handheld terminals also has to respect limits coming from practical considerations. First, integrated antennas are often desired to be built on single- or multi-layered PCBs on which the subcomponents are mounted to save manufacturing cost. Second, mechanical properties are other crucial aspects. Durable encapsulation of integrated antennas as well as other electronics is always desired. A protruding antenna configuration is often not a good choice. Moreover, robust integrated antenna solutions are preferred to relax the manufacturing tolerance.

Wireless communications in portable devices can be categorized to low data rate (wireless sensors and RFID tags) and high data rate communications (mobile voice, on-line TV, navigation, FM radio, and satellite communications). For low data rate communication systems, impedance bandwidth of integrated antennas does not seem to be a problem, sometimes less than one percent is sufficient. Yet antennas with very small bandwidths often pose many difficulties in the design procedure. For example, they usually necessitate a number of design iterations to achieve the right operation frequencies, and thus result in costly and time-consuming prototyping processes. In the case of high data rate communications, system bandwidths can be larger, so antenna designers must be extra cautious to make the best use of the available volume.

## 2.1 Novel Antenna Designs

While handheld terminals are getting more and more popular in daily life, the demand for capacity as well as improved services increase. These terminals are traditionally for voice but more and more for advanced services at different bands, requiring transfer of large amounts of data.

Today handheld terminals for mobile communication, e. g. cellular phones, often contain a number of antennas functioning at different frequencies. Each of them typically covers a rather small bandwidth for a specific function, but together achieve multiple functionalities. In the future, an increasing demand on fitting more antenna functionalities into the handheld terminal with a constant, or even shrinked volume, is foreseen. So far, most resonant antennas like the F-antenna [39],[40], monopole, and loop, have been used, but such antennas typically feature narrow bandwidth. Hence, an interesting question arises: is it possible to implement a single broadband enough antenna covering all frequency bands [41]-[43]? Of course, such antenna must operate in association with filters or switches for isolation between the different bands.

An antenna element with extremely broadband performance has been presented by Suh [44],[45]. It is actually a variant of the conventional inverted cone antenna, but with a planar radiating element, so-called planar inverted cone antenna (PICA), cf Fig. 2.2. At its lowest frequency, it acts as a monopole. At higher frequencies, it works more like a notch antenna, maintaining a good impedance matching up to more than a decade above the lowest frequency of operation. The upper operational frequency limit is primarily determined by how small the gap between the leaf-shaped protruding part and the ground plane can be made. Even though this antenna is named PICA, it actually features a 3D configuration rather than planar, as its radiating element is mounted perpendicular to the ground plane. This fact brings difficulties in integrating such an antenna into small handheld terminals.

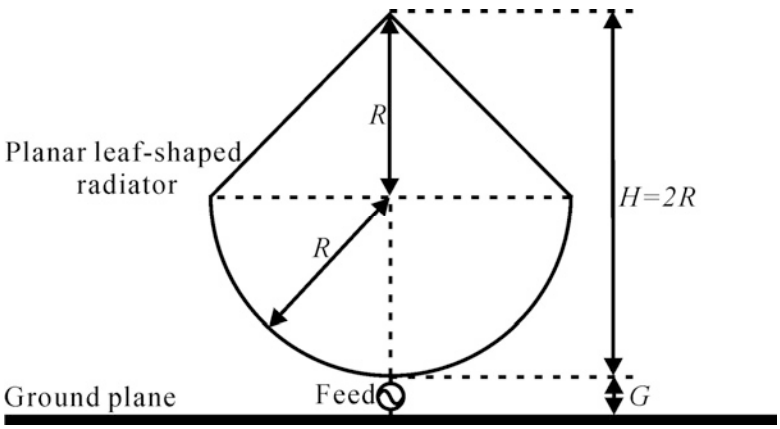


*Figure 2.2: Simplified drawing of PICA by Suh, presented in [44],[45].*

### 2.1.1 Slot PICA

Based on the PICA concept, a purely planar printed slot antenna for integration in a printed circuit board (PCB) for ultrawideband (UWB) applications

is proposed and evaluated in *Paper IV*, as shown in Fig. 2.3. This slot antenna resembling the PICA, so-called "slot PICA", can be implemented using either chemical etching or mechanical milling from two metal layers of the PCB. It maintains the advantages of the PICA such as extremely large bandwidth, omnidirectional radiation pattern, and relatively small size, while featuring some additional attractive merits like ease of integration, low cost manufacturing, and planarity.

The slot-PICA consists of a leaf-shaped metal radiating element in one plane, and a large leaf-shaped slot in a second metal plane. A 50-Ω microstrip feed line is connected to the metal radiator in the first plane. The second plane acting as ground plane for the microstrip line can be utilized for integration of other electronics without affecting the electrical performance of the antenna. The leaf-shaped slot in the ground plane leads to strong electromagnetic coupling to the feeding structure. The antenna impedance can thereby be tuned by adjusting the slot and feed. The lower operational frequency limit is primarily determined by the height of the radiator $2R_f$, which approximately corresponds to a quarter wavelengths in free space at the lowest frequency. Impedance matching at higher frequencies can be improved by varying the size of the leaf-shaped slot. The distance $G$ between the bottom edges of the leaf-shaped slot and the feed is crucial for the impedance matching, especially at the highest frequencies. By carefully optimizing the above dimensions, a broad impedance bandwidth of a decade or even a couple of decades above the lowest frequency of operation can be achieved as well as good radiation characteristics.

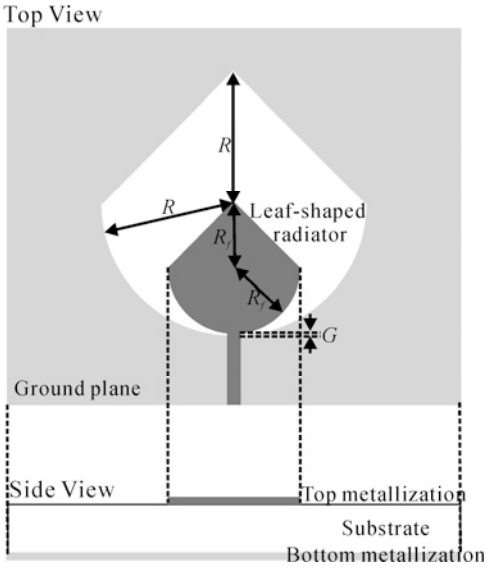


*Figure 2.3: Drawing of the printed slot PICA described in Paper IV.*

### 2.1.2 Broadband Handset Antenna

A basic PICA is modified to a low-profile configuration that fits in a handset of typical dimensions. In the modified PICA presented in *Paper III*, the leaf-shaped radiating element is bent so that the upper part is parallel to the ground plane, as depicted in Fig. 2.4. The folded radiator occupies about the same volume and circuit board area as the standard inverted F-antenna used in many handsets, and placed on a 100 mm × 50 mm ground plane resembling the chassis of a mobile handset. Different heights of the bent radiating element $H$ are tested, and it is found that a higher radiator features better electrical performance. Furthermore, different feed points on the ground plane are investigated. The one that is found to exhibit the best performance is the center of the short edge of the ground plane. The gap $G$ between the ground plane and the radiating element at the feed point is a critical dimension at higher frequencies, where impedance matching can be improved using a smaller gap.

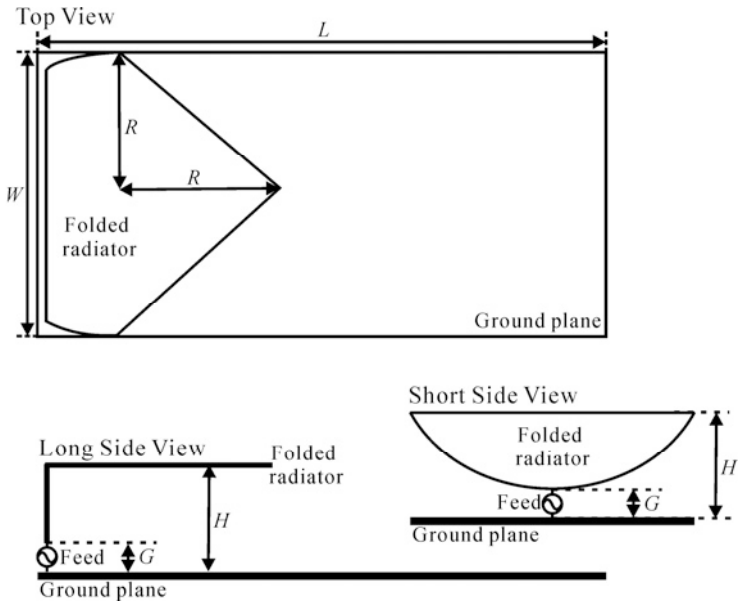


*Figure 2.4: Drawing of the modified handset PICA, with the radiating element folded at height H above the ground plane, evaluated in Paper III.*

### 2.1.3 Antenna System Integration

When integrating an antenna into a system, integration compatibility must be taken into account. Designing nice appearance for the entire device often poses the first priority, rather than antenna electrical performance. Good

compatibility here means a small and inconspicuous antenna. Naturally, planar or low-profile antenna configuration usually suits planar systems, and a 3D system may require a 3D antenna configuration.

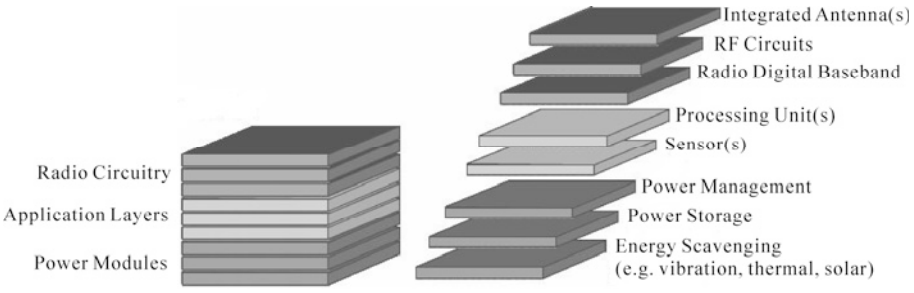


*Figure 2.5: General architecture of wireless sensor node, proposed in e-CUBES [46].*

Recently, 3D integration technologies enabling high density of integration have been proposed for miniaturizing the overall size of wireless sensor nodes and lowering the losses of interconnects, as shown in Fig. 2.5. Using 3D integration technologies, all electronics can be densely integrated into a miniaturized cube-like architecture [46]. This in turn requires an integrated antenna to fit into such a cube, as depicted in Fig. 2.6. For this specific case, (2.1) is reformulated as

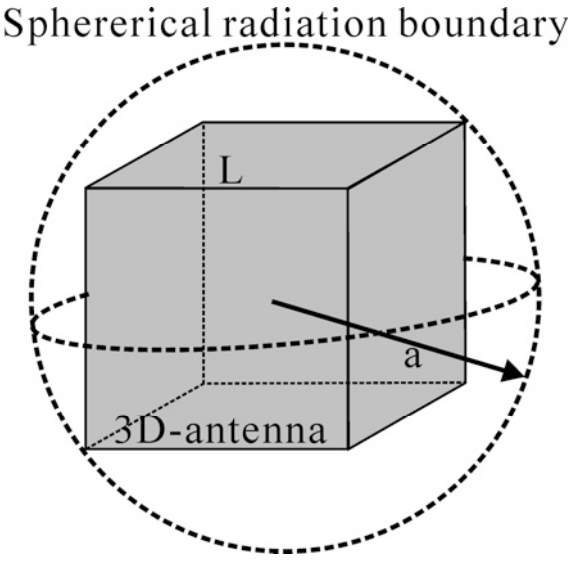


*Figure 2.6: 3D integrated antenna (L is the lateral length of the cube, and a is the radius of the spherical radiation boundary).*

$$a = \frac{\sqrt{3}}{2} L \tag{2.3}$$

$$Q = \left(\frac{1}{k^3 a^3} + \frac{1}{ka}\right)\eta \tag{2.4}$$

$k$ is the wave number at the centre frequency.
$Q$ is the quality factor.
$\eta$ is the radiation efficiency.

to describe the fundamental limitations of a 3D integrated antenna, in which both radiation efficiency and impedance bandwidth are counted. But the theoretical limitation is just an ideal case and very hard to achieve in practice.

When designing integrated antennas for miniaturized devices, antenna designers must make use of all available techniques to achieve optimal performance within the often highly limited available space. The fact that integrated systems contain a large number of various electronic modules poses many challenges in the design procedure, with additional problems of coupling and interference. Various loading techniques, e.g. capacitive, inductive and dielectric loading, can be used to implement electrically small antennas for miniaturized devices or systems, yet electrical performance of the antennas will certainly be degraded. A tradeoff between antenna performance and size sometimes has to be made.

Moreover, antennas are sensitive to the surroundings. Not only other electronics in the device itself, but also the operating environment will affect the performance of an antenna. For example, when a wireless sensor node is placed on a human body, both the port impedance and the radiation characteristics of its internal antenna are affected. This can be a severe problem for portable devices, as it is linked to the transmit power and link budget, which in turn determine battery lifetime. However, as the operating environment varies from case to case, it is very hard to define a universal optimal antenna solution for all cases. Instead, antennas should be especially adapted to the specific environment at hand.

Direct impedance matching between the integrated antenna and radio circuitry without any external balun or matching network is often preferred as a means to lower the cost. This may significantly complicate the integrated antenna design, especially for a differential radio circuitry with complex optimal load impedance. Additionally, specific impedance matching techniques, e.g. folding or T-match, might be needed to match the antenna port impedance to the optimal load impedance of the radio.

Characterization techniques are especially difficult for integrated antennas. Differing from the measurements on stand-alone antennas, integrated antennas must be characterized together with the other electronics in the system. Port impedance, radiation patterns, and radiation efficiency are the most interesting parameters in passive measurements. In such experiments, antennas are often connected to the measurement instruments via RF cables. Sometimes, it can be difficult to access the interface for connecting to the antenna in a miniaturized system. Furthermore, as the feed cable may act a part of the antenna, its influence has to be taken into account in the measurements [47],[48]. The effect of the feed cable can be eliminated in active measurements such as the overall radiated power or active radiation patterns, where the antenna is directly fed by the radio unit.

### 2.1.4 T-Matched Dipole Antenna and Characterizations

One of the primary application areas for wireless sensor nodes as well as wireless sensor networks is remote healthcare and fitness monitoring, where body-worn sensor nodes are in great favor [49]-[51]. Communications can then be either among a number of sensor nodes configured as a body area network on the same body, or between a body-worn node and a base station at certain distance. The presence of a base station enables further access to existing systems such as GSM, GPRS, CDMA and Internet, and thus provides long range data transfer to a clinic or a hospital.

A small and light body-worn sensor node powered by an internal battery is often desired to enhance the comfort of the user. The capacity of the battery is restricted by the available volume within the senor node. Hence, efficient energy handling including efficient circuits and an efficient antenna is critical for the system design. This challenges the physical limitations for electrically small antennas, because of the contradictory requirements of both small size and high efficiency [33]-[35]. Furthermore, a robust antenna that can tolerate the severe body influence is also of importance to a node placed in the proximity of the body [52],[53].

An integrated antenna is expected to be directly matched to the optimal load impedance of the radio circuitry to lower the manufacturing cost. In the case of a differential transceiver with complex optimal load impedance, a differential antenna off its resonance, featuring complex input impedance, is preferred, as illustrated in Fig. 2.7.

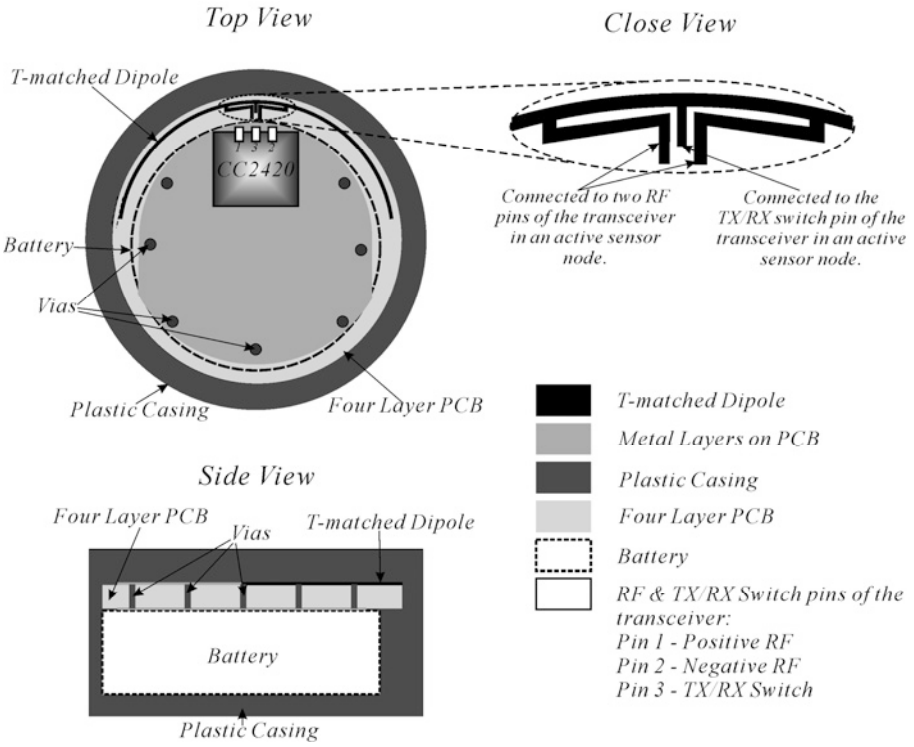


*Figure 2.7: Schematic drawing of the T-matched dipole integrated in a small body-worn sensor node presented in Paper VII.*

The sensor node used in *Paper VII* has a cylindrical plastic housing with an outer radius of 15 mm and a height of 7 mm. The maximum cross dimension of the node corresponds to a quarter wavelengths at 2.45 GHz, which is the operational frequency of the ZigBee transceiver (CC2420) used in the node. Most of the interior space is occupied by the battery and a PCB. Around the periphery of the circuit board, on the top metallization, is a space allocated for the antenna. A T-matched dipole antenna that eliminates any external balun between the antenna and the RF transceiver is proposed and implemented in the small node [54],[55]. The choice of a differential antenna is also based on the idea that it might be less sensitive to the surroundings. The T-match is employed to increase the antenna input impedance to compensate for the low antenna radiation resistance resulting from the strong coupling effect of the surrounding subcomponents, and thus achieve a good impedance match.

In passive characterization without any circuitry, the antenna is fed by a semi-rigid cable via an Anaren 0404 balun. The antenna port impedance is first measured at the end of the cable using a vector network analyzer, and then recalculated using the formulas derived in *Paper VII*. The radiation

efficiency is characterized in a reverberation chamber, and found to be around -4 dB within the frequency range of 2.4-2.48 GHz. In active measurements such as radiated power and active radiation patterns, the antenna is directly fed by the sensor node transceiver programmed to the unmodulated transmitter test mode. Moreover, the antenna performance in the fully functional sensor node with 3D acceleration and 2D magnetic field monitoring functions is also evaluated at Philips in the Netherlands. A communication range up to 20 m is successfully demonstrated, which is sufficient for real applications.

Following the successful demonstration of the sensor node at 2.4 GHz, a further miniaturized sensor node operating at 17 GHz is implemented. Thanks to the advanced 3D integration technologies, the entire size of the sensor node including the encapsulation is reduced to 20 mm × 11.4 mm × 7.4 mm, with the same functionalities as the one at 2.4 GHz are kept, cf. Fig. 2.8.

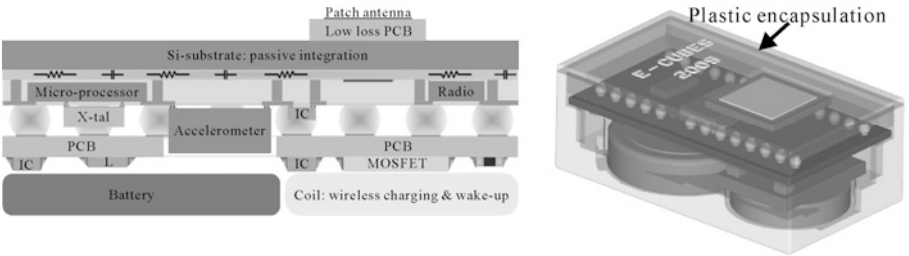


*Figure 2.8: Physical architecture of 17 GHz 3D integrated sensor node (left) and mechanical design drawing with encapsulation (right), proposed in e-CUBES [46].*

As the operational frequency is increased, the sensor node at 17 GHz is no longer electrically small, and sufficient volume can be found in such a sensor node to fit a standard antenna, i.e. patch, monopole or loop. A linearly polarized patch antenna including a ground plane acting as a shield to suppress the coupling to other electronics is chosen. It is fed by a 50-Ω microstrip line on the Si-stack, using aperture coupling through an H-shaped slot in the ground plane. Instead of metalizing the back of the Si substrate, the patch etched on a 508 μm thick Rogers 5880 substrate ($\varepsilon_r$=2.2, tan$\delta$=0.009) is glued on the back of the Si-stack. The antenna input impedance match and resonance frequency can be easily tuned by varying the patch width and length on the Rogers substrate. It is apparently a cost-effective solution to optimize the antenna performance, because the antenna feed on the Si-stack can remain the same and the costly production of the Si-stack is minimized.

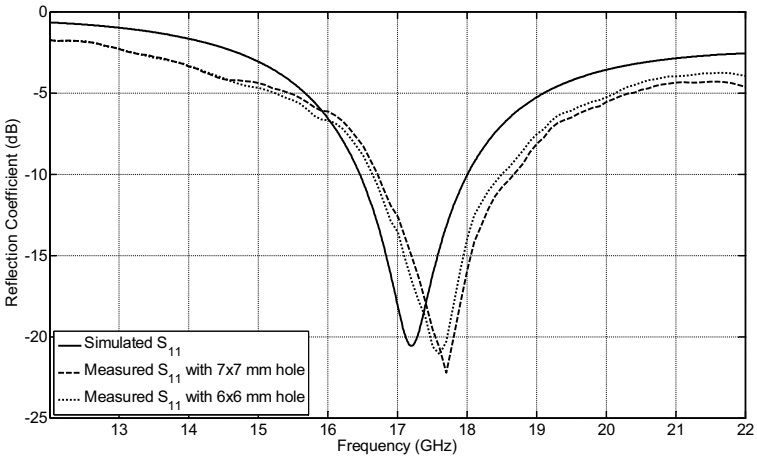


*Figure 2.9: Simulated and measured reflection coefficient of the integrated antenna.*

Simulated and measured reflection coefficients of the antenna integrated in the sensor node are presented in Fig. 2.9. Experimental results agree well with the simulations. It is shown that an impedance bandwidth of 10 % is achieved at 17.2 GHz. Moreover, the influence of the opening in the plastic housing on the antenna port impedance is also investigated. Only slight variations in the measured reflection coefficient can be seen between the housings with the 6 mm × 6 mm and 7 mm × 7 mm openings, respectively.

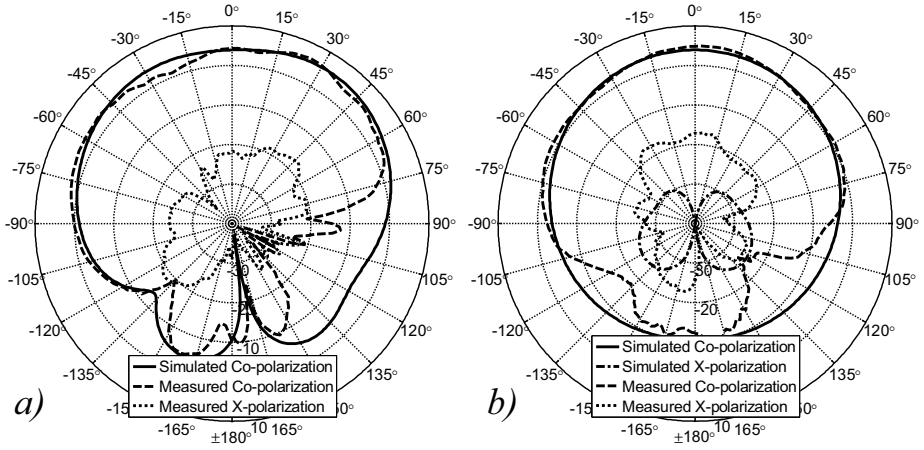


*Figure 2.10: Simulated and measured a) xz- and b) yz-plane radiation patterns of the integrated antenna at 17.2 GHz.*

Fig. 2.10 shows the simulated and measured radiation patterns at 17.2 GHz. The presented antenna exhibits a gain of 5.0 dBi, and a front-to-back ratio of 13.4 dB at 17.2 GHz. Efficient radiation characteristics owes to the use of low loss Rogers substrate and high resistivity silicon. This antenna mainly radiates upwards, which is a favorable feature in off-body communication.

### 2.1.5 Stretchable Liquid Metal Antennas

In contrast to miniaturized 3D nodes, body-worn sensors can also be made in very thin planar configurations covering a large surface with flexibility, twistability, and stretchability. In some sense, these kinds of nodes resemble textile electronics based sensors. The difference is that it offers a higher degree of flexibility that is not possible in textile electronics. Furthermore, it can also overcome some crucial technical issues in textile electronics, for instance moisture absorption, poor manufacturing precision, and relatively high conductive losses.

A variety of approaches to implement stretchable large area electronics have been proposed by several research groups [7]-[9],[56]-[60]. Most of them use planar or 3D meandered solid wires in combination with elastic materials to achieve a certain degree of stretchability. Still, stretchability in these approaches is restricted by the solid metals due to the severe mechanical mismatch between the solid metals and elastic materials. Recently, room temperature liquid metal filled elastomeric micro-structured channels have been utilized for stretchable interconnects, which feature very impressive performance in terms of high multiaxial stretchability and low resistance in DC [11]. However, studies on stretchable antennas other than the previously reported low frequency ICs or relative simple interconnects are still absent.

Flexible, stretchable and twistable antennas based on liquid metal are demonstrated for the first time. This concept incorporates room temperature liquid metal alloy into micro-structured channels in a sheet of elastic substrate, polydimethylsiloxane (PDMS). In brief, the manufacturing process consists of the following steps: master fabrication, molding, liquid-metal injection, and encapsulation, as illustrated in Fig. 2.11.

The design pattern is first transferred to a 100 μm thick SU-8 layer on a silicon wafer carrier using standard soft lithography [61]. It is then developed and thermally stabilized at 150$^{o}$C for 30 min. The mixed PDMS prepolymer and cross linker is first poured onto the SU-8 master, and degassed afterwards. The PDMS mixture is then cured at 70$^{o}$C for 30 min. Later, the structured PDMS thin layer is peeled off and a couple of through-holes are punched out for injecting the liquid metal. In parallel to the PDMS replication process, a blank PDMS lid is cast on a flat silicon wafer carrier. Using corona discharging activation, the above two PDMS layers are bonded together. The liquid metal (Galinstan, 68.5 %, Ga, 21.5 % In, 10 % Sn, $\sigma$=3.46·10$^{6}$ S/m) is injected into the micro-structured channels via the through-holes, and finally the openings are encapsulated with uncured PDMS mixture.

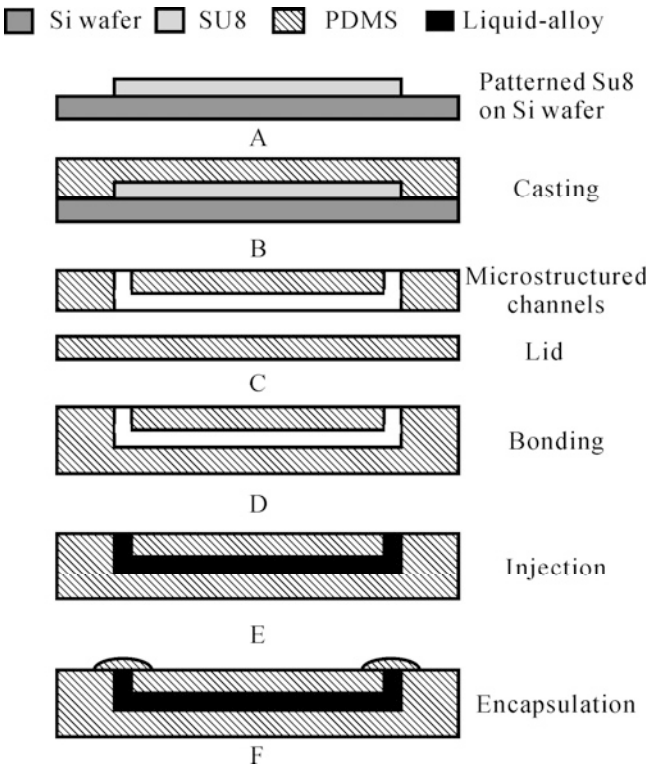


*Figure 2.11: Manufacturing process flowchart.*

The first prototype, an unbalanced loop antenna operating at 2.4 GHz, is demonstrated in *Paper VIII*, as shown in Fig. 2.12. In the lower semicircular ground plane, a large number of PDMS posts are aligned to space the top and bottom PDMS membranes. In addition, several cylindrical reservoirs are placed along the upper channel of the antenna to ensure good electrical connection of the liquid metal while folding, stretching, or twisting the antenna.

Prior to characterizations on the antenna electrical performance, mechanical test on stretching, folding, and twisting the antenna are carried out. A relative stretching of 40 % along two orthogonal orientations can be achieved without any damage. The uneven PDMS layer thickness and the heterogeneous antenna pattern result in slight mechanical heterogeneity while stretching. In addition to the mechanical tests on the stretchability, folding with a small curvature, as well as severe twisting of the antenna, is also demonstrated with no mechanical damage found.

According to characterizations of electrical performance, the non-stretched antenna exhibits a good impedance matching around 2.4 GHz. While stretching the antenna, the length of the upper radiating arm ($L_{\text{loop}}$) increases, leading to a lower resonance frequency. Measured radiation pat-

terns at 2.4 GHz feature almost perfect omnidirectionality, which is similar to that of conventional unbalanced loop antennas. The maximum gain of the non-stretched antenna is found to be around 2.7 dBi, and the measured cross-polarization is approximately 15 dB lower than the corresponding co-polarization. Variations can be seen in the measured radiation patterns of the stretched antenna. Not only the omindirectionality of the radiation patterns degrades, but the cross polarization level also increases. This fact can mainly be explained by the increasing cable influence and the asymmetrical geometry when the antenna is stretched. Apart from the radiation pattern measurements, the antenna radiation efficiency at 2.4 GHz is characterized in a reverberation chamber. It is verified that the antenna maintains a radiation efficiency higher than 80 % at 2.4 GHz even if stretched by 40 %.

The resonance frequency detuning resulting from stretching has to be taken into account in future studies. A robust antenna whose electrical performance is insensitive to stretching is of great interest. This target requires good knowledge both in electrical and mechanical properties of stretchable antennas.

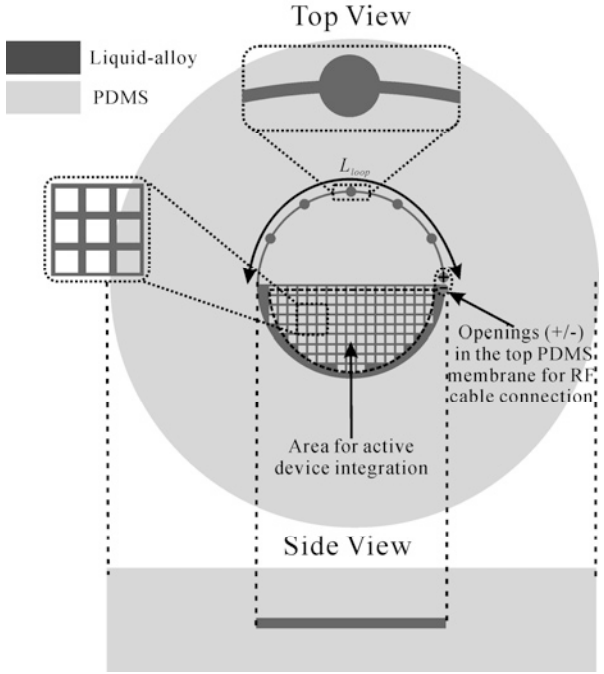


*Figure 2.12: Mechanical drawing of the first stretchable antenna prototype, stretchable unbalanced loop antenna introduced in Paper VIII.*

In *Paper X*, the PICA concept is implemented as a stretchable antenna in order to enhance the robustness of the antenna electrical performance while stretching, Fig. 2.13. This antenna resembles the previously presented “slot

PICA" in *Paper IV*, but has a uniplanar configuration. This makes it suitable for folding, stretching, and twisting, and simplifies the fabrication process as well.

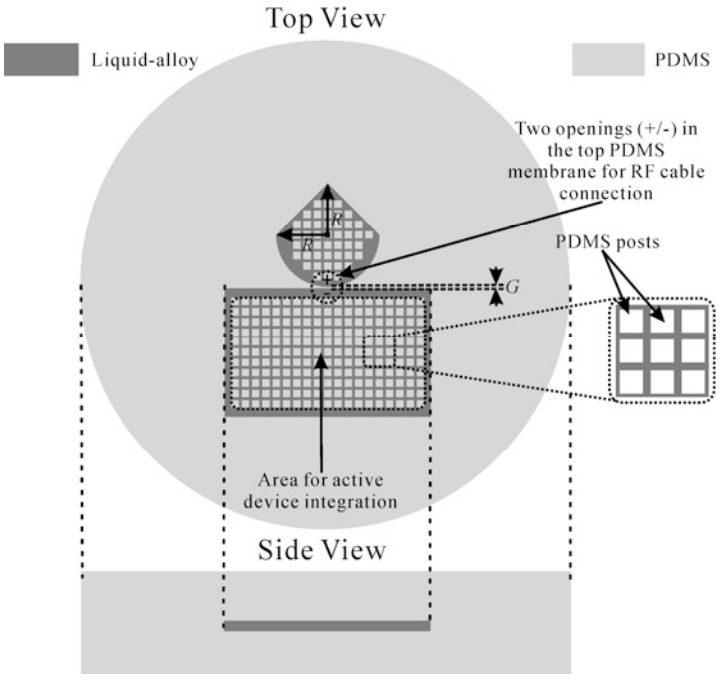


*Figure 2.13: Mechanical drawing of the stretchable PICA, evaluated in Paper X.*

The height *2R* of the leaf-shaped radiator determines the lowest antenna resonance frequency, but the antenna input impedance matching at higher frequencies is not very sensitive to the exact shape of the radiator. This feature might enable a robust antenna that can tolerate severe stretching over a broad impedance bandwidth. At the highest frequencies, the antenna input impedance matching depends on the size of the gap *G* between the leaf-shaped radiator and the ground plane.

Experimental results on the mechanical properties of the stretchable PICA are very similar to that of the unbalanced loop antenna. However, the stretchable PICA exhibits much more stable electrical performance while stretched. Measured data verifies that this antenna achieves a return loss better than 10 dB within 3-11 GHz and a radiation efficiency of >70 % over 3-10 GHz, also when stretched. Such kind of electrical performance is sufficient for UWB applications.

## 2.2 Summary and Conclusion

Several antenna solutions investigated within the scope of this chapter share a common design target, which is compatible integration of appropriate antennas into various systems. Differences of the systems and applications lead to differences in the antenna designs. For handheld terminals, the focus lies in the enhancement of the antenna impedance bandwidth within very limited available volume in handsets. Low radiation efficiency is one of the most critical issues for electrically small antennas integrated in miniaturized sensor nodes. A couple of effective integrated antenna solutions have been addressed and examined. New measurement techniques for characterizing integrated antennas either in a completely passive or fully functional active node are introduced. For stretchable large area electronics, studies of integrated antennas are dedicated to improve the antenna stretchability while maintaining favorable electrical performance. Two liquid metal based stretchable antenna prototypes have been successfully demonstrated with good mechanical and electrical performance. This concept opens remarkable potentials for future applications of large area electronics.

Nevertheless, technical issues in many systems and applications have not been solved yet. Sufficient isolation, using filters or switches, among various bands can be an interesting research topic for broadband antennas integrated in mobile handsets. The influence of different communication systems can also be of importance. For body-worn sensor nodes, better understanding of the body influence on the integrated antenna performance and the implementation of robust antennas with high performance are definitely needed. Stretchable large area electronics is a relatively new research field, where many new research topics can be found. One of the key subjects is to develop a reliable interface between stretchable interconnects and rigid components. Successful implementation of such an interface will enable stretchable fully functional devices and systems, fulfilling the requirements of a wide range of applications, and bring this concept a step further towards the market.

# 3 Electrically Steerable and Switchable Array Antennas

Phased array antennas with electrical beam steering or switching functionality, so-called electrically steerable or switchable arrays (ESA), have received significant attention in recent years. This concept enables beam scanning of a physically stationary antenna. It thus eliminates mechanical adjustment, i.e. gimbal or motor. The ESA technique is traditionally applied to radar systems. A majority of these systems are dedicated to military applications, in which high cost usually is not an issue. ESAs have also been implemented in many satellites, another type of costly systems. Beam steering functionality allows an antenna to be fixed onto a satellite. The antenna beam can then be electrically steered towards any desired direction to avoid any additional physical movement of the satellite, which is costly in space. So far not many consumer applications of ESAs can be seen on the market.

Due to enhanced performance and decreasing cost of semiconductor and MEMS devices, implementation of cost-effective ESAs with high performance now becomes feasible. ESAs using varactor or pin diode-based phase shifters can be realized at a few gigahertzes for communication systems, such as cellular networks. At higher frequencies, i.e. millimeter-wave frequencies, MEMS-based phase shifters or switching matrix can be employed to implement electrically steerable or switchable array antennas. As an alternative solution, digital beam forming (DBF) with parallel radios and beam forming at baseband frequencies is also possible. However, this technique requires complicated digital processing, weighting algorithm, and calibration technology. Thus the key to this approach is advanced software and circuitry rather than specific antenna technology.

A phased array antenna usually consists of a number of radiating elements and a tunable feed network. The radiation characteristics of a phased array antenna is mainly determined by the excitation of each radiating element, the radiation properties of each element, relative spacing, and coupling among the radiating elements. In some cases, radiation from the feed network should also be taken into account, because it might significantly affect the overall radiation performance of a phased array. Once a phased array antenna is constructed, its physical architecture, i.e. configuration of the feed

network or relative spacing of the radiating elements, is very hard to change. Varying the excitation of each radiating element is however feasible by electrically tuning the feed network. Therefore, ESAs are often realized by introducing electrically tunable components, i.e. phase shifters or switch matrix, into the feed network.

A general architecture of a 1-D ESA is illustrated in Fig. 3.1, where a number of radiating elements are placed in a row with certain spacing. Such linear array can be incorporated to a tunable feed network either in parallel or series. The tunable feed network can be implemented using various approaches, but here only the factors of the coupling effect and excitation to each element through the feed network are of interest. To simplify the analysis, it is assumed that the feed network is perfectly shielded without any contribution to the overall radiation of the array antenna.

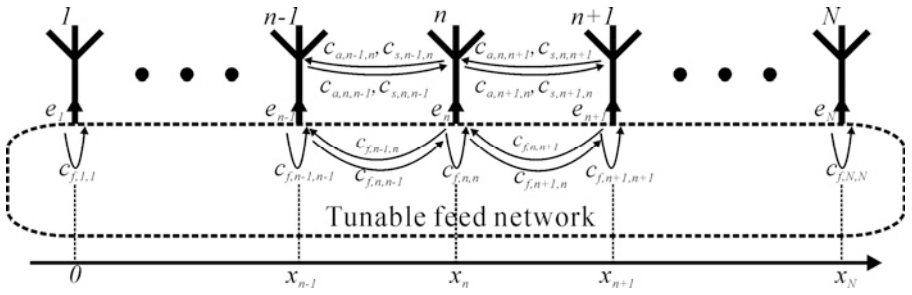


*Figure 3.1: General architecture of an ESA.*

$n$ is integer representing different radiating element.

$c_{a,n,m}$ is the coupling through the air from element $m$ to $n$.

$c_{s,n,m}$ is the coupling through the substrate from element $m$ to $n$. If there is no substrate in the antenna, this coefficient is equal to zero.

$c_{f,n,m}$ is the coupling through the feed network from element $m$ to $n$.

$e_n$ is the complex of drive of element $n$.

$x_n$ is the location of the center of radiating element $n$.

The overall coupling matrix **C** contains the coupling through the feed network $\mathbf{C_f}$, the substrate $\mathbf{C_s}$, and the air $\mathbf{C_a}$, and the ideal coupling to the radiating elements **I**, which is an identity matrix. It can be formulated as

$$\mathbf{C} = \mathbf{C_f} + \mathbf{C_s} + \mathbf{C_a} + \mathbf{I} \tag{3.1}$$

The individual matrices consist of coefficients according to the following.

Coupling through the feed network:

$$\mathbf{C_f} = \begin{bmatrix} -c_{f,1,1} & -c_{f,1,2} & \bullet & -c_{f,1,N-1} & -c_{f,1,N} \\ -c_{f,2,1} & -c_{f,2,2} & \bullet & \bullet & -c_{f,2,N} \\ \bullet & \bullet & \bullet & -c_{f,N-2,N-1} & \bullet \\ -c_{f,N-1,1} & \bullet & -c_{f,N-1,N-2} & -c_{f,N-1,N-1} & -c_{f,N-1,N} \\ -c_{f,N,1} & -c_{f,N,2} & \bullet & -c_{f,N,N-1} & -c_{f,N,N} \end{bmatrix} \quad (3.2)$$

Coupling through the substrate:

$$\mathbf{C_s} = \begin{bmatrix} -c_{s,1,1} & -c_{s,1,2} & \bullet & -c_{s,1,N-1} & -c_{s,1,N} \\ -c_{s,2,1} & -c_{s,2,2} & \bullet & \bullet & -c_{s,2,N} \\ \bullet & \bullet & \bullet & -c_{s,N-2,N-1} & \bullet \\ -c_{s,N-1,1} & \bullet & -c_{s,N-1,N-2} & -c_{s,N-1,N-1} & -c_{s,N-1,N} \\ -c_{s,N,1} & -c_{s,N,2} & \bullet & -c_{s,N,N-1} & -c_{s,N,N} \end{bmatrix} \quad (3.3)$$

Coupling through the air:

$$\mathbf{C_a} = \begin{bmatrix} -c_{a,1,1} & -c_{a,1,2} & \bullet & -c_{a,1,N-1} & -c_{a,1,N} \\ -c_{a,2,1} & -c_{a,2,2} & \bullet & \bullet & -c_{a,2,N} \\ \bullet & \bullet & \bullet & -c_{a,N-2,N-1} & \bullet \\ -c_{a,N-1,1} & \bullet & -c_{a,N-1,N-2} & -c_{a,N-1,N-1} & -c_{a,N-1,N} \\ -c_{a,N,1} & -c_{a,N,2} & \bullet & -c_{a,N,N-1} & -c_{a,N,N} \end{bmatrix} \quad (3.4)$$

Excitation of the array including the coupling effect can then be derived as

$$\mathbf{A}=\mathbf{C}^{-1}\mathbf{e} \quad (3.5)$$

where **e** is expressed as

$$\mathbf{e} = \begin{bmatrix} e_1 \\ e_2 \\ \bullet \\ e_N \end{bmatrix} \quad (3.6)$$

The radiation pattern **G** of the complete array is obtained by letting

$$\psi_n = \exp(-j2\pi x_n \sin\theta/\lambda_a) \tag{3.7}$$

after which

$$\mathbf{G} = 20\log|\mathbf{A}^T \cdot \mathbf{\Psi}| \text{ [dB]} \tag{3.8}$$

where $\lambda_a$ is the free-space wavelength.

Often, only the direct coupling **I** from the drive towards each radiating element is desired and the remaining terms $\mathbf{C_f}$, $\mathbf{C_s}$, and $\mathbf{C_a}$ should be equal to zero. Perfect isolation is usually not achievable and there is always a certain amount of coupling between the radiating elements. The undesired coupling can degrade the performance of the entire array, and should be suppressed in the design procedure. The level of the coupling through the substrate and the air usually decreases with increased spacing. But unwanted substrate modes or standing waves may be excited and contribute to the coupling, causing unexpected results. Good isolation among the ports that are connected to the radiating elements in a feed network is desired, and sometimes resistors are needed within a feed network to suppress multiple reflections, e.g. Wilkinson power dividers instead of purely reactive dividers.

Classical electrically steerable phased array antennas are usually comprised of a number of individual antenna elements and a parallel feed network containing phase shifters, as shown in Fig. 3.2a. Each element is connected to the feed network via a phase shifter. Since different phase shifts are required to be able to steer the antenna beam, phase shifters in this class of antennas often need to be controlled individually. This results in complex biasing circuits, large phase tuning range of the phase shifters as well as complicated calibration for each beam tilt angle. In contrast, in a traveling wave array antenna all phase shifters can be biased identically with relatively small phase tuning range, and tuned synchronously to alter the beam tilt angle, as illustrated in Fig. 3.2b. This concept therefore simplifies the biasing, relaxes the phase shifter requirements, and avoids complicated calibration. The traveling wave array antenna is fed at one end and the injected RF power then exponentially decays due to antenna radiation and phase shifter losses, while propagating through the array. At the other end of the array, the remaining RF power is terminated by a load to suppress the reflections and enhance the impedance bandwidth. In the case of a traveling wave array, only one radiating element next to the feed port is directly excited, and the remaining elements are then excited by the coupling through the feed network.

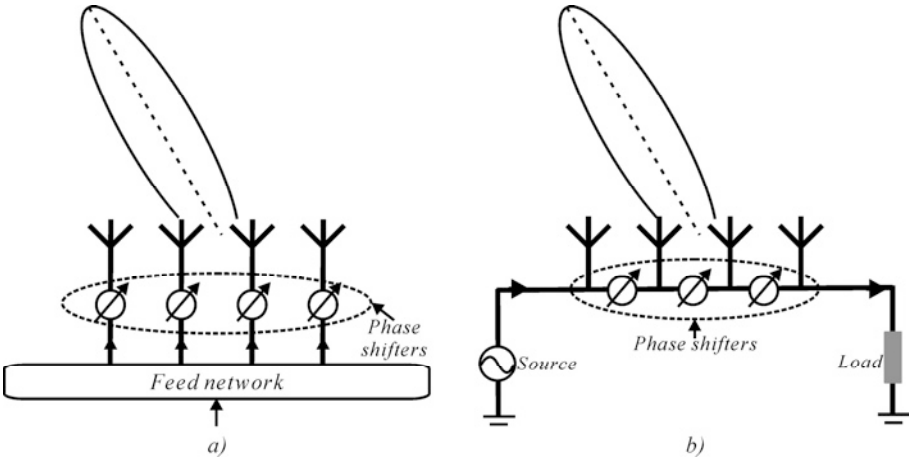


*Figure 3.2: Schematic description of the a) parallel feed and b) traveling wave electrically steerable array antenna configuration.*

When all radiating elements are excited in phase, a beam tilt angle of $0^o$ is achieved. While the phase response of the phase shifters decreases, a beam tilt moving towards the feed port can be observed and vice versa. For a symmetrical array, radiation patterns with respect to the broadside direction can be mirrored by feeding the antenna from the opposite direction. The overall beam scanning range is thereby doubled for a given phase tuning range of the phase shifters.

When it comes to practical implementation of ESAs, more technical issues, e.g. nonlinearity, power handling as well as extra losses might arise. These factors should be cautiously analyzed for each system and application.

## 3.1 Varactor-Based Steerable Phased Array Antennas

Current cellular communication systems are often limited in their capacity by interference from other users. The base station antenna that provides service to the users within a cell should also suppress the radiation to/from other cells as much as possible. Interference between neighboring cells mainly depends on the radiation characteristics of the base station antennas. One of the feasible approaches to minimize the interference between neighboring cells is to tilt the beam vertically, typically within the range 0-$10^o$ below the horizon, as shown in Fig. 3.3. The down tilt angle of each individual base station antenna varies from case to case, and is primarily determined by the interference and system capacity at hand.

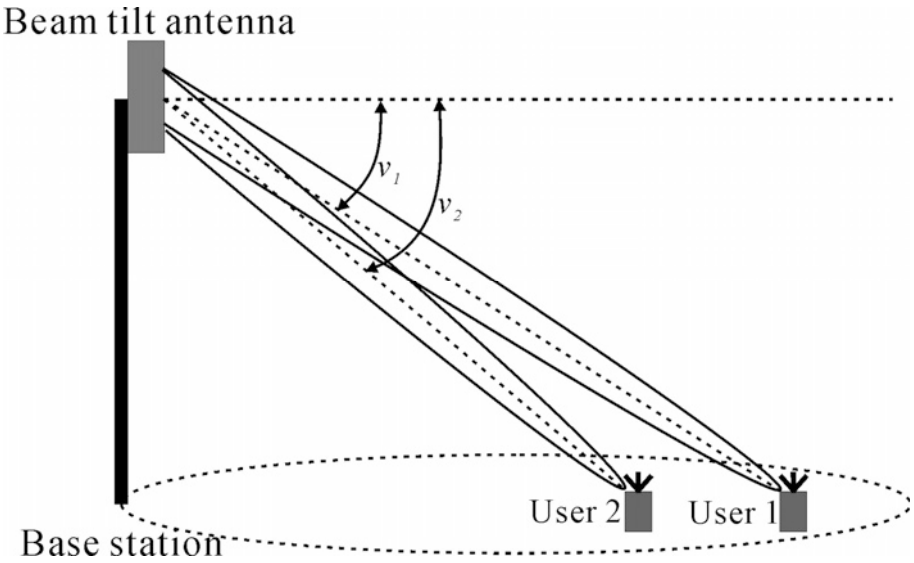


*Figure 3.3: Application scenario of the vertical beam tilt base station antenna in cellular communication systems.*

Since most base station antennas in present cellular communication systems are simple designs with fixed beams, mechanical beam tilt with a bracket is a common solution. Changing the beam tilt mechanically is elaborate and therefore typically done only once during installation. In addition to mechanical beam tilt, electrical beam tilt is also sometimes used, where the phase shifters contained in the antenna feed network are mechanically actuated. Such phase shifters are very slow, with a response time typically in the order of seconds. An enhancement to cellular systems would be to implement rapid base station antenna beam tilt, with a response time of fractions of a second [62]. In time division multiple access (TDMA) systems where the different time slots can be allocated to different terminals, it could be of great interest to be capable to tilt the antenna beam within microseconds, to serve each user terminal with an optimal base station antenna beam tilt. Fast beam steering necessitates truly electrical devices to alter the excitation of the antenna elements. Typical semiconductor phase shifters or switches are apparently good candidates. When replacing the mechanically actuated phase shifters with semiconductor ones, additional parameters such as insertion loss, power handling as well as nonlinearity, must however be taken into account. As an alternative solution, MEMS devices certainly offer better electrical performance than semiconductor ones, yet their response time is longer [63]. A 5.8 GHz ten-element traveling wave microstrip patch array antenna incorporated with varactor-based transmission-type phase shifters (TTPS) in the same radiating aperture is depicted in Fig. 3.4. Both antenna radiating elements and TTPSs are fabricated on the top metallization of a 0.76 mm thick PTFE substrate. The choice of this substrate is a compromise

between the performance of the patches and the phase shifters. While being vertically installed and fed from the lower end, the presented array antenna features an electrically adjustable beam down tilt in the range of $0^{o}$-$13^{o}$. Nine identical TTPSs as inter-components are placed between each neighboring patch pair in the array. Each TTPS consists of a high impedance transmission line loaded with two identical varactor-based tunable stubs, as illustrated in Fig. 3.5. The phase tuning stubs in the shunt tunable loads can either be open or short-circuit at the far ends by adding or subtracting a quarter wavelength transmission lines. In the case of the presented array, all the phase tuning stubs are connected to the bottom ground plane through metal vias, which provides easy access for DC biasing the varactors. In this case, both RF signal and DC control voltage can be applied to the antenna feed port via a bias-T, and the beam tilt angle can be easily adjusted by varying the DC voltage. Compact phase shifters are needed to be able to fit to the restricted spacing between two neighboring patches. For minimizing the coupling effect between the phase shifters and the adjacent radiating elements, the phase tuning stubs are folded towards the center.

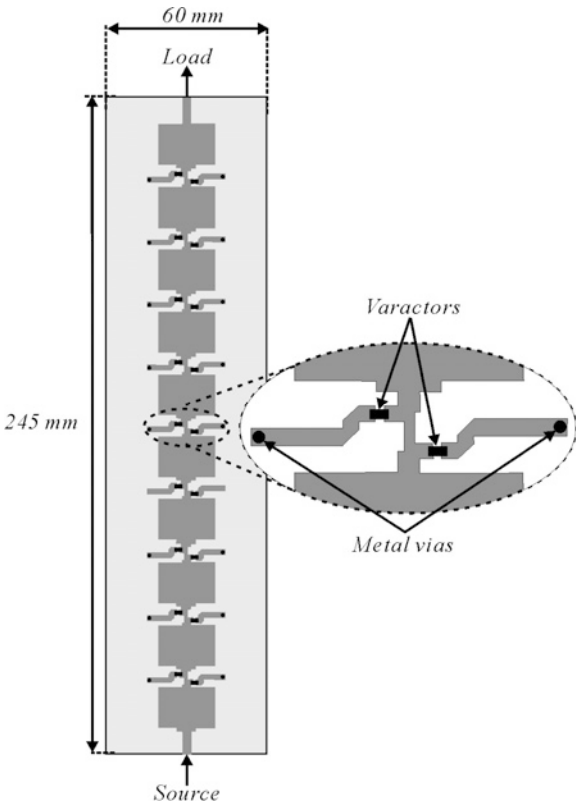


*Figure 3.4: Layout of the ten-element vertical beam tilt traveling wave array antenna presented in Paper II.*

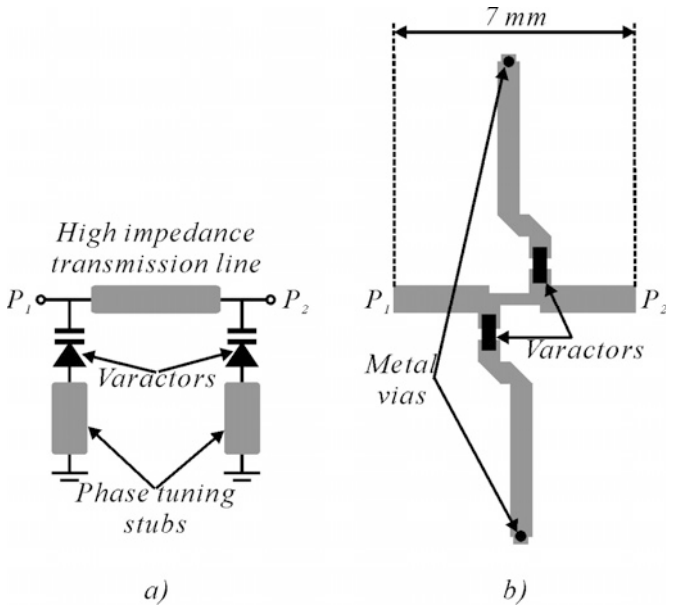


*Figure 3.5: Transmission-type phase shifter with varactor-based parallel loads a) schematic, b) layout presented in Paper II.*

When a varying bias voltage of -1 V to -30 V is applied, the implemented TTPS exhibits a return loss of better than 16 dB, an insertion loss of lower than 0.3 dB, and a continuous phase tuning range of -144$^{o}$ to -119$^{o}$ around 5.8 GHz. By lowering the bias voltage down to 0 V, an extra phase tuning range of -158$^{o}$ to -144$^{o}$ can be obtained at the expense of high insertion loss.

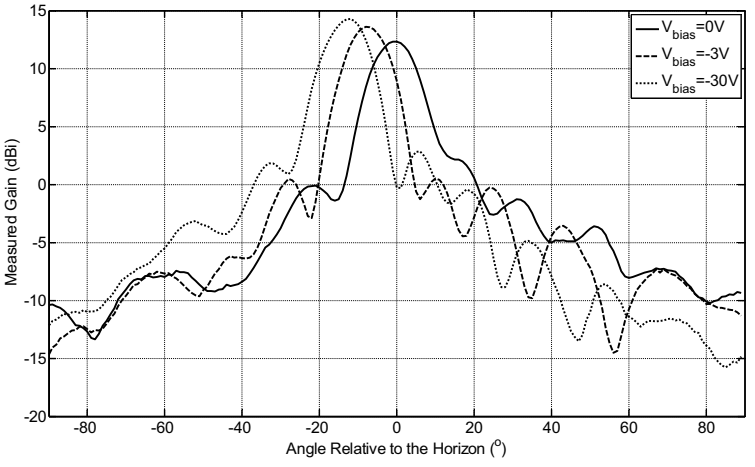


*Figure 3.6: Measured vertical radiation patterns of the beam tilt antenna for various bias voltages at 5.8 GHz.*

Measured data demonstrated in Fig. 3.6 shows that the antenna beam can be electrically steered from the horizon downwards and reaches a maximum beam tilt angle of 13°. The presented array antenna achieves a maximum antenna gain of 14.4 dBi at the maximum beam tilt, with a bias voltage of -30 V. When the bias voltage approaches 0 V, the antenna gain decreases down to 12.3 dBi along the horizon. The decreasing antenna gain can be explained by the increasing losses in the varactor diodes due to the low reverse bias [64], but also by effects of coupling in the array.

Apart from the vertical beam tilt functionality, a base station antenna enabling broad electrical beam steering in the horizontal plane is also of interest to cellular systems. Nowadays, most base station antennas are designed to provide coverage within a wide sector in the horizontal plane, e.g. 120°, and for this reason they have a wide beam. Using a narrow beam instead would bring the advantage of further interference reduction by spatial filtering. Another reason to use a narrow beam could be to increase the antenna gain. In order to fully cover a section of 120° with a narrow beam, a much broader beam tilt range in the horizontal plane other than that in the vertical plane has to been realized. This translates to higher requirements on the phase shifters.

Implementing a TTPS with wide phase tuning range is challenging because of the degraded port impedance matching. This type of phase shifters can not fulfill the requirements of wide scanning array antennas. Reflective-type phase shifters (RTPS), cf. Fig. 3.7a, often feature broad phase tuning range as well as good return loss [65]. The RTPS utilizes the property of a 90° hybrid terminated by two identical reactive impedances at the lower ports, and causes all the incident RF power from $P_1$ to be reflected to the normally isolated $P_2$. In the case of a continuously tunable RTPS, the two lower ports of the hybrid are connected to varactor-based reactive loads. In principle, perfect port impedance matching should be achieved over the entire phase tuning range, and the insertion loss is determined by the losses of the hybrid and varactors.

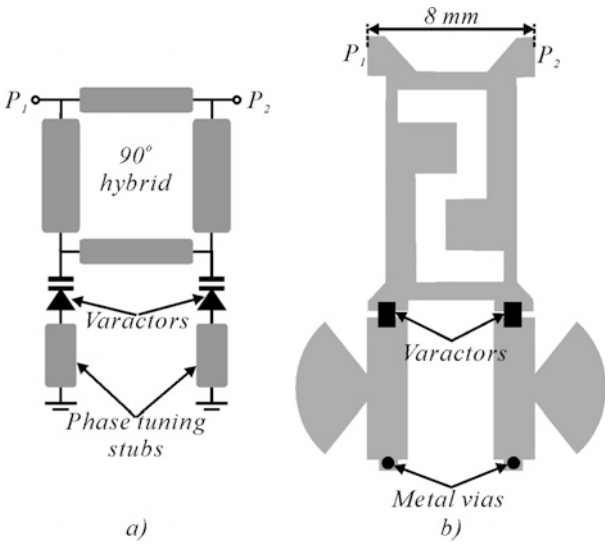


*Figure 3.7: Varactor-based reflective-type phase shifter a) schematic, b) layout reported in Paper I.*

Conventional 90° hybrids comprising four 90° transmission lines are too large to be integrated in the same microstrip layer as the patch radiators. A possible solution would be to use an unequal length hybrid instead [66]. However, such hybrid requires a pair of parallel low impedance transmission lines that are very wide on the substrate in use and difficult to be fit to the restricted spacing between two neighboring patches. In *Paper II* a modified compact hybrid is implemented and evaluated, which makes the use of asymmetric T-shaped transmission lines to replace those wide low impedance lines in a regular unequal length hybrid for further size reduction, cf Fig. 3.7b. According to the experimental data at 5.8 GHz, the implemented RTPS features a broad phase tuning range of -97° to -35° as well as a return loss of better than 13 dB and an insertion loss of less than 0.6 dB, for bias voltages within 0 V to -30 V (see Fig. 3.8). A more detailed description is presented in *Paper II*.

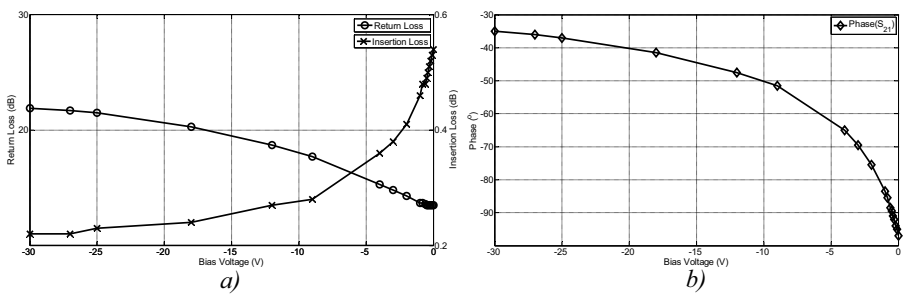


*Figure 3.8: Measured a) return loss and insertion loss, b) phase shift versus bias voltage, at 5.8 GHz, of the implemented compact RTPS.*

The proposed compact RTPSs are integrated in the radiating aperture of a five-element traveling wave patch array, as illustrate in Fig. 3.9. The presented wide scanning antenna is built in a symmetrical configuration to relax the severe phase tuning range requirements on the phase shifters. By switching the feed between either ends of the array, mirroring of the beam scanning range with respect to the broadside direction can be obtained.

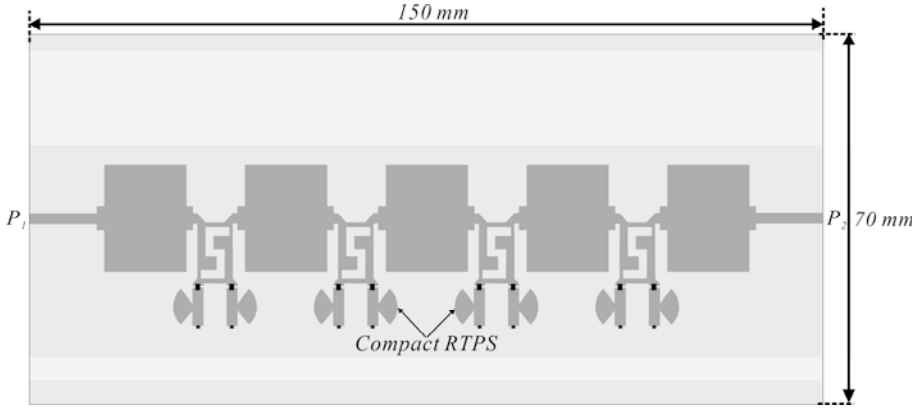


*Figure 3.9: Layout of the five-element wide scanning traveling wave array antenna demonstrated in Paper II.*

Fig. 3.10 shows the measured broadside radiation patterns of the wide scanning array with various bias voltages. Continuous beam scanning angles of -32° to -10° and 10° to 32° in the broadside direction can be achieved by varying the bias voltage from 0 V to -30 V as well as switching the antenna feed and termination between $P_1$ and $P_2$. The remaining range of -10° to 10° can be covered by the relatively wide antenna beam from both directions.

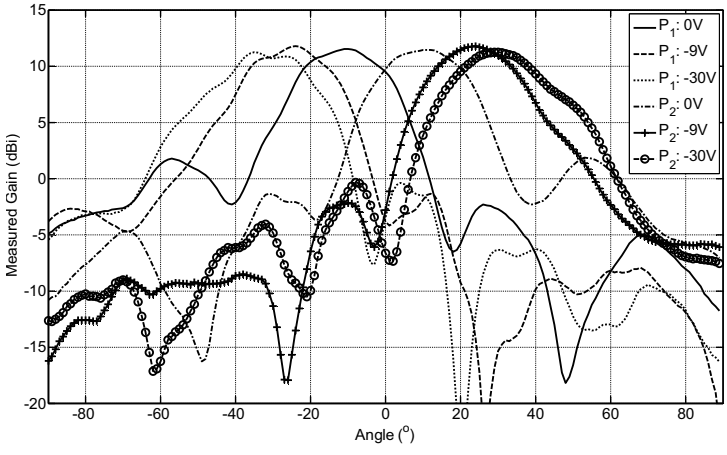


*Figure 3.10: Broadside radiation patterns, at 5.8 GHz, of the wide scanning antenna fed from either end, for various bias voltages.*

## 3.2 RF MEMS-Based Switched Beam Antenna

When moving to higher frequencies such as millimeter-wave frequencies, electrically steerable or switchable antennas based on solid-state components often suffer from degraded electrical performance. A great need for high performance switchable or tunable components, i.e. electrically actuated switches or variable capacitors as basic building blocks for advanced tunable antennas as well as other microwave devices, can be seen.

During the past years, RF Micro Electromechanical Systems (MEMS) have experienced tremendous progress in terms of technology development, device architecture, and circuit applications. Outstanding RF properties, for instance, high isolation, low losses, high linearity, and low power consumption, have already been demonstrated when using RF MEMS in single components such as switches, variable capacitors, and transmission lines [67]-[72]. These components are well suited for integration with antennas, phase shifters, matching networks, filters, etc. [73]-[79]. Nowadays, RF MEMS is regarded as a promising technology to significantly enhance performance of next generation RF communication and sensor systems. Novel types of MEMS technology is expected to be an essential part of cognitive RF systems, wireless sensors (e.g. radars), and millimeter-wave systems (such as RFID or MMID and point-to-point communication) in the 20-100 GHz range. Although RF MEMS technology features highly attractive advantages, there still remain unsolved issues that currently prevent a successful integration of RF MEMS (i.e. low cost and high reliability) into practical RF systems and commercial products.

Using RF MEMS switches, antennas with a variety of reconfigurabiliy in terms of resonance frequency, impedance bandwidth, polarization, and radiation patterns, have been recently introduced [80]-[85]. The goal of such reconfigurable apertures is to reduce the system complexity for operation over a wide frequency band or with diverse radiation characteristics. A microwave antenna router based on MEMS switches is a novel and application driven integration method. A simple, compact, low-cost and nearly zero-power consumption MEMS router is envisaged as a cost-effective solution for certain applications related to wireless communication, automotive radar and RF-sensing, traffic control and safety.

A 20 GHz two element array antenna integrated with a single-pole double-throw (SPDT) router based on capacitive RF MEMS switches is demonstrated in *Paper IX*, as shown in Fig. 3.11. Monolithic integration is used in order to avoid inter-chip connects that usually introduce additional losses at millimeter-wave frequencies. Quasi-Yagi antenna is chosen due to its compact size, sufficient impedance bandwidth, and end-fire radiation patterns

[86],[87]. Moreover, such an array antenna is compatible with RF MEMS manufacturing processes.

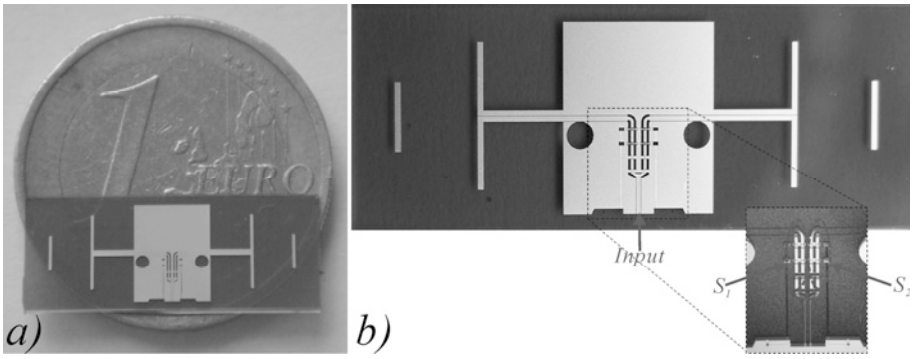


*Figure 3.11: Photographs of the array antenna integrated with RF MEMS-based SPDT router on quartz substrate. a) Scale in relation to 1 Euro coin. The size of the router device is 21 mm × 8 mm. b) Details of the switch network.*

The MEMS-based SPDT switch matrix and quasi-Yagi antennas are designed individually. The former is designed at VTT, Finland, based on the equivalent lumped circuit models and full-wave simulations of the coplanar-waveguide (CPW) transmission lines. The latter is modeled in pure full-wave simulations. The complete demonstrated prototype is fabricated on a 525 µm thick quartz substrate ($\varepsilon_r$ = 3.8 and tan$\delta$ = 0.001) using a capacitive RF MEMS process at the Ferdinand Braun Kessler (FBK) institute in Trento, Italy. The integrated quasi-Yagi antenna is expected to feature a gain of higher than 4 dBi and relative impedance bandwidth of wider than 20 % at 20 GHz. In addition to good isolation in the SPDT switch matrix, directive antenna radiation patterns with a front-to-back ratio of greater than 10 dB are required to achieve highly diverse directivity of the entire router.

Port impedance and radiation patterns of the implemented antenna router are characterized by applying actuation voltages with various combinations to the two switch pairs, $S_1$ and $S_2$. Fig. 3.12 shows the measured reflection coefficients of the complete router. The 10 dB return loss bandwidth is found to be around 28.2 % at 20 GHz when an actuation voltage is applied to either switch pair.

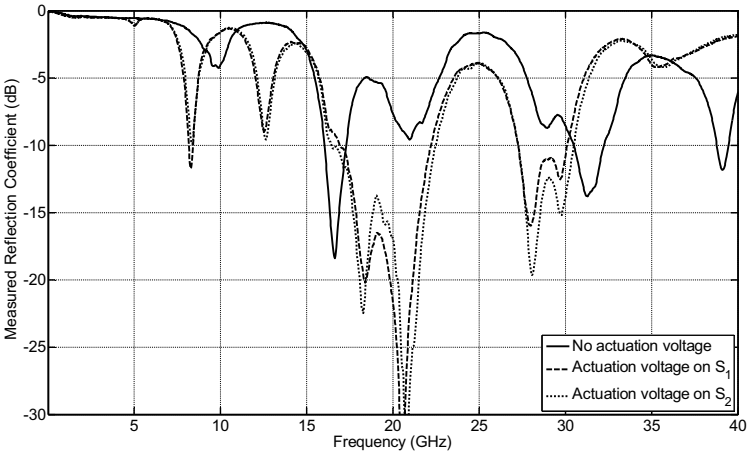


*Figure 3.12: Measured reflection coefficient of the complete SPDT router.*

Good isolation in the measured antenna radiation can be seen, as shown in Fig. 3.13. By applying the actuation voltages on both switches, the radiation decreases more than 10 dB compared to no actuation voltages. It is also indicated by the measured data that the antenna beam can be switched between two opposite directions with a gain of 4.6 dBi, a half power beam width (HPBW) of 82$^{o}$, and a front-to-back ratio of 14 dB. Moreover, as expected, the cross-polarization is much lower than the co-polarization in all the experimental results.

The demonstrated monolithically integrated MEMS-based switched beam antenna router is feasible to be scaled to other frequencies and thus opens up great potentials for many systems operating at millimeter-wave frequencies.

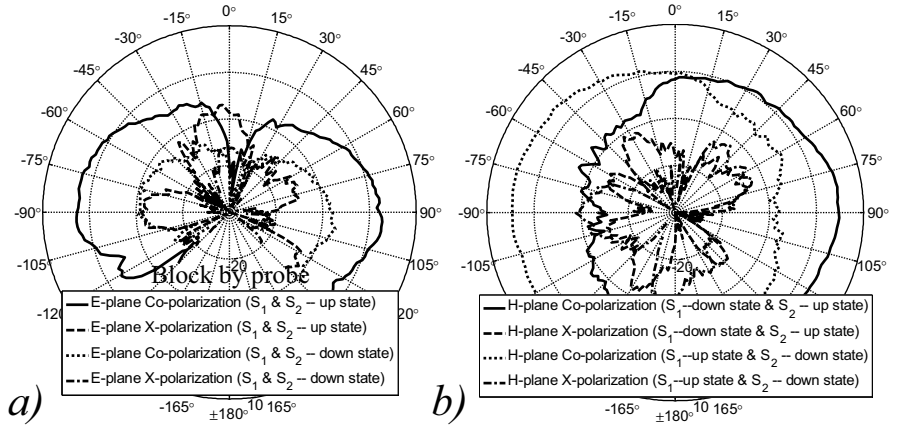


*Figure 3.13: Measured a) E- ($S_1$ & $S_2$ -- up-state and $S_1$ & $S_2$ -- down-state) and b) H-plane ($S_1$ -- down-state & $S_2$ -- up-state and $S_1$ -- up-state & $S_2$ -- down-state) radiation patterns at 20 GHz.*

## 3.3 RF MEMS-Based Switchable Phased Array Antenna

Investigations on more advanced antenna systems compared to the previously mentioned antenna router are needed to bring the MEMS-based reconfigurable antenna concept one step further towards the market. A switched beam steering array antenna at 24 GHz based on conventional solid-state switches has been implemented recently. In this design, the switches represent a large part of the losses [88]. An interesting attempt would be to replace those lossy semiconductor switches with MEMS switches to improve the electrical performance of the array antenna. A switched beam array antenna concept based on RF MEMS switches is therefore proposed and implemented. The concept consists of a single-pole-six-throw (SP6T) router (beam steering switch matrix) using RF MEMS switches on high resistivity silicon substrates fabricated at Fraunhofer ISIT, Hamburg, Germany, and two traveling wave array antennas on low temperature co-fired ceramic (LTCC: $\varepsilon_r = 7.5$ and $\tan\delta = 0.001$) manufactured at Via Electronics, Hermsdorf, Germany, cf Fig. 3.14.

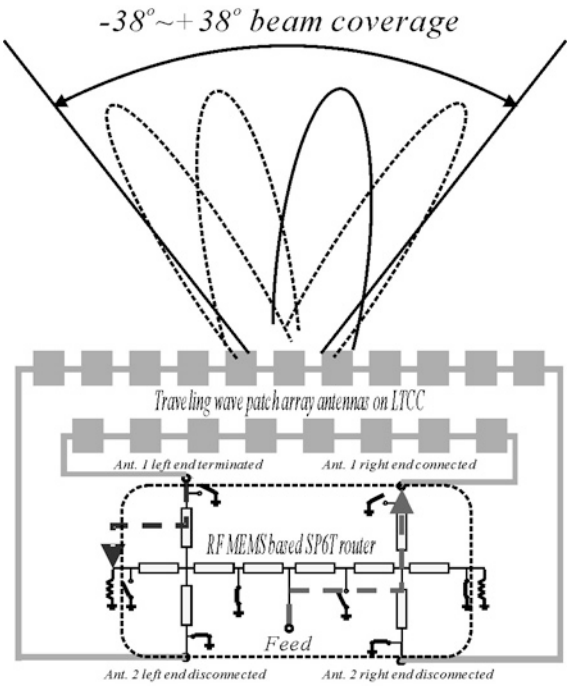


*Figure 3.14: Schematic of the 24 GHz switched beam steering array antenna concept.*

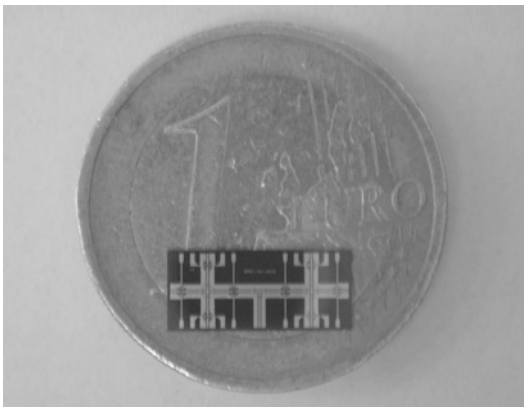

*Figure 3.15: Photograph of the SP6T router (beam steering switch matrix) fabricated by Fraunhofer ISIT.*

Fig. 3.15 shows the photograph of the implemented SP6T router, and the working mechanism of the router is described in Fig. 3.16. When the switches $S_2$, $S_4$, $S_5$ and $S_6$ are actuated to the down-state, the RF input from $P_1$ is directed to $P_2$ and one of the traveling wave array antennas is fed from the left end. The other end of this antenna is connected to $P_3$ and terminated by a 50-Ω load at $P_4$. Excellent isolation of the MEMS switches yields good RF signal rejection and thus the other array antenna is efficiently switched off. In this case, an antenna beam tilt towards the left hand side can be obtained, whereas an antenna beam pointing to the right hand side can be obtained with the antenna fed in the opposite way.

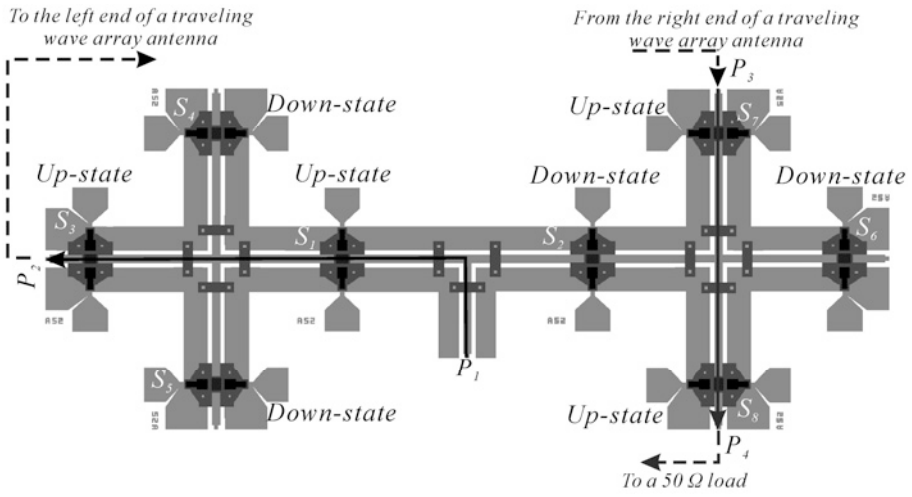


*Figure 3.16: Schematic of the SP6T router when $S_1$, $S_3$, $S_7$, and $S_8$ are in the up-state, $S_2$, $S_4$, $S_5$, and $S_6$ are in the down-state.*

Simulated and measured reflection and transmission coefficients of the SP6T router are demonstrated in Fig. 3.17. According to the experimental results, the SP6T router exhibits an impedance bandwidth of approximately 24 % and an insertion loss of 1.9 dB at 24 GHz. The performance is much better than commercial semiconductor switches in terms of isolation and losses at this frequency range.

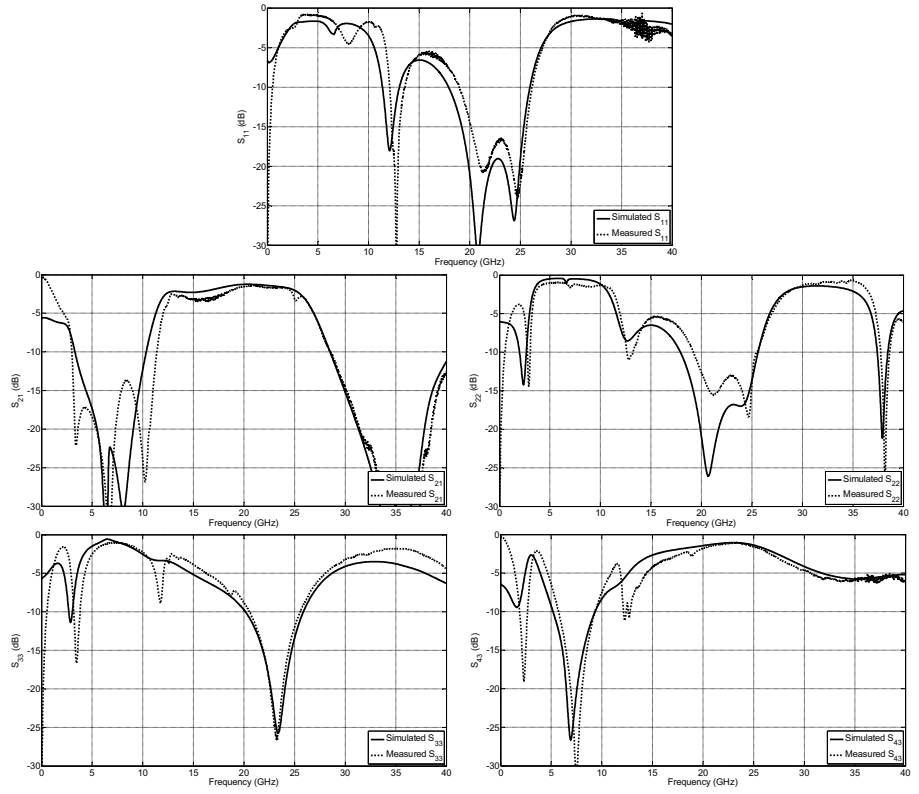


*Figure 3.17: Simulated and measured $S_{11}$, $S_{21}$, $S_{22}$, $S_{33}$, and $S_{43}$ of the SP6T router ($S_1$, $S_3$, $S_7$, $S_8$: up-state; $S_2$, $S_4$, $S_5$, $S_6$: down-state).*

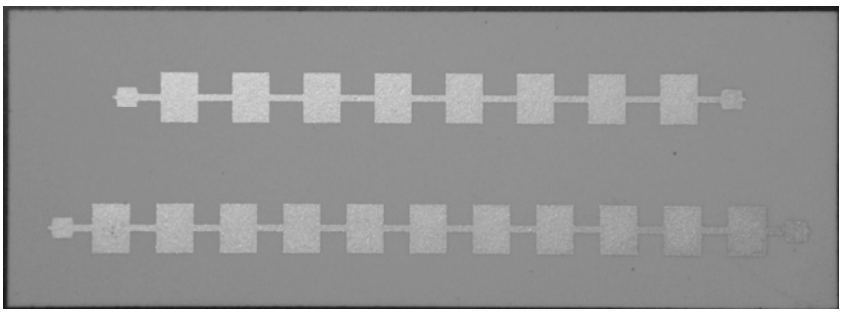

*Figure 3.18: Photograph of the 8-(upper) and 11-(lower) element traveling wave array antennas on LTCC.*

Photograph of the fabricated 8- and 11-element array antenna samples is shown in Fig. 3.18. Fig. 3.19 presents the simulated and measured reflection and transmission coefficients of the two antennas. Experimental results verify that both antennas feature broad impedance bandwidth at 24 GHz.

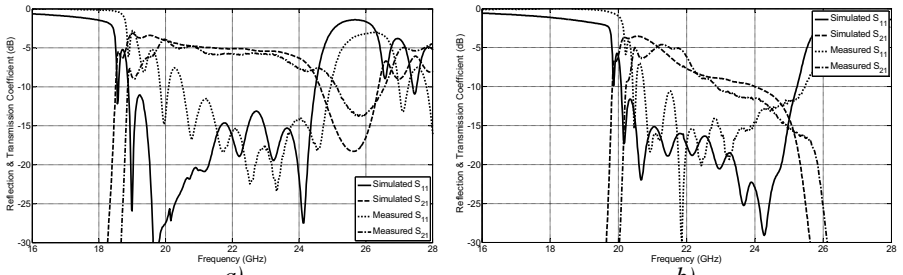


*Figure 3.19: Simulated and measured $S_{11}$ and $S_{21}$ of the a) 8- and b) 11-element traveling wave array antennas.*

When characterizing the radiation performance, the antenna is fed by an RF probe at one end and terminated by a 50-Ω load at the other end. Simulated and measured E-plane radiation patterns of the 8- and 11-element traveling wave array antennas are displayed in Fig. 3.20. By combining the beams of the two antennas, an overall coverage of ±38$^{o}$ in the broadside direction can be achieved with an average gain of 10 dBi at 24 GHz. Both antennas exhibit broad beam coverage in the H-plane.

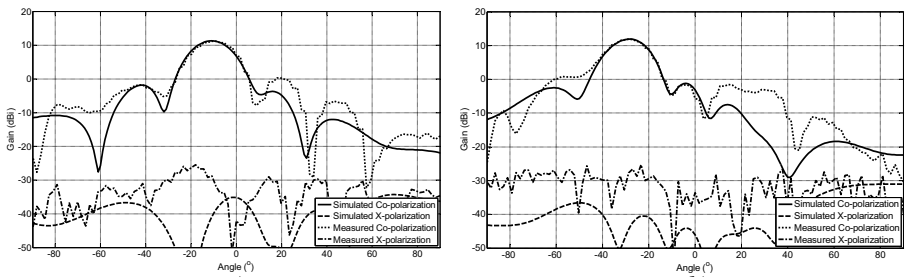


*Figure 3.20: Simulated and measured E-plane radiation patterns of the a) 8- and b) 11-element traveling wave array antenna at 24 GHz.*

As shown in the measurements, both the RF MEMS-based beam switching matrix and traveling wave array antennas feature good RF performance. Hence, the same designs are employed for the complete 24 GHz switched beam steering array antenna test vehicle with minor adaption for the packaging. A schematic of the packaging concept is depicted in Fig. 3.21 where the SP6T router chip is flip-chip bonded to the LTCC part using thermal compression bonding. The RF MEMS chip is sealed by an LTCC frame and a glass lid afterwards. The connects for the control voltages of the RF MEMS

switches are distributed on the top metal layer of LTCC and well isolated from the array antennas at the bottom metal layer by a large ground plane.

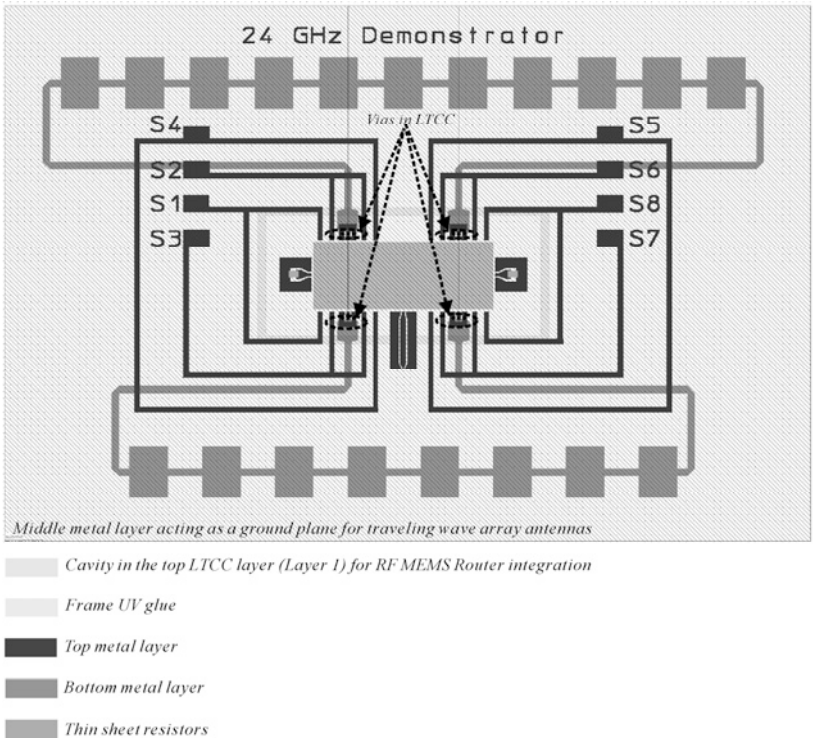


*Figure 3.21: Schematic of the packaged 24 GHz switched beam steering array antenna.*

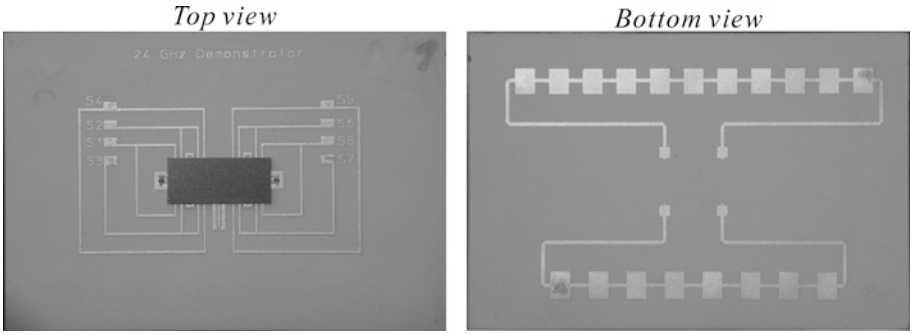


*Figure 3.22: Photograph of the LTCC chip for 24 GHz switched beam steering array antenna.*

Unfortunately, the assembled module does not function, cf. Fig. 3.22. Some tests indicate that all the MEMS switches do not work at all after flip-chip bonding. It is preliminarily deduced that the thermal expansion mismatch between the MEMS and LTCC chips, resulting from the high operation temperature of the thermal compression bonding process, might have damaged the bridges of the MEMS switches, and caused the failure. However, in-depth investigations and more evidences are needed to draw a definite conclusion.

## 3.4 Adaptive Array Antenna

Beam scanning of phased array antennas can also be implemented at baseband. Digital beamforming (DBF) is a fast developing technology, and enables full utilization of the degrees of freedom in the array. Compared to traditional techniques, this technology can lead to significant improvements in adaptive pattern nulling, space-time adaptive processing (STAP), beamforming of simultaneous multiple independent beams, and direction finding (DF). Due to its high flexibility, DBF might find use in a broad range of phased array antenna applications.

One interesting application is automotive radar systems. Increasing demand on automotive radars to improve road safety is currently being seen all over the world. Attractive functions like anti-collision, lane change assistance, and blind spot monitoring have been employed in these devices. Advanced cruise control systems “long-range radar” operating at 77 GHz enable a vehicle to maintain a cruising distance from a vehicle in front. While an anti-collision “short-range radar” at 79 GHz is being developed as a part of a system to warn the driver of a pending collision, enabling automatic braking in case of inevitable collision to minimize injury to passengers. Such systems have been implemented in several high class vehicles, like Mercedes S-class, Volkswagen Phaeton or Audi A8. Nevertheless, existing automotive radar technologies are not mature yet. A great amount of further development in adding more functions, extending detection range, and increasing resolution in target range, azimuth angle as well as Doppler frequency is needed to ensure reliable driver assistance and safety systems. The DBF technique is regarded as one of the most promising solutions for significantly enhancing the performance of automotive radars. However, developing DBF phased arrays for automotive radar systems necessitates state-of-the-art technologies. First, digital challenges includes increasing ADC sampling rate, implementing digital time delays, and processing enormous data loads associated with complicated algorithms. Second, RF hardware requires high performance mixers and efficient array antennas. Third, elaborate calibration processes at installation are necessary for ensuring high measurement accu-

racy in real applications. Of course, hardware integration should also be taken into account. Integrating RF subcomponents at millimeter-wave frequencies is always challenging.

All these technical challenges should be considered on system level, as various sub-modules are tightly linked and can be affected by the others. Sometimes, an intelligent solution for one sub-component might be in great favor of many sub-modules, because it may help to relax their rigorous requirements. A requirement is the compatible integration. The multi-layer benzocyclobutene (BCB, $\varepsilon_r$ = 2.65 and tan$\delta$ = 0.0008) process on low resistivity silicon substrates at Acreo AB, Sweden, is chosen for the system integration of all sub-modules at RF frequencies. The cross view of the build-up of this process is depicted in Fig. 3.23. This technology enables high degrees of freedom in routing. The bottom 1 μm thick copper layer can act as a ground plane for microstrip lines using either top signal or middle bridge metallization. Since the top and middle copper layers are isolated by a 14 μm thick BCB membrane, cross lines can be easily constructed in these two layers without any additional air bridges or bond wires. Micro-vias as well as stacked ones through both BCB layers provide the possibilities of direct connections of the three metal layers. This feature is of importance for DC biasing and direct RF grounding with low parasitics. Owing to the excellent dielectric properties of BCB, transmission lines and feed networks implemented in this process exhibit very low losses at millimeter-wave frequencies. Moreover, high-Q integrated passive devices (IPDs) such as capacitors, inductors, and resistors, are also achievable at very high frequencies. Additionally, the multi-layer BCB process also opens up potentials of integrations with other commercial processes like GaAs, SiGe BiCMOS, and CMOS.

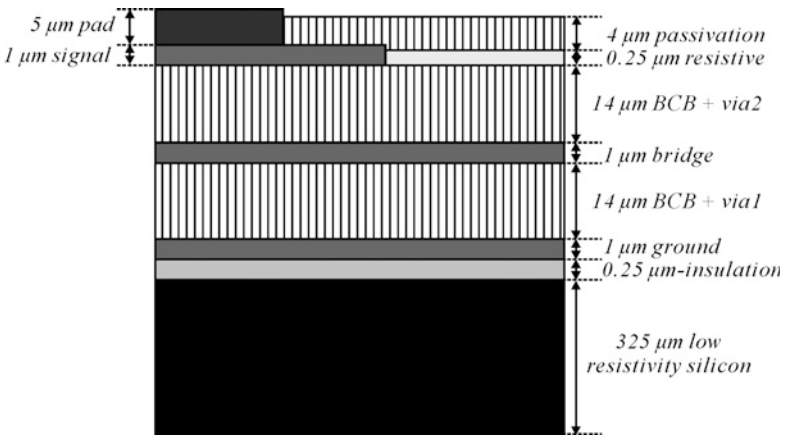


*Figure 3.23: Build-up of the multi-layer BCB on low resistivity silicon substrate. Dimensions are not to scale.*

The 5-20 Ω·cm low resistivity silicon substrates in use are widely available in semiconductor industry. But such substrates are not favorable for antenna designs at millimeter-wave frequencies due to high dielectric constant and significant losses. The deep reactive-ion etching (DIRE) process is therefore employed to etch away the lossy silicon and form an air-cavity beneath each radiating element, folded slot antenna, in phased arrays operating at 79 GHz, see *Paper XIII*. Due to the multi-layer BCB process, a relatively thick BCB layer of approximately 32 μm can be realized, which allows BCB membranes with large areas associated with reliable mechanical properties for suspending radiators, and lowers the losses in microstrip based feed networks for large arrays.

The implemented phased array module consists of one Tx and eight Rx array antennas, as illustrated in Fig. 3.24. Each array is comprised of eight identical folded slot antennas that are suspended on BCB membrane and connected by a symmetrical parallel feed network. The choice of parallel feed network is because squintless arrays are desired to simplify the calibration of the DBF. Since these folded slot antennas exhibit bi-directional radiation characteristics, a large metallic cavity is introduced to direct the radiation forward. A number of metallic bars are placed on the ceiling of the cavity to suppress unwanted cavity modes as well as coupling among subarrays.

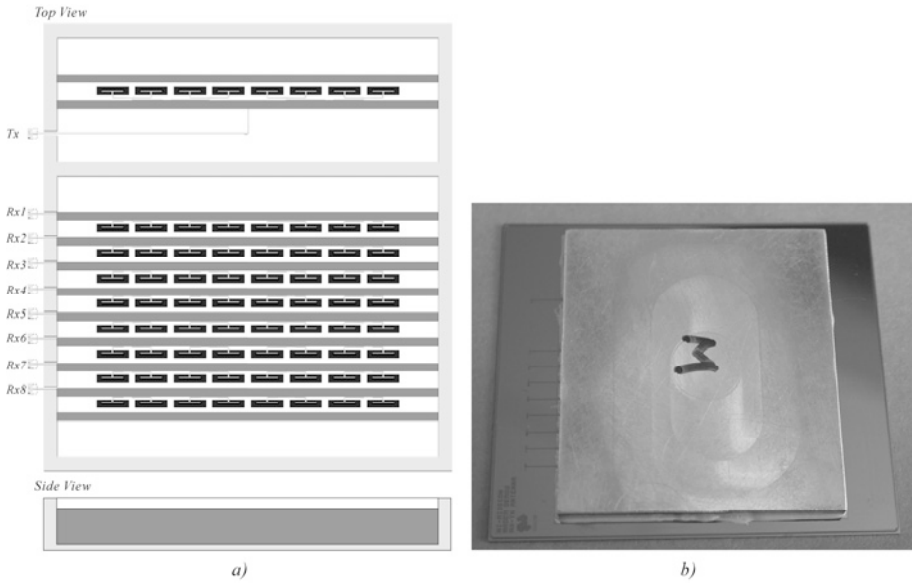


*Figure 3.24: Implemented Tx/Rx array antenna. a) Schematic drawing. b) Photograph.*

In real applications, the presented module will be installed with all the sub-arrays perpendicular to the horizontal plane. The single Tx array will transmit RF power covering a broad sector in the horizontal plane, while the Rx arrays will be horizontally steered using DBF technique to detect the reflections from pedestrians, bicyclists, motorcyclists, or other vehicles in front. In the vertical plane, a very directive antenna beam, approximately $10^{o}$ half power beamwidth (HPBW), is required. This way the radar detection range can be increased and the reflections from the ground and some regular objects above the roads, including bridges or traffic signs, will be suppressed. For the same reasons, excitations of the radiating elements from the parallel feed network are optimized to reduce the sidelobe levels of the arrays instead of maximizing the antenna gain. Hence, the radiators in Tx and Rx arrays are not uniformly excited.

Fig. 3.25 presents the measured vertical plane radiation patterns of the first Rx array, Rx1, at 79 GHz. This array exhibits a maximum gain of 6.6 dBi, a HPBW of $11^{o}$, and a sidelobe level of 18 dB below the main beam. The presence of the large metallic cavity effectively enhances the forward radiation of about 3 dBi compared to without the cavity, and the backward radiation is suppressed down to approximately -20 dBi.

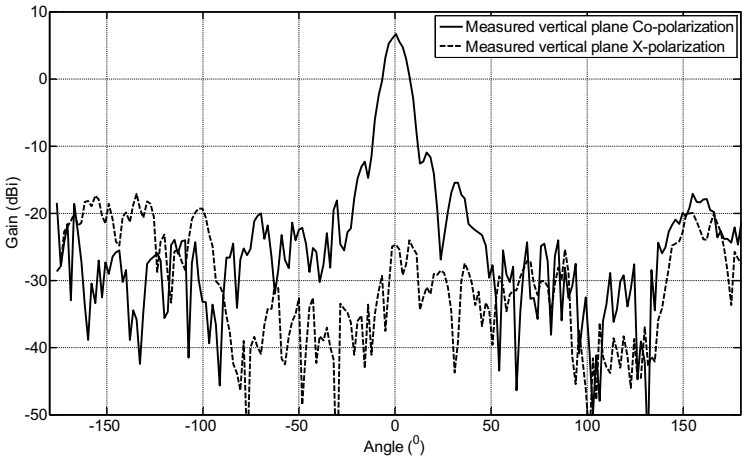


*Figure 3.25: Measured vertical plane radiation patterns of the Rx1 array at 79 GHz.*

## 3.5 Summary and Conclusion

In this chapter, various electrically steerable or switchable phased array antennas at different frequencies have been proposed and evaluated. The concept of utilizing electrically tunable varactor-based phase shifters in series

with the radiating elements of a traveling wave microstrip patch array to steer the beam has been verified by the successful demonstration of two 5.8 GHz arrays. Measured port impedance as well as radiation characteristics of the presented traveling wave array antennas are in good agreement with theoretical and numerical results. The proposed concept enables extremely fast beam scanning within a couple of microseconds or even a few hundred nanoseconds, mainly restricted by the varactor charging or discharging. In principle, the demonstrated arrays are feasible to be scaled to other frequencies from a few hundred megahertz to tens of gigahertz. However, a practical limitation is the increasing losses of the varactors at high frequencies, which will introduce significant losses to the array antennas and result in poor radiation performance. If a hybrid integration approach is chosen, appropriate assembly processes are of great importance when implementing this concept at very high frequencies, for instance, millimeter-wave frequencies. Instead of standard soldering, advanced assembly technologies, i.e. thermal compression bonding, are preferred. Additionally, limited power handling capability as well as nonlinearity of the varactors set a limit for realizing this concept in high power applications. Although some special diode configurations can be employed to reduce the intermodulation distortion, the linearity will likely be insufficient for most high power applications.

RF MEMS certainly features much better electrical performance in terms of isolation, linearity, and losses. Using capacitive MEMS switches, a simple monolithically integrated antenna router has been implemented at 20 GHz, where electrically antenna beam switching between two opposite directions has been successfully demonstrated. Following the simple antenna router demonstration, a more advanced electrical beam switched array antenna concept has been investigated, where a hybrid integration solution was utilized. Implemented traveling wave patch array antennas on LTCC and MEMS-based switching matrix have been tested separately with good electrical performance. However, failure of the MEMS switches was found after the assembly process. Thus, none of the assembled modules was functional at the end. Although RF MEMS technologies are becoming mature and the reliability of stand-alone RF MEMS components have been significantly improved in the past few years, many technical issues in hybrid integration of RF MEMS components with other microwave devices with maintained reliability have not been solved yet. Interesting research activities on developing RF MEMS technologies compatible to commercial IC processes, e.g. CMOS, SiGe, and GaAs, have been conducted with promising outcomes. It is foreseen that the marriage of RF MEMS and commercial IC processes will open up great potential for many systems and applications. Nevertheless, these IC compatible RF MEMS technologies are still on the laboratory prototype level and not yet commercially available.

Silicon micromachined array antennas have been proposed for DBF phased arrays for automotive radar applications. It is verified by experimental results that the severe requirements on the Rx and Tx arrays are fulfilled. However, due to difficulties in developing beamforming algorithms as well as delicate calibration at the frequencies of operation, a fully functional DBF phased array module has not been successfully demonstrated. From the RF hardware perspective, the presented multi-layer BCB process enables a cost-effective integration solution for many millimeter-wave systems.

# 4 Millimeter-Wave Integrated Antennas

Millimeter-wave technologies ranging from 30 GHz to 300 GHz can be dated back to the end of the 19th century. J. C. Bose, a great Indian scientist, pioneered the investigations of millimeter-waves, and first made the remarkable public demonstration of ringing a bell at a distance using millimeter-waves. However, over the last century, millimeter-wave technologies have been mainly applied to radio astronomy and military systems, but not widespread in commercial applications. This is primarily due to difficulties and significant cost of generating and testing radio signals at millimeter-wave frequencies.

Various millimeter-wave frequency bands have recently been allocated for different commercial applications by US Federal Communications Commission (FCC). Most of these bands are essentially undeveloped and available for use in a broad range of new products and services, including high-speed point-to-point or point-to-multipoint communications, broadband Internet access, radar devices, as well as high resolution imaging systems. Owing to shorter wavelengths, these bands allow the use of smaller antennas than would be needed for similar circumstances at lower frequencies, to achieve the same high directivity. The immediate consequence of this high directivity, associated with the significant free space loss at millimeter-wave frequencies, is the possibility of a more efficient use of the spectrum for point-to-multipoint applications. Since a greater number of highly directive antennas can be placed in a given area, compared to less directive antennas, the net result is more efficient reuse of the spectrum, and higher density of users, as compared to lower frequencies. Furthermore, highly directional "pencil-beam" radiation characteristics are also favored in many radar systems to enhance their resolution.

Although many attractive features at millimeter-wave frequencies have been noticed, widespread use of millimeter-wave electronics has not been seen yet. Components are still expensive, as are the test instruments to characterize them. Solid state sources have limited maximum frequencies and output powers. This fact reflects on the strict requirements on highly efficient circuits as well as highly efficient antennas. In addition, interconnects or transitions for connecting various sub-components may sometimes introduce parasitics and significant losses. In case of unavoidable interconnects,

attention must be paid to designing appropriate transitions and minimizing their parasitics. Delicate integration techniques are commonly utilized as a means to avoid transitions and minimize their losses. Subsequently, integration compatibility becomes a crucial factor in the design.

For antennas at millimeter-wave frequencies, technical challenges lie in high efficiency, ease of integration, and high precision manufacturing. Advanced fabrication technologies associated with low loss materials provide feasible solutions for implementing highly efficient antennas. Challenging integration issues can be solved by choosing appropriate manufacturing techniques and cautiously optimizing all transitions.

Once a millimeter-wave antenna is implemented, accurate characterizations are required. Traditional measurement techniques using coaxial cables and connectors to feed antennas are not suitable at millimeter-wave frequencies. This is because millimeter-wave antennas can be very small and contain many physically small features, causing difficulties in accessing antenna feed ports. Moreover, connecting an RF cable to an antenna at millimeter-wave frequencies may also introduce strong parasitics and thus significantly degrade the antenna electrical performance.

On-wafer measurement techniques are regarded as a promising approach to accurately characterize antennas at millimeter-wave frequencies, especially for impedance characteristics. Component characteristics like DC I-V curves have been measured with needles already a few decades ago. Scattering parameter (S-parameter) measurement is a basic tool in microwave and millimeter-wave circuit characterization. The first broadband on-wafer measurement systems at microwave frequencies were developed at the beginning of 1980s [89],[90]. Since then, development activities to extend on-wafer measurements to millimeter-wave frequencies have been conducted. W-band on-wafer S-parameter measurement systems were presented for the first time at the beginning of 1990s [91]-[93]. In the late 1990s and the beginning of the 21$^{st}$ century, on-wafer S-parameter measurements have been extended to 200 GHz [94]-[96]. Recently, WR-3 band measurement setup has been successfully demonstrated, where an upper frequency range of 325 GHz has been reached [97],[98].

The merits of on-wafer measurement systems are good repeatability and very low parasitics at high frequencies, which can ensure high accuracy in millimeter-wave characterizations. However, standard on-wafer S-parameter measurement setups are primarily optimized for characterizing circuits instead of antennas, in which under-test-devices (UTD) are often fixed on metal chucks using vacuum pumps and RF probes are employed to feed the UTDs from the top side. This fact may introduce difficulties in the case of

measuring antennas without shields underneath. Consequently, modified sample fixtures are usually needed to adapt standard on-wafer measurement setups to antenna port impedance characterization. For instance, the UTA can be mounted on the edge of a metal chuck with its radiator sticking out in free space. Alternatively, a low dielectric constant and low loss materials based fixture can replace the standard metal chuck.

When measuring antenna radiation characteristics at millimeter-wave frequencies, major modifications of standard on-wafer measurement systems are required to eliminate blockage, scattering, and reflections from different metal parts. Instead of measuring radiation patterns on bulky metal probe stations, the W-band UTA is mounted on a piece of rigid foam glued on the bottom side of a probe holder, and fed by an RF probe, as illustrated in Fig. 4.1. The receiving end, including a W-band standard horn and an OML (Oleson Microwave Labs) W-band vector network analyzer (VNA) extender receiving module, is mounted on a stepper motor controlled arm. Prior to radiation pattern measurements, gain of the standard horn antenna as well as losses in free space, cables, adaptors, connectors, and waveguides, must be considered in calibration.

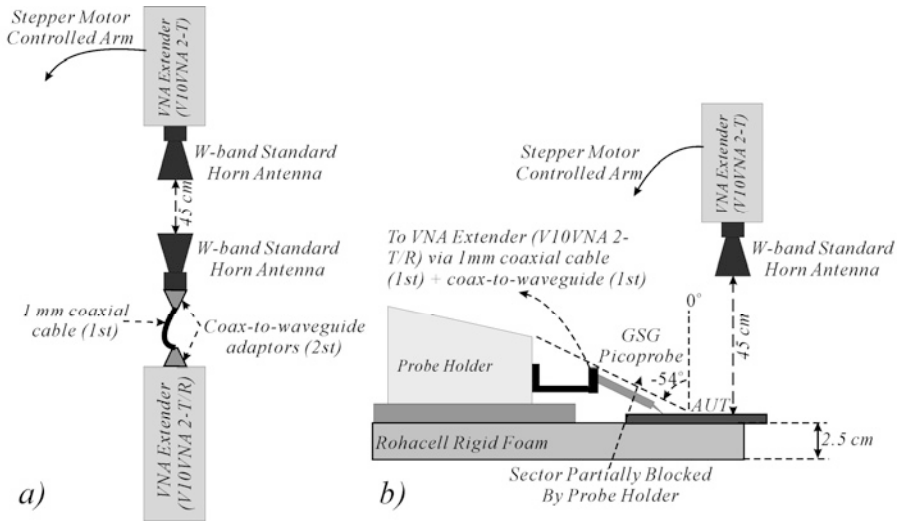


*Figure 4.1: Schematic drawing of W-band antenna radiation characteristics measurement setup at Uppsala University, a) calibration, b) radiation pattern measurement setup.*

Fig. 4.2 shows photographs of the W-band antenna radiation pattern measurement setup at Uppsala University, where two external synthesizers are triggered by a performance network analyzer (PNA) and employed for pumping the RF and LO ports of the two millimeter-wave VNA frequency extension modules.

*Figure 4.2: Photographs of W-band antenna radiation characteristics measurement setup at Uppsala University, a) complete view of the measurement setup, b) close view of the probe fed UTA.*

## 4.1 Substrate Integrated Waveguide (SIW) Based Antennas

Transmission lines usually play an essential role in millimeter-wave systems and applications. Low loss transmission lines are favored in many millimeter-wave distributed components. When implementing large array antennas at millimeter-wave frequencies, feed networks often represent a large part of the losses. The demand for highly efficient millimeter-wave array antennas therefore reflects on severe requirements on low loss transmission lines.

Rectangular waveguides are commonly used at millimeter-wave frequencies due to their attractive features, e.g. low losses, high power handling, and excellent isolation. However, manufacturing of such waveguides necessitates sufficient accuracy so as to allow for operation at very high frequencies. Making use of advanced micromachining technologies, hollow waveguides have been successfully demonstrated at millimeter-wave or even submillimeter wave frequencies [99],[100]. Drawbacks like costly manufacturing, relative large volume and mass, as well as difficulties in integration to planar circuitry still set a limit for the use of waveguides in many applications.

The concept of substrate integrated waveguides (SIW) has been proposed recently by K. Wu [24]. It maintains the advantages of rectangular waveguides as well as additional merits, e.g. ease of integration, low manufacturing cost, and compact size. Conventional printed circuit board (PCB) processes are a cost-effective approach to fabricate SIWs and SIW-based microwave devices up to Ka-band. Successful demonstrations of a variety of

microwave components including filters, couplers, Rotman lenses, and antennas, have been reported [101]-[107]. When moving to higher millimeter-wave frequencies, SIWs or SIW-based structures implemented by conventional PCB processes often suffer from increased radiative waveguide losses [26],[27]. A need for a feasible solution for realizing low loss SIWs at very high frequencies is seen.

A new concept of nano-wire based SIWs is proposed in *Paper V*. It is the marriage of ion track technologies and conventional SIWs, where the lateral walls of SIWs are built in the form of closely-packed 'forest' of nickel wires, as shown in Fig. 4.3. The spacing and diameter of such wires are in the order of a few hundred nanometers instead of several hundred micrometers as in conventional SIWs. Thus, leakage losses from the lateral walls of the presented SIWs are significantly reduced [26],[27], in turn enabling a significant increase in the upper operational frequency limit.

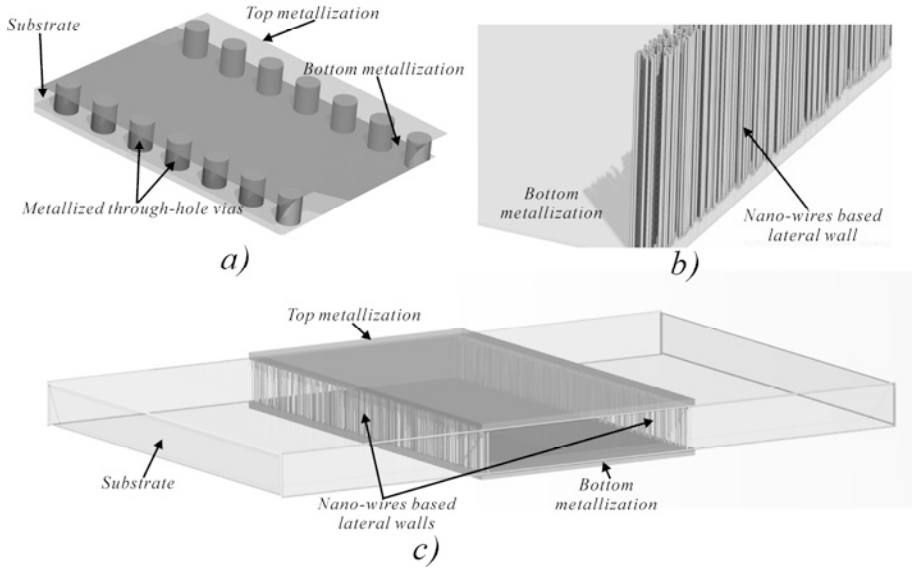


*Figure 4.3: 3D schematic drawings of a) conventional SIW, b) segment of a nano-wire based SIW, and c) complete view of a nano-wire based SIW.*

For evaluating the proposed nano-wire SIW concept, first prototypes at 79 GHz are implemented in 76 μm thick Kapton HN® polyimide foils with 3 % porosity, see *Paper V*. The choice of polyimide is mainly due to lightness, high degree of flexibility, and low cost manufacturing techniques, as well as moderate electric properties.

The fabrication process of the nano-wire based SIWs are described in detail in *Paper V*. According to our experiments, the used polyimide foil features a relative permittivity ($\varepsilon_r$) of 3.1 and a loss tangent (tan$\delta$) of 0.011 around 79 GHz. Fig. 4.4 shows the schematic of 79 GHz SIW prototypes with different lengths. Each of them consists of a piece of nano-wire based SIW and an identical microstrip-to-SIW transition connected at each end.

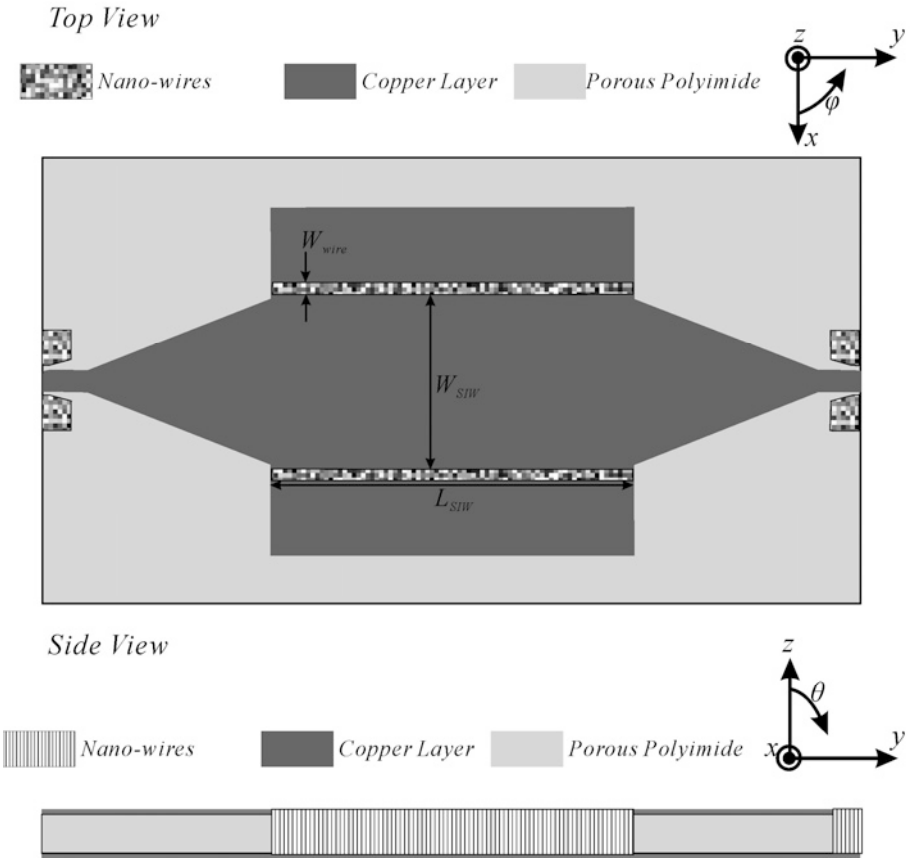


*Figure 4.4: Schematic drawings of the SIWs connected to a microstrip-to-SIW transition at each end. Dimensions are: $W_{SIW}$=1.5 mm, $W_{wire}$=100 μm, and $L_{SIW}$=3.1/6.1 mm.*

Analytical studies are carried out to estimate various losses in the presented SIW prototypes [108]. As shown in Figs. 4.3.b and 4.3.c, the nano-wires in the demonstrated SIWs are closely-packed and small. Thus, the lateral walls can be seen as solid ones when calculating the cut-off frequency. The cut-off frequency for the $TE_{10}$ mode is found to be 56.8 GHz using

$$f_c = \frac{c_0}{2a\sqrt{\varepsilon_r}} \tag{4.1}$$

where $f_c$ is the $TE_{10}$ cut-off frequency, $c_0$ is the velocity of light, $\varepsilon_r$ is the relative permittivity of the dielectric, and $a$ is the width of the SIW.

However, the approximation of the solid lateral walls is not valid in the analysis of the losses. The extra conductor and leakage losses resulting from the discrete walls have to be taken into account. The total attenuation constant is given by

$$\alpha_{total} = \alpha_d + \alpha_{copper} + \alpha_{wire} + \alpha_{leakage} \tag{4.2}$$

where $\alpha_d$ is the attenuation constant of the dielectric loss, $\alpha_{copper}$ and $\alpha_{wire}$ are the conductive attenuation constant of the top and bottom copper layers and the vertical nano-wires, and $\alpha_{leakage}$ is the attenuation constant of the leakage loss.

The attenuation constant of the dielectric loss for the $TE_{10}$ mode can be obtained as

$$\alpha_d = \frac{\sqrt{\varepsilon_r} k_0 \tan\delta}{2\sqrt{1-(\frac{f_c}{f})^2}} \tag{4.3}$$

where $f$ is the operation frequency, $k_0$ is the free-space wavenumber, and $\tan\delta$ is the loss tangent of the dielectric.

The conductive attenuation constant of the two flat copper layers for the $TE_{10}$ mode is calculated by noting that

$$\alpha_{copper} = \frac{R_{copper}}{b\sqrt{1-(\frac{f_c}{f})^2}} \sqrt{\frac{\varepsilon_0 \varepsilon_r}{\mu}} \tag{4.4}$$

where $b$ is the height of the SIW, $\varepsilon_0$ is the permittivity of free-space, $\mu$ is the permeability of the dielectric. $R_{copper}$ is the surface resistivity of copper defined as

$$R_{copper} = \sqrt{\frac{\omega\mu}{2\sigma_{copper}}} \tag{4.5}$$

where $\omega$ is the radian frequency, and $\sigma_{copper}$ is the conductivity of copper ($5.8 \times 10^7$ S/m).

The conductor and leakage losses of the nano nickel wires in the SIW lateral walls are difficult to estimate. However, the sum of them can be extracted from the measured data and theoretical results. For comparison, the attenuation constant of the conductor loss of solid nickel walls is calculated. This gives the attenuation constant

$$\alpha_{nickel} = \frac{2R_{nickel}}{a\sqrt{1-(\frac{f_c}{f})^2}}\sqrt{\frac{\varepsilon_0\varepsilon_r}{\mu}}(\frac{f_c}{f})^2 \tag{4.6}$$

where $R_{nickel}$ is the surface resistivity of nickel formulated as

$$R_{nickel} = \sqrt{\frac{\omega\mu}{2\sigma_{nickel}}} \tag{4.7}$$

where $\sigma_{nickel}$ is the conductivity of nickel ($1.45 \times 10^7$ S/m).

The attenuation per unit length in each case can then be calculated from the corresponding attenuation constant using

$$\alpha_{dB} = -20\log e^{-\alpha}. \tag{4.8}$$

It is indicated by experimental results that the overall attenuation per unit length of the presented SIWs is approximately 0.3 dB/mm at 79 GHz. Using (4.2)-(4.8). The theoretical attenuation due to the dielectric, copper layers and solid nickel walls are calculated as 0.2 dB/mm, 0.056 dB/mm, and 0.006 dB/mm, respectively. These values together with (4.2) imply that the sum of the conductor and leakage losses of the nano-wires is much less than the dielectric loss and comparable to the conductor loss of solid nickel walls.

In addition to the nano-wire based SIWs, a single slot antenna, longitudinal and four-by-four slot array antenna, operating at 79 GHz, are also implemented on 76 μm thick Kapton HN® polyimide foils with 3 % porosity, see *Paper VI*.

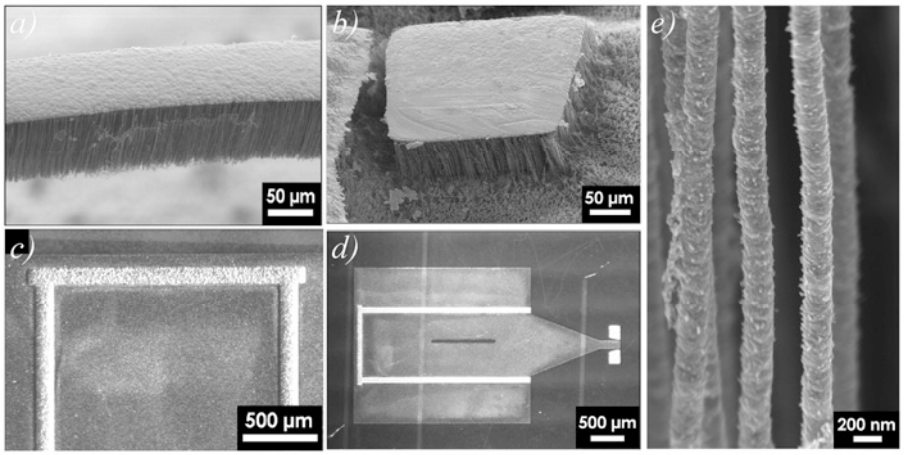


*Figure 4.5: SEM images of a nano-wire SIW-based single slot antenna. The polyimide substrates are removed by oxygen ashing to reveal the embedded structures. a) Segment of a lateral wall of the antenna. b). Grounding via. c). Top view of lateral walls. d). Top view of the complete antenna. e). Close view of nano-wires.*

Micro-photographs of different parts of a SIW-based single slot antenna are presented in Fig. 4.5. Measurements show that this antenna exhibits approximately 4.7 % impedance bandwidth ($S_{11}$<-10 dB) and 2.8 dBi maximum gain around 79 GHz.

Higher antenna gains of 6.0 dBi and 11.0 dBi are obtained in a 79 GHz longitudinal slot array and a four-by-four slot array. The demonstrated four-by-four array is comprised of a parallel one-to-four feed network and four identical longitudinal slot array antennas uniformly excited to achieve the maximum antenna gain along the *z*-axis, cf. Fig. 4.6. Fig. 4.7 displays a photograph of a four-by-four slot array antenna folded by hand. Mechanical tests verify that all prototypes can tolerate moderate bending and slight twisting because of the flexibility of polyimide foils and nano-wires. This feature makes them interesting for large conformal array antennas at millimeter-wave frequencies. If a sample is severely folded or twisted, its top metal layer might peel off. This issue can however be solved by improving the adhesion between the porose polyimide foils and the metal layers.

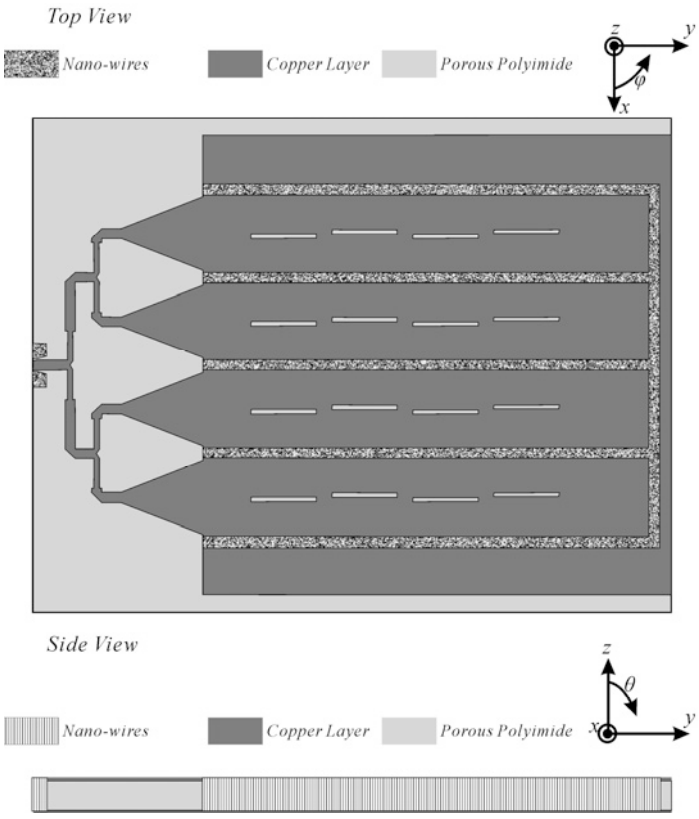


*Figure 4.6: Schematic of the SIW-based four-by-four slot array antenna.*

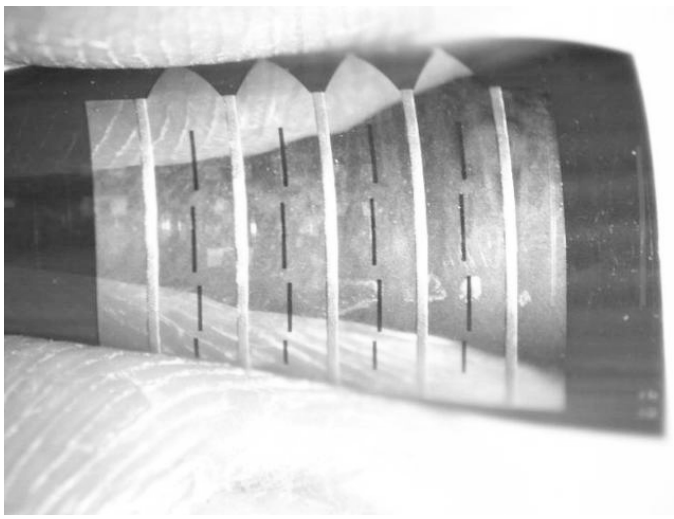

*Figure 4.7: Photograph of the folded four-by-four slot array antenna.*

Good agreement between simulations and measurements is seen in Fig. 4.8, which further confirms negligible leakage losses in nano-wire SIWs at the frequencies of operation. Furthermore, it also proves that those lateral walls in the form of densely packed nano-wires can be equivalently modeled as solid ones in numerical simulations.

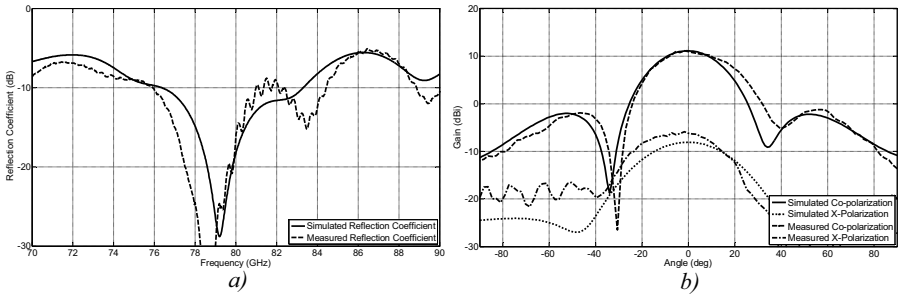


*Figure 4.8: Simulated and measured a) port impedance and b) radiation patterns, at 79 GHz, of the nano-wire SIW-based four-by-four slot array antenna in the xz-plane (with the coordinate system in Fig. 4.6).*

## 4.2 Micormachined Millimeter-Wave Antenna

Due to its competitive manufacturing cost, silicon is the dominating semiconductor material for low frequency electronics. In the past few years, remarkable progress in silicon technologies have been made, allowing silicon to be used as a cost-effective alternative to traditional III-V materials like GaAs and InP at microwave and millimeter-wave frequencies. In most commercial CMOS, BiCMOS, and SiGe HBT processes, low resistivity silicon is the only available substrate material. In radio frequency integrated circuits (RFIC), the high dielectric losses of low resistivity silicon is not a big issue, as passive components are predominately designed in the form of lumped elements, such as spiral inductors. However, integration of antennas or distributed transmission line components on this kind of substrate poses problems. First of all, the presence of lossy silicon can introduce high losses to antennas, resulting in poor radiation characteristics. Secondly, minimized chip sizes of RFICs are often needed to save manufacturing cost in mass production. As most antennas, especially array antennas, are much larger than ICs, integration of these antennas to RFIC chips requires relative large chip sizes, yielding a significant cost increase.

Micromachining techniques have been employed as a means to improve electrical performance of on-chip antennas on low resistivity silicon at millimeter-wave frequencies. Many such micromachined antennas are referred

to as membrane suspended antennas. This concept was originally developed at the University of Michigan, and demonstrated at 94 GHz [109] and 13 GHz [110]. Later, a variety of membrane suspended antennas have been reported [111]-[116]. Large membranes are usually beneficial for achieving better antenna electrical performance, but mechanical properties become poor. Such membranes are very fragile and easily damaged in real applications.

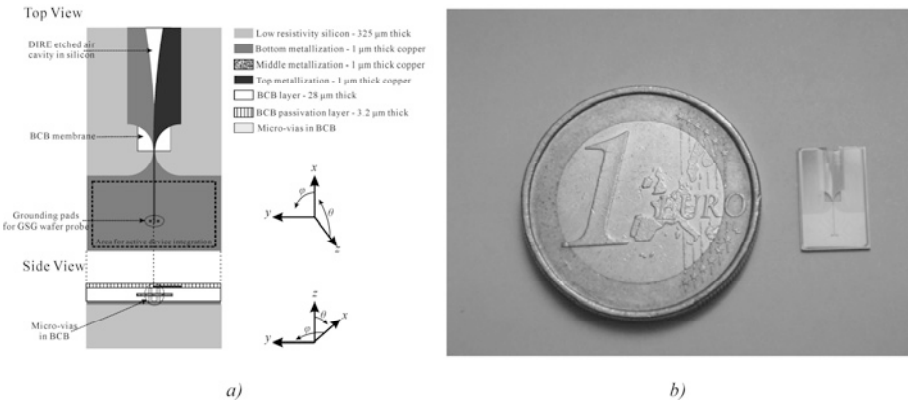


*Figure 4.9: Micromachined millimeter-wave TSA, a) schematic, b) photograph.*

In *Paper XII*, a W-band benzocyclonbutene (BCB) membrane suspended tapered slot antenna (TSA) integrated on a micromachined low resistivity silicon substrate is demonstrated, as shown in Fig. 4.9. The use of multi-layer BCB permits the implementation of a relatively large membrane with maintained mechanical performance, which is desired for suspending the large radiating element of a TSA. Moreover, the multi-layer BCB process associated with micro-vias enables complex routing in multiple metallization layers as well as low loss microstrip based feed networks for large arrays. In addition, this process is also compatible with advanced hot-via [117]-[119] or embedded thin die [120],[121] processes, in which hybrid integration to active circuitry can be realized at millimeter-wave frequencies using low loss interconnects. In the case of applications that are not strictly limited by cost, the presented antenna can also be monolithically integrated with transceiver circuits manufactured in commercial SiGe HBT, BiCMOS or CMOS processes.

Measurements verify that the demonstrated micromachined TSA features good impedance match with $S_{11}$ less than -10 dB, and favorable radiation characteristics with an antenna gain higher than 5 dBi within the frequency range of 67 GHz to 114 GHz. The end-fire radiation patterns can be seen in both numerical and experimental results presented in Fig. 4.10. Good electrical performance of this antenna is mainly owing to the presence of the 5.5

mm × 1.5 mm large BCB membrane that effectively suppresses dielectric losses and unwanted substrate modes in the silicon substrate.

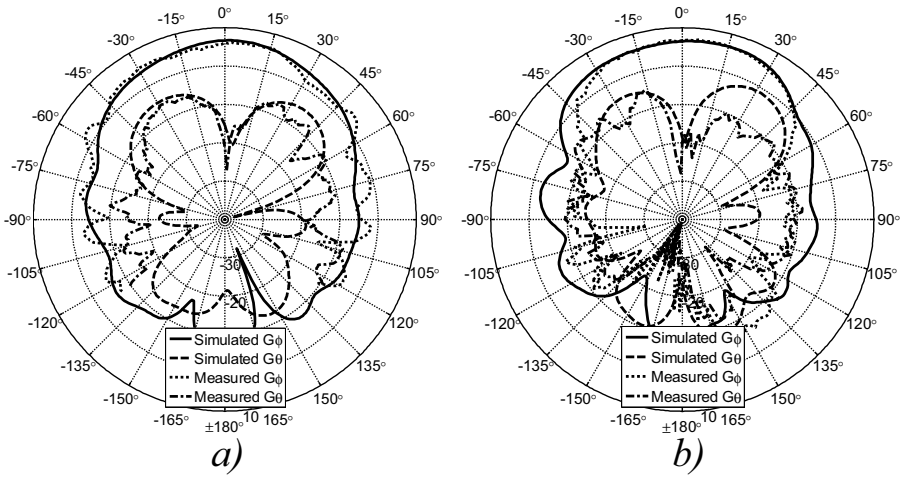


*Figure 4.10: Simulated and measured radiation patterns in the xy-plane (with the coordinate system in Fig. 4.9) at a) 79 GHz and b) 94 GHz.*

## 4.3 Body-Worn Automotive Radar Tag Antenna

Vulnerable road users (VRU) such as pedestrians, cyclists, and motorcyclists run a high risk of being seriously injured in traffic accidents. In contrast to their relatively low involvement in road accidents, a large number of all fatalities are VRUs. According to published statistics, pedestrians, cyclists, and motorcyclists counted 42.5 % of all fatalities in road accidents in Europe in 2005 [122].

Automotive radar devices are becoming standard equipment in luxury vehicles, and expected to be commonplace also in medium and economic class vehicles, as a means to improve road safety and assist driving. Most commercially available radars are either for blind spot detection (BSD) or automatic cruise control (ACC). In addition to these functionalities, multipurpose radar sensors could also be used to detect road conditions [123] or identify VRUs. One possible solution for identifying VRUs using automotive radars is to add a harmonic receiver to existing radars and equip VRUs with nonlinear radar reflectors generating backscattering at harmonic frequencies [124]. Because of its frequency offset from the transmitted and all other reflected signals, this harmonic frequency can be easily singled out from the reflections from other objects or clusters. Successful demonstrations of the harmonic radar concept have been reported [125],[126]. However, the large

frequency offset of such harmonic radars poses difficulties in fulfilling the frequency regulations set for automotive radars.

A slightly different solution using intermodulation radars for detecting and identifying VRUs wearing radar reflectors is proposed in the European Commission (EC) funded ADOSE project [127]. This concept resembles the conventional harmonic radar concept, but with reduced frequency offset between transmitted radar signals and non-linear reflections from radar reflectors. The reduced frequency offset allows the frequency regulations for automotive radars to be easily fulfilled and also simplifies electronics implementation. Fig. 4.11 describes the proposed intermodulation radar concept, where the radar transmits two tones $f_1$ and $f_2$ with a small frequency offset around the frequency of operation. When the transmitted radar signals at $f_1$ and $f_2$ are received by a nonlinear radar reflector, so-called tag, the nonlinear load of the tag will produce signals at the intermodulation frequencies of $f_1$ and $f_2$, such as $2f_1 - f_2$. Reflections from other targets like vehicles or trees are only at the fundamental frequencies $f_1$ and $f_2$.

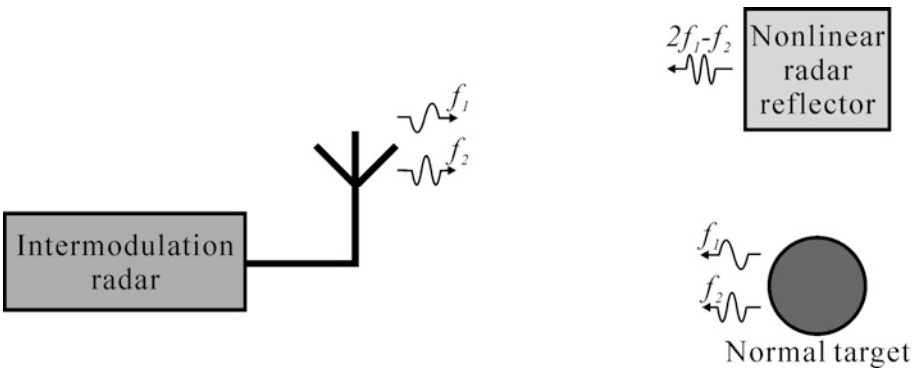


*Figure 4.11: Schematic of the proposed intermodulation radar concept.*

A nonlinear radar reflector consists of an antenna and a nonlinear load. The nonlinear load is in effect a reflective mixer, which can be implemented with for example Schottky diodes. Optimal antenna gain and beamwidth must be taken into account in the antenna design to meet the system requirements on detection range and full azimuthal coverage.

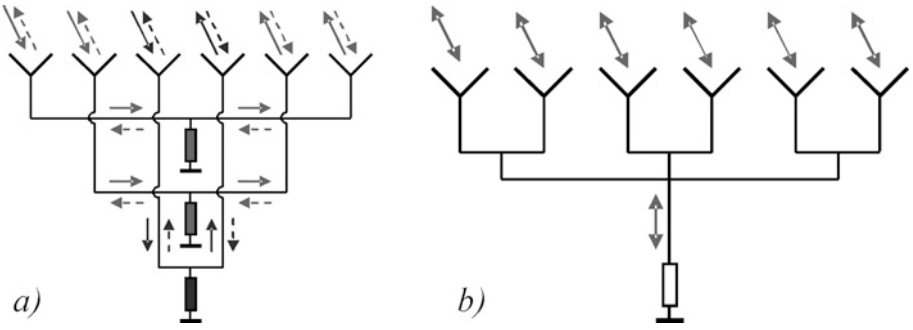


*Figure 4.12: Comparison between two alternative solutions: a) Van Atta array with several transmission-type nonlinear loads, b) standard resonance array antenna with a single reflective-type nonlinear load.*

An interesting attempt would be to use retrodirective array concept [128],[129] to combine high gain with broad coverage. However, as illustrated in Fig. 4.12a, the received power in a retrodirective array is divided into several loads. This in turn reduces the power at each nonlinear load, yielding drastic increase of conversion loss in the mixing and decrease of detection range. In a standard array antenna, all received power is directed into a single nonlinear load, see Fig. 4.12b. A standard array antenna solution is therefore chosen for nonlinear tags.

The preliminary system calculations suggest that an antenna gain of >15 dBi, an impedance bandwidth ($S_{11}$<-10 dB) of >1 GHz, and vertical beamwidth of $20^{o}$ are required. Apart from these requirements, the horizontal beamwidth is expected to be as wide as possible to reduce the number of nonlinear tags that are needed for full coverage in azimuth. Since several tags might be necessary for a VRU, each of them must be inexpensive to keep the overall cost down.

Implementing highly efficient millimeter-wave antennas at low cost is challenging. A successful design necessitates a substrate material with low cost and favorable electrical performance at millimeter-wave frequencies. As integration of nonlinear radar reflectors into clothes is desired, flexible tags are beneficial for the comfort of the user. All these aspects lead to the choice of a single layer microstrip patch array antenna etched on a 100 µm Rogers liquid crystal polymer (LCP) Ultralam 3000 flex foil substrate, cf. Fig. 4.13. The LCP substrate is chosen for its attractive merits, e.g. excellent electrical properties at millimeter-wave frequencies, extremely low moisture absorption, high flexibility, and low cost [130],[131]. Furthermore, a commercially available PCB manufacturing process is chosen for fabricating the first tag antenna prototypes, which then can be easily adapted to mass production.

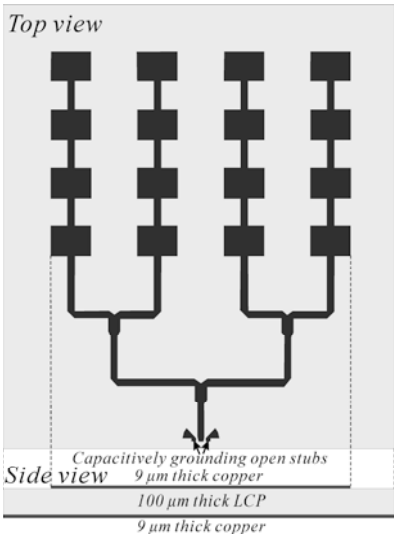


*Figure 4.13: Layout of the presented tag antenna.*

Measured results on the antenna samples indicate that the antenna achieves 2.5 GHz bandwidth, 16.4 dBi gain, 21° vertical beamwidth, and 16° horizontal beamwidth, at 80 GHz. The 16° beamwidth in azimuth implies that at least 23 tags are needed for full horizontal coverage. When integrating this antenna into clothes, its electrical performance will not be affected by objects behind it due to the ground shield. Anything in front of the antenna might have an impact though. Therefore, the influence of various textiles on the antenna performance, including detuning of the antenna resonance frequency and attenuation due to reflection and absorption, is experimentally investigated, see Table 4.1.

**Table 4.1.** Resonance frequency detuning and attenuation (gain reduction) due to various textile layers in front of the tag antenna.

| Textile | Detuning, dry | Detuning, wet | Attenuation, dry | Attenuation, wet |
|---|---|---|---|---|
| Cotton | ±0.0 GHz | -0.4 GHz | 0.2 dB | 10 dB |
| Wind poplin | +0.2 GHz | -0.1 GHz | 0.1 dB | 2 dB |
| Wool | +0.1 GHz | +0.2 GHz | 0.4 dB | 18 dB |
| Felt | +0.1 GHz | -0.4 GHz | 0.2 dB | 31 dB |
| Thick felt | ±0.0 GHz | ±0.0 GHz | 0.6 dB | No data |
| Synthetic | +0.2 GHz | +0.2 GHz | 0.1 dB | 14 dB |
| Wadding | +0.1 GHz | No data | 0.0 dB | 56 dB |
| Cotton | ±0.0 GHz | -0.4 GHz | 0.2 dB | 10 dB |
| Wind poplin | +0.2 GHz | -0.1 GHz | 0.1 dB | 2 dB |

To summarize, all dry textiles have a very small effect on the antenna port impedance and radiation attenuation. In the case of wet textiles, the detuning effect is negligible. Significant differences, from a couple of decibel to tens of decibel, can be found in the measured attenuation with various wet textiles. The measured data indicates that the attenuation is proportional to the amount of water absorbed by the textiles.

## 4.4 Summary and Conclusion

In this chapter, several integrated antenna solutions at millimeter-wave frequencies have been demonstrated. The proposed nano-wire based SIW concept provides a new cost-effective solution for implementing SIW technology at very high frequencies. Based on this concept, three slot antennas have been demonstrated at 79 GHz with good electrical performance. It is verified by experimental and analytical studies that the dielectric loss in the presented nano-wire SIWs are dominating. Consequently, further development of adapting this technology to low loss substrate materials like LCP or PTFE would be a feasible approach to improve the performance of these nano-wire SIWs and SIW-based devices. Using silicon micromachining associated with multi-layer BCB process, a W-band membrane suspended TSA has been implemented and tested. Good impedance and radiation characteristics of this antenna are mainly owing to the large BCB membrane that suspends the big antenna radiator in free space. The used multi-layer BCB technology not only improves the mechanical properties of large membranes, but also opens up possibilities for hybrid integration of passive components like antennas to active circuitry at millimeter-wave frequencies. For the nonlinear radar reflector, a single layer four-by-four microstrip patch array antenna have been proposed and evaluated. Excellent electrical performance of this tag antenna has been verified in measurements. Experiments also confirm the possibilities of integrating the presented tag antennas into clothes. The utilizations of low cost LCP substrates and commercial PCB manufacturing processes lead to a cost-effective solution for large volume production.

# 5 Conclusion and Future Work

In this thesis, several integrated antenna solutions and studies related to various applications from a few hundred megahertz up to millimeter-wave frequencies have been presented. The theme of this thesis is the exploration and evaluation of appropriate solutions for wireless sensor and millimeter-wave systems. Varactor-based electrically steerable array antennas at 5.8 GHz, intended for use in future advanced base stations, have been demonstrated. When moving to higher frequencies such as millimeter-wave frequencies, high performance electrically steerable arrays or switched beam antennas have been implemented using advanced RF MEMS and digital beamforming technologies. A conventional T-matched dipole antenna has been integrated into a body-worn wireless sensor node, with emphasis on new measurement techniques for characterizing an electrically small antenna in a miniaturized system. Standard PCB and silicon micromachining technologies have been employed to implement various W-band antennas. Possibilities of realizing highly efficient millimeter-wave antennas at low cost using commercial PCB manufacturing processes have been investigated experimentally. Integration of planar inverted cone antenna (PICA) based broadband antennas into a handheld terminal and a planar PCB has been verified in experiments.

A new concept of liquid metal stretchable RF electronics has been proposed. Experiments on two stretchable antenna prototypes verify their high degree of flexibility as well as excellent electrical performance. The demonstrated technology opens up a curvy and stretchy future for RF electronics in a broad range of applications. Many technical issues remain, however. First of all, integration of the stretchable parts with rigid components by reliable interfaces is a key to realize fully functional stretchable electrics and boost the commercialization of this technology. Second, the present manufacturing processes should be adapted to mass production. For instance, manual injection of liquid metal alloy into microstructured elastic channels should be replaced by automated injection or parallel filling processes. Present state-of-the-art stretchable active electronics are restricted by a maximum operational frequency of merely a couple of megahertz. Moreover, the demonstrated stretchable RF devices have not been optimized in terms of reliable mechanical properties and robust electrical performance. Further investigations of stretchable RF electronics that are insensitive to strain would be of

interest. This necessitates in-depth understanding of both electrical characteristics and mechanical properties of stretchable structures.

Nano-wire based SIW is another new concept presented in this thesis, with implementations in antenna design demonstrated. For further development of nano-wire based SIWs, the first priority would be to transfer the technology to low loss substrates at millimeter-wave frequencies, such as LCP and PTFE. This would significantly reduce the dominating dielectric losses, and thus improve the electrical performance of SIW-based devices. Moreover, the nickel nano-wires used in the present SIW processes may introduce extra losses and cause problems at very high frequencies due to the high permeability and low conductivity of nickel. An interesting attempt would be to replace nickel with other low loss metals like copper or gold. Integration of active circuits at millimeter-wave frequencies would also be of interest. Integration technologies such as flip-chip bonding and hot-via processes could be proved useful.

With respect to MEMS-based reconfigurable antennas, the reliability of MEMS components is one of the key technical issues. Appropriate packaging solutions can be employed as a means to enhance the reliability of integrated MEMS devices. Excellent reliability of RF MEMS in terms of switching cycles of more than 10 billion cold-switching cycles has been demonstrated, but the long-term reliability has not been verified yet.

In Chapter 4, a W-band antenna measurement setup has been demonstrated. Further investigations on developing a sub-millimeter wave antenna measurement setup have been initiated. Fig. 5.1 illustrates the WR3-band on-wafer measurement setup with two external synthesizers. A clear dynamic range enhancement can be achieved by using two external synthesizers, as shown in Fig. 5.2.

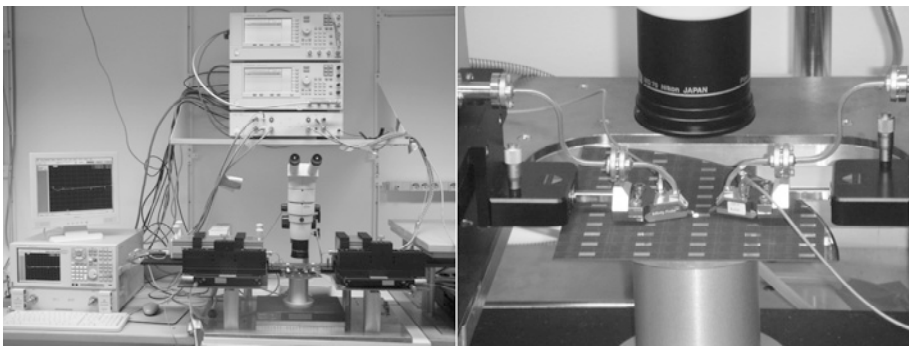

*Figure 5.1: WR3-band measurement setup with two external synthesizers.*

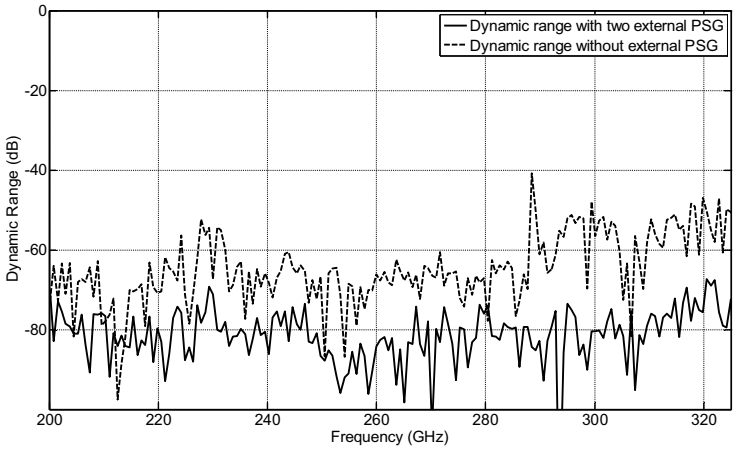


*Figure 5.2: Dynamic range comparison between measurements made with and without external synthesizers.*

Still, the dynamic range of better than 70 dB at the WR-3 band is not sufficient for measuring antenna radiation characteristics, because of the high free-space losses within this frequency range. A possible solution would be to build a compact antenna measurement setup by placing a transmitting/receiving antenna at a very short distance from an RF probe fed UTA. This however may raise practical issues while rotating the transmitting/receiving module in radiation pattern measurements.

There is still much to be done in the areas of integrated antennas. Instead of designing stand-alone antennas, a broad view from a system perspective is needed in order to better understand and effectively solve the numerous technical issues in this field.

# 6 Summary of Papers

Thirteen papers are included in this thesis. *Papers III*, *IV*, *VII*, *VIII*, and *X* deal with integrated antennas for handheld terminals, wireless sensor nodes, as well as large area electronics. Electrically steerable and switched beam array antennas based on either varactor-diodes or MEMS switches operating at different frequencies are presented in *Papers I*, *II*, and *IX*. *Papers V*, *VI*, *XI*, *XII*, and *XIII* demonstrate millimeter-wave antennas realized using conventional PCB, silicon micromachining, or nano-wire based SIW technology.

## 6.1 Paper [I]: Compact Reflective Microstrip Phase Shifter for Traveling Wave Antenna Applications

Tunable phase shifters are one of the key components in electrically steerable array antennas at low frequencies. Microstrip phase shifters can be integrated as inter-elements on the same radiating aperture as traveling wave patch array antennas to achieve electrical beam steering. Reflective-type phase shifters (RTPS) based on varactors feature wider continuous phase tuning range and lower return loss compared to transmission-type phase shifters (TTPS). However, relatively large sizes of conventional RTPSs pose difficulties in fitting them between each pair of neighboring radiating elements on the same metallization layer. A 5.8 GHz compact RTPS based on modified unequal length branch line coupler is therefore proposed in this paper. Asymmetric T-shaped microstrip equivalents are utilized to replace wide branch lines of a conventional hybrid for minimizing its overall size. Measured electrical performance indicates that the implemented coupler exhibits a 2 % impedance bandwidth ($S_{11}$<-10 dB), an insertion loss of less than 0.6 dB, and a continuous phase tuning range of 62$^{o}$ at 5.8 GHz.

## 6.2 Paper [II]: Electrically Steerable Single-Layer Microstrip Traveling Wave Antenna with Varactor Diode Based Phase Shifters

Analysis and design of electrically steerable traveling wave patch array antennas are presented in this paper. Two 5.8 GHz array antennas, intended for

use in advanced base stations, are implemented and characterized. A vertical beam tilt array antenna, equipped with varactor-based TTPSs, shows a gain of 14.4 dBi and a tunable downtilt within the range $0^o$ to $-13^o$. Compact RTPSs proposed in *Paper I* are integrated on the same layer of a five-element traveling wave microstrip patch array antenna to obtain broader beam scanning range. Measured radiation patterns show that the antenna beam can be horizontally steered within a range of $\pm 32^o$ with a gain of approximately 11.0 dBi. Sufficient impedance bandwidths ($S_{11}$<-10 dB) are also achieved in both array antennas.

## 6.3 Paper [III]: Modified Planar Inverted Cone Antenna for Mobile Communication Handsets

The need for integrating more wireless communication functionalities and services into mobile terminals is increasing. This trend leads to high requirements of antenna impedance bandwidth. Differing from conventional multi-band handset antennas discretely covering all required bands, one broadband antenna is proposed and evaluated in this paper. The presented antenna resembles a well-known broadband antenna, the planar inverted cone antenna (PICA), but with a modified low-profile configuration. The leaf-shaped radiating element of the modified PICA is placed on the short edge of a 100 mm × 50 mm ground plane, and bent with its upper part parallel to the ground. The modified configuration allows it to be fit into a mobile handset with large bandwidth ($S_{11}$<-6 dB) from 1 GHz to 30 GHz. Measured radiation efficiency shows values of approximately 75 % at frequencies around 1 GHz, and 90 % or more at frequencies above 1.2 GHz.

## 6.4 Paper [IV]: Printed Slot Planar Inverted Cone Antenna for Ultrawideband Applications

Integration of the PICA on a single PCB is demonstrated in this paper. The proposed design comprises a leaf-shape radiator in the top metallization, and a large leaf-shaped slot in the bottom metallization. It features extremely large bandwidth, omnidirectional radiation pattern, and compact size, just as the original PICA, but with additional merits like ease of integration, cost-effective manufacturing, and planarity. Measured results show that the implemented antenna prototype achieves at least 13:1 impedance bandwidth ($S_{11}$<-10 dB), and a radiation efficiency of 80 %-90 % over the operational frequency range.

## 6.5 Paper [V]: Substrate Integrated Waveguides (SIWs) in a Flexible Printed Circuit Board for Millimeter Wave Applications

This paper reports a new concept of substrate integrated waveguides (SIWs) in a flexible PCB for 79 GHz automotive radar applications. The vertical lateral walls of the demonstrated SIWs in this paper consist of thousands of densely packed electrodeposited metallic wires. The diameters and spacing of these wires are on the order of a few hundred nanometers. Hence, such lateral walls can be regarded as continuous metallic walls, and the leakage losses through them are negligible. This feature allows the presented SIWs to operate at higher frequencies compared to conventional SIWs realized by standard PCB manufacturing processes. Attenuation per unit length of nano-wire based SIWs with different porosities is experimentally investigated. Also, a slot antenna based on nano-wire SIWs is demonstrated, with good port impedance match at 79 GHz.

## 6.6 Paper [VI]: 79 GHz Slot Antennas Based on Substrate Integrated Waveguides (SIW) in a Flexible Printed Circuit Board

This paper is an extension of the preliminary studies reported in *Paper V*. The design, fabrication, and characterization of a 79 GHz single slot antenna, as well as longitudinal and four-by-four slot array antennas based on nano-wire SIWs are presented in this paper. A flexible polyimide foil with 3 % porosity is chosen for the fabrication of all antenna prototypes. The choice of the substrate is based on the experimental results in *Paper V*. Measured port impedance and radiation characteristics show that the three antennas achieve 4.7 %, 5.4 % and 10.7 % bandwidth ($S_{11}$<-10 dB) with 2.8 dBi, 6.0 dBi and 11.0 dBi gain around 79 GHz, respectively. Moreover, analysis of radiation efficiency and finite ground plane influence on antenna gain is carried out in numerical simulations. It is verified by analytical and experimental studies that dielectric losses of the used porose polyimide substrate represent a large part of the losses in the presented SIWs and SIW-based structures. However, considering the frequency of operation, electrical performance of the demonstrated antenna prototypes is very good.

## 6.7 Paper [VII]: T-Matched Dipole Antenna Integrated in Electrically Small Body-Worn Wireless Sensor Node

Integration of a 2.4 GHz balanced antenna into an electrically small body-worn wireless sensor node for monitoring body parameters like motion and orientation is described in this paper. The choice of a T-matched dipole antenna is due to its compatibility with the used differential RF transceiver in the sensor node, and its high degree of freedom in impedance matching. Also, a balanced antenna is expected to be less sensitive to other parts of the node. However, such an antenna introduces difficulties in characterization, as measurement cables, connectors, and instruments usually are unbalanced. Different methods for passive and active characterization of port impedance and radiation performance are proposed, and simulations are used for comparison. In addition to electrical performance in free space, the integrated sensor node antenna is also characterized in proximity of a human body, with severe attenuation and blockage of RF signals as results. Finally, a complete system demonstration is performed, where a communication range up to 20 m is achieved.

## 6.8 Paper [VIII]: Liquid Metal Stretchable Unbalanced Loop Antenna

Stretchable RF electronics is a new growing field in the microwave and antenna world. Its strict requirements on high degree of flexibility and stretchability associated with good electrical performance pose challenges to conventional manufacturing technologies, where electronics are typically built in rigid formats. A new concept of stretchable RF electronics is presented in this paper, with implementation in a 2.4 GHz unbalanced loop antenna. This antenna prototype is realized by incorporating room temperature liquid metal alloy into microstructured elastic channels. A 2D stretchability of 40 % as well as severe 3D foldability and twistability are experimentally verified. Measurements of electrical performance show that the non-stretched antenna achieves good impedance matching at 2.4 GHz, and its resonance frequency shifts while stretching. Although electrical performance degradation of the strained antenna occurs, its radiation efficiency is greater than 80 % at 2.4 GHz.

## 6.9 Paper [IX]: Switched Beam Antenna Based on RF MEMS SPDT Switch on Quartz Substrate

A 20 GHz switched beam antenna based on RF MEMS switches on quartz substrate is demonstrated in this paper. Compared to p-i-n or field-effect transistor (FET) diode switches, MEMS switches offer highly attractive merits such as high isolation, low insertion loss, high linearity, low cost, and near-zero power consumption. The switched beam antenna presented in this paper consists of two identical quasi-Yagi antenna elements monolithically integrated with a single-pole double-throw (SPDT) MEMS switch router network on a 21 mm × 8 mm chip. The quasi-Yagi antenna is chosen for its compact size, sufficient impedance bandwidth, and end-fire radiation characteristics. Measured results show that the antenna features a 27 % impedance bandwidth ($S_{11}$<-10 dB), a gain of 4.6 dBi, and front-to-back ratio of 14.0 dB, at 20 GHz.

## 6.10 Paper [X]: Foldable and Stretchable Liquid Metal Planar Inverted Cone Antenna

This paper demonstrates a mechanically flexible and stretchable PICA for ultrawideband (UWB) applications. The elastic substrate together with the room temperature liquid metal used in the antenna prototype enables bending with a very small radius, twisting, and straining along any direction. Experimental results verify that this antenna exhibits more stable impedance characteristics while stretching compared to that of the unbalanced loop antenna presented in *Paper VIII*. A return loss better than 10 dB within 3-11 GHz, and a radiation efficiency of >70 % over 3-10 GHz are achieved, even when it is stretched. Tests confirm that stretching up to 40 % is possible with maintained electrical performance. Potential applications of the presented antenna in body-worn electronics or harsh environments are foreseen.

## 6.11 Paper [XI]: Millimeter-Wave Tapered Slot Antenna for Integration on Micromachined Low Resistivity Silicon Substrates

The tapered slot antenna (TSA) is an antenna type with wideband performance as well as favorable radiation characteristics. Implementation of a TSA covering several millimeter-wave frequency bands is of interest in a broad range of applications. This paper presents a millimeter-wave TSA integrated on a 325 μm thick low resistivity silicon substrate. To minimize substrate

losses and unwanted substrate modes, silicon micromachining technique is employed to form a 5.5 mm × 1.5 mm large benzocyclonbutene (BCB) membrane for suspending the antenna radiator. Measured results show that this antenna achieves good impedance match ($S_{11}$<-10 dB) and a gain of >4.6 dBi, from 75 GHz to 100 GHz.

## 6.12 Paper [XII]: Array Antenna for Body-worn Automotive Harmonic Radar Tag

Automotive radar systems operating within the range of 77-81 GHz have been identified as a critical technology for the improvement of road safety. A new added functionality to existing automotive radars would be to distinguish persons among "dead" targets and clutter. The intermodulation radar technique associated with body-worn nonlinear radar reflectors is studied as a means to accomplish this. This paper demonstrates a W-band four-by-four microstrip patch array antenna, intended for use in automotive intermodulation radar tags. The antenna is implemented on 100 μm thick liquid crystal polymer (LCP) flex foil, using commercial PCB manufacturing processes. Owing to excellent dielectric properties of LCP at millimeter-wave frequencies, good antenna electrical performance with a 2.5 GHz impedance bandwidth ($S_{11}$<-10 dB) and a 16.4 dBi gain is achieved.

## 6.13 Paper [XIII]: Compact Integrated Slot Array Antennas for the 79 GHz Automotive Band

Due to the widespread use of low resistivity silicon substrates in microelectronics industry, antennas integrated on such substrates of interest in many systems and applications, especially at millimeter-wave frequencies. However, as a result of significant substrate losses, millimeter-wave antennas implemented on low resistivity substrates usually suffer from poor radiation characteristics. When implementing array antennas, severe losses in feed networks might also be an issue. An advanced technology of incorporating silicon micromachining with multi-layer BCB process is proposed in this paper, with implementations in a 79 GHz compact Tx/Rx slot array antenna demonstrated. To enhance forward radiation and suppress potential cavity modes, the presented antenna prototype is backed by a metallic cavity with a number of metallic bars mounted in its ceiling. It is shown in the measurements that this cavity-backed array antenna achieves good impedance matching (S11<-10 dB) within the range 70-90 GHz as well as a gain of approximately 6.6 dBi at 79 GHz. Moreover, high sidelobe suppression of 18 dB is measured.

# 7 Summary in Swedish

## Integrerade Antennlösningar för Trådlösa Sensor- och Millimetervågssytem

Avhandlingen presenterar ett antal integrerade antennlösningar för olika typer av trådlösa system, för frekvenser från några hundra megahertz till sub-millimetervågsfrekvenser. De presenterade lösningarna är intressanta för många tillämpningar, till exempel trådlösa sensornätverk (WSN) på kroppen, bredbandiga handburna terminaler, avancerade basstationer, front-ends baserade på mikroelektromekaniska system (MEMS), RFID-taggar, antikollisionsradar för fordon, s.k. large area electronics och fjärranalys. Mer specifikt består det presenterade arbetet av innovativa antenntyper och tillverkningsmetoder, nya metoder för antennkarakterisering, avancerad integration, samt experimentella studier av känd antennteknik men för högre frekvenser än tidigare använts. Forskningen som lett fram till avhandlingen har bedrivits inom ett antal nationella och internationella forskningsprojekt, finansierade av Vinnova och Europeiska Kommisionen.

Mobila enheter för trådlös kommunikation har funnits länge, och under de senaste 20 åren fått stor spridning, framför allt för mobiltelefoni. Under de senaste åren har utvecklingen även börjat ta fart inom så kallade trådlösa sensornätverk. Dessa karakteriseras av att små enkla sensorer, för t ex temperatur eller acceleration, kommunicerar med en central nod. Syftet är typiskt övervakning av tekniska system eller av människors hälsa. I det senare fallet ska ett trådlöst system placeras på kroppen. Liten storlek och låg effektförbrukning är då speciellt viktiga. Möjlighet att sy in antenn och elektronik i kläder är också efterfrågad i vissa tillämpningar. Detta innebär att nya lösningar krävs för antenner och för integration av antenner och övrig elektronik. Studier av elektrisk funktion såväl som mekaniska egenskaper är nödvändiga, men forskningen bör även behandla aspekter som rör produktutveckling och tillverkning, t ex material, tillverkningsprocesser, och konstruktionsverifiering. Även för mobiltelefon sker en snabb utveckling med allt större funktionalitet, vilket ställer krav på nya antennlösningar. Både själva telefonerna och basstationerna som de kommunicerar med är föremål för

snabb utveckling. Antennegenskaper som efterfrågas mer och mer är exempelvis ökad bandbredd samt elektriskt styrbara basstationsantenner.

En annan allmän trend inom trådlös kommunikation är användandet av allt högre frekvenser. Frekvenser på tiotals gigahertz blir allt vanligare, t ex fordonsradar vid 79 GHz. Högre frekvens innebär mindre våglängd. Eftersom antenners storlek är proportionell mot våglängden betyder det att antennerna blir mindre och mindre. Detta öppnar för möjligheten att införa mer avancerade antenner inom en liten volym, vilket också ofta är skälet till att söka sig mot högre frekvenser. Å andra sidan innebär mindre antenner också att tillverkningen försvåras. Vid millimetervågsfrekvenser är forskningen på antenner och integration i hög utsträckning fokuserad på materialval och tillverkningsprocesser.

I det presenterade arbetet föreslås för trådlösa sensornätverkstillämpningar en miniatyriserad dipolantenn med T-anpassning, integrerad i en elektriskt liten kroppsburen sensornod. Specifika mättekniker är utvecklade för karakterisering av komplexa portimpedansen och strålningsegenskaperna hos den integrerade antennen. Möjligheter och begränsningar hos den plana inverterade konantennen (PICA) för små handburna terminaler är experimentellt undersökta. PICA-antenner för ultrabredbandiga (UWB) handburna terminaler demonstreras, en antenn av slitstyp etsad på ett substrat, samt en krympt PICA-antenn för små terminaler.

Vidare föreslås olika lösningar för elektriskt styrbara och omkopplingsbara gruppantenner, baserade på monolitiska tekniker såväl som på hybridteknik. För elektriskt styrbara gruppantenner på låga frekvenser har hybridintegration av avstämbara fasvridare inom en gruppantenn av vandringsvågstyp realiserad på ett enlagerssubstrat undersökts. En kompakt varaktordiodbaserad fasvridare som ryms inom antennaperturen på samma lager som antennelementen har utvecklats. Omkopplare baserade på radiofrekvensmikroelektromekaniska system (RF-MEMS) har använts för att förbättra elektriska prestanda hos rekonfigurerbara gruppantenner vid höga frekvenser. En enkel 20 GHz switched beam-antenn som utnyttjar monolitisk integration av kapacitiva omkopplare på kvarts-substrat har realiserats och utvärderats. Till skillnad från tidigare arbeten publicerade av andra har här kompletta experimentella resultat rapporterats. Dessutom föreslås en hybridlösning för en switched beam-antenn av vandringsvågstyp på 24 GHz. En router bestående av en sexvägs kapacitiv omkopplare är tillverkad på substrat av högresistivt kisel, och en gruppantenn är tillverkad med en LTCC-process.

Ett innovativt koncept för nanotrådbaserade substratintegratede vågledare (SIW) presenteras. Tekniken antas bli betydelsefull för framtida millimeter-

vågs och sub-millimetervågstillämpningar, såsom till exempel vågledarantenner. Ett antal antennprototyper baserade på detta koncept har med framgång demonstrerats för fordonstillämpningar på 79 GHz. Experiment visar att de presenterade antennerna har goda impedans- och strålningsegenskaper inom det aktuella frekvensområdet.

Personburna ickelinjära radarreflektorer på 79 GHz föreslås som en teknik för att förbättra funktionaliteten hos fordonsradar. Den tidigare kända tekniken för harmonisk radar har här tillämpats för att ge befintliga fordonsradarer möjlighet att skilja människor från döda föremål i trafiken. Såväl passiva, semi-passiva som aktiva ickelinjära reflektorer bestående av gruppantenner och ickelinjära kretsar tillverkade på tunn flexfilm har undersökts. Mätresultat visar på utmärkta antennprestanda. Tester av integration i olika typer av textiler visar att reflektorerna kan sys in i kläder.

Ett nytt koncept för töjbar RF-elektronik, avsett för s.k. large area electronics med ett flertal tillämpningar, är uppfunnet och demonstrerat. Antennprototyper är realiserade genom att inkorporera en legering av metall (galinstan) som är flytande vid rumstemperatur i kanaler i det elastiska materialet polydimetylsiloxan (PDMS). På så sätt erhålls elektriska ledningar som kan töjas, böjas, och vridas utan nämnvärt mekaniskt slitage. Olika antenntyper kan sedan realiseras med dessa ledningar. Prototyper i form av en loopantenn och en PICA-antenn är tillverkade, elektriskt uppmätta, och mekaniskt testade. Prototyperna klarar en töjning på 40 % längs två ortogonala riktningar såväl som vikning och vridning. Goda elektriska egenskaper har påvisats, även under töjning.

Sammanfattningsvis konstateras att det finns mycket att forska på inom området integrerade antenner. Istället för att konstruera separata antenner bör ett brett perspektiv anläggas för att förstå de många problemen inom detta område och kunna hitta effektiva lösningar.

# Acknowledgements

Since March 2006 I have been fortunate enough to take part in nine different research projects at the Microwave Group at the Signals and Systems Division, Uppsala University, Sweden. The projects have been funded by the European Commission and VINNOVA, I would hereby like to take the opportunity to express my thankfulness to everyone who helped me during the past four years to accomplish this important goal in my life.

Starting with the colleagues at the Signals and Systems Division at Uppsala University, my first and foremost thanks go to my supervisor Prof. Anders Rydberg, the head of the Microwave Group in the Signals and Systems Division, for his support and encouragement during these years, and for providing me the opportunity to work in a number of highly interesting and challenging research projects, while giving me the freedom to develop my own ideas. Secondly, I am very grateful to my co-supervisor Dr. Paul Hallbjörner, for his scientific support and invaluable help in various forms, and for guiding me from a fresh undergraduate student to a researcher in the microwave and antenna world. My sincerest gratitude goes to former colleagues Dr. Erik Öjefors and Dr. Peter Lindberg for their kind help and countless interesting discussions. In the last year of my PhD studies, I have enjoyed the collaboration and friendship with present colleagues at the Microwave Group M.Sc. Mathias Grudén, M.Sc. Magnus Jobs, Dr. Robert Malmqvist, and Dr. Xin Hu. Prof. Anders Ahlén, the head of the division, deserves special thanks for a friendly and creative atmosphere. Thanks also to Ylva Johansson for all help with administration, as well as Jonatan Bagge and Mikael Österberg for their continuous support in maintaining computers and software. I also thank staff members Lars Ericsson, Nora Masszi, Dr. Ping Wu, and others in our group for their help. I take this opportunity also to thank all the PhD students for the fun and for sharing their experience in the previous years.

Some guys from other groups at Uppsala University also deserve my special thanks for the fruitful collaboration and friendship. I would like to acknowledge Dr. Hanna Yousef and Dr. Henrik Kratz for the great collaboration in nano-wire based SIWs, as well as Dr. Zhigang Wu for the cooperation in stretchable RF electronics. Thanks very much for all the spare time you spent after your work and during weekends. Also, I express my thank-

fulness to colleagues at the MST group, Prof. Klas Hjort, M.Sc. Sam Ogden, and M.Sc. Joakim Magrell, for their kind help with manufacturing various test structures. Special thanks to Dr. Arnaud Ferrari and Prof. Volker Ziemann for the research collaboration in the nearly-confocal resonators, to M.Sc. Gerald Pettersson at Forskarpatent i Uppsala AB for the patent drafting, to UU Innovation and INNOVATIONSBRON for financial support of the patent filing and dissemination, and to Dr. Roger Karlsson for all the interesting discussions related to antennas.

A major part of my PhD work has been carried out in close collaboration with many academic and industrial research groups all over the Europe. During the years, I have received constant and invaluable support from a number of partners. It has been my pleasure to work with you guys.

My sincere appreciation goes to Dr. Piet van Engen and Ir. Ric van Doremalen at Philips Applied Technologies, Dr. De Raedt Walter, Dr. Muller Philippe, and M.Sc. Jansen Roelof at IMEC, Dr. Werner Weber, Dipl.-Ing. Thomas Herndl, and Dipl.-Ing. Martin Flatscher at Infineon, as well as Dipl.-Ing. Thomas Fritzsch at Fraunhofer IZM, for the fruitful and creative research cooperation in 3D integrated wireless sensors. Dr. Tauno Vähä-Heikkilä, Dr. Jussi Varis, and M.Sc. Markku Lahti at VTT, Prof. Hermann Schumacher and Dipl.-Ing. Tatyana Purtova at the University of Ulm, Dr. Afshin Ziaei at Thales, Dipl.-Ing. Thomas Lisec and Dr. Joachim Janes at Fraunhofer ISIT, as well as Dipl.-Ing. Thomas Bartnitzek at VIA Electronic GmbH, are greatly appreciated for their contributions to collaborative research related to RF MEMS. I am also grateful to M.Sc. Michael Salter, M.Sc. Duncan Platt, and M.Sc. Lars Pettersson at Acreo AB for the collaboration, support and technical discussions. Dr. Lorenzo Tripodi at Philips Research is acknowledged for his kind help and extra hours in finalizing the layout at the last moment of the tape-out. I would also like to thank Dr. Ville Viikari and Dr. Timo Varpula at VTT, as well as Dr. Jone Saebboe at Triad, for the productive collaboration in the ongoing ADOSE project.

Of course, my acknowledgements also go to all my friends at Uppsala, Song Sun, Na Guan, Siwei Peng, Yanwu Yang, Lin Jiang, Xiaochun Shi, Bingwen He, Hao Li, Wei Sun, Xuping Wu, Jia Mi, Chen Wang, Li Lv, Jun Lu, Shuxi Zhao, Wei Xia, Miao Wu, Xin He, Shuyi Li, Zhuo Bao, Lunmei Huang, Mei Hong, Lianghui Ding, Hao Wang, and Johannes Hjerdt, for their friendship during these years.

I express my greatest gratitude to my wife Yiwen Jiang for all her love, support and patience, as well as my parents and parents-in-law for their unselfish love.

Finally, I thank all those not mentioned who have supported me during the past years.

*Shi Cheng*
*December, 2009*

# Bibliography


[1] C. C. Enz, A. El-Hoiydi, J.-D. Decotignie, and V. Peiris, "WiseNET: an ultralow-power wireless sensor network solution," *Computer*, vol. 37, no. 8, pp. 62–70, Aug. 2004.

[2] J. Kumagai and S. Cherry, "Sensors and sensibility," *IEEE Spectrum*, vol. 41, no. 7, pp. 22–26, Jul. 2004.

[3] Smart Dust Project [online]. http://robotics.eecs.berkeley.edu/~pister/SmartDust/.

[4] V. Lumelsky, M. Shur, and S. Wagner, "Sensitive skin," *IEEE Sensors Journal*, vol. 1, no. 1, pp. 41–51, Jun. 2001.

[5] R. H. Reuss et al., "Macroelectronics: perspectives on technology and applications," *Proceedings of the IEEE*, vol. 93, no. 7, pp. 1239–1256, Jul. 2005.

[6] J.A. Rogers and Y. Huang, "A Curvy, Stretchy Future for Electronics," *Proceedings of the National Academy of Sciences USA*, vol. 106, no. 27, pp. 10875–10876, Jul. 2009.

[7] D.-H. Kim, J.-H. Ahn, W. M. Choi, H.-S. Kim, T.-H. Kim, T.-H. Kim, J. Z. Song, Y. Y. Huang, Z. J. Liu, C. Lu, and J. A. Rogers, "Stretchable and foldable silicon integrated circuits," *Science*, vol. 320, no. 5875, pp. 507–511, Apr. 2008.

[8] D. Kim, J. Z. Song, W. M. Choi, H. Kim, R. Kim, Z. J. Liu, Y. Y. Huang, K. Hwang, Y. Zhang, and J. A. Rogers, "Materials and noncoplanar mesh designs for integrated circuits with linear elastic responses to extreme mechanical deformations," *Proceedings of the National Academy of Sciences USA*, vol. 105, no. 48, pp. 18675–18680, Dec. 2008.

[9] J. Baca, J.-H. Ahn, Y. G. Sun, M. A. Meitl, E. Menard, H.-S. Kim, W. M. Choi, D.-H. Kim, Y. Huang, and J. A. Rogers, "Semiconductor wires and ribbons for high-performance flexible electron-

ics," *Angewandte Chemie International Edition*, vol. 47, no. 30, pp. 170–188, Jul. 2008

[10] STELLA Project IST-028026 [Online]. Available: http://www.stellaproject.de/.

[11] H.-J. Kim, C. W. Son, and B. Ziaie, "A multiaxial stretchable interconnect using liquid-alloy-filled elastomeric microchannels," *Applied Physics Letters*, vol. 92, no. 1, pp. 011904–1–3, Jan. 2008.

[12] M. W. Pospieszalski, E. J. Wollack, N. Bailey, D. Thacker, J. Webber, L. D. Nguyen, N. Le, and M. Lui, "Design and performance of wideband, low-noise, millimeter-wave amplifiers for Microwave Anisotropy Probe radiometers," in *Proc. IEEE MTT-S International Microwave Symposium Digest*, Jun. 2000, pp. 25–28.

[13] J. Tuovinen, P. Kangaslahti, P. Haapanen, N. Hughes, P. Jukkala, T. Karttaavi, O. Koistinen, M. Lahdes, H. Salminen, J. Tanskanen, and S. Urpo, "Development of 70 GHz receivers for the Planck LFI," in *Proc. Astrophysics Letters and Communications,* vol. 37, no. 3–6, Jun. 2000, pp. 181–187.

[14] P. J. Napier, D. S. Bagri, B. G. Clark, A. E. E. Rogers, J. D. Romney, A. R. Thompson, and R. C. Walker, "The very long baseline array," *Proceedings of the IEEE*, vol. 82, no. 5, pp. 658–672, May 1994.

[15] L. H. Eriksson and B. As, "A high performance automotive radar for automatic AICC," *IEEE Aerospace and Electronic Systems Magazine*, vol. 10, no. 12, pp. 13–18, Dec. 1995.

[16] H. Meinel, J. Wenger, H. Hentling, G. Rollmann, and H. Dominik, "Automotive radar: from long range collision warning to short range urban employment," in *Proc. International Joint Conference of the 7th Topical Symposium on Millimeter Waves (TSMMW2004) and the 6th MINT Millimeter-Wave International Symposium (MINT-MIS)*, Feb. 2005, pp. 244–247.

[17] J. Wenger, "Automotive radar—status and perspectives," in *Proc. IEEE Compound Semiconductor Integrated Circuit Symposium*, Oct.-Nov. 2005, pp. 21–24.

[18] P. Mikkonen, "Modern 60 GHz radio link," in *Proc. 29th European Microwave Conference*, vol. 3, Oct. 1999, pp. 83–86.

[19] J. Burns, “The application of millimetre wave technology for personal communication networks in the United Kingdom and Europe: A technical and regulatory overview,” in *Proc. IEEE MTT-S International Microwave Symposium Digest*, vol. 2, May 1994, pp. 635–638.

[20] E. C. Niehenke, R. A. Pucel, and I. J. Bahl, “Microwave and millimeterwave integrated circuits,” *IEEE Transactions on Microwave Theory and Techniques*, vol. 50, no. 3, pp. 846–857, Mar. 2002.

[21] Y. Takimoto, “Recent activities on millimeter-wave indoor LAN system development in Japan,” in *Proc. IEEE MTT-S International Microwave Symposium Digest*, vol. 2, May 1995, pp. 405–408.

[22] L. Yujiri, M. Schucri, and P. Moffs, “Passive millimeter-wave imaging,” *IEEE Microwave Magazine*, vol. 4, no. 3, pp. 39–50, Sep. 2003.

[23] M. Kantanen, M. Lahdes, and J. Tuovinen, “A millimeter wave imager,” in *Proc. International Joint Conference of the 7th Topical Symposium on Millimeter Waves (TSMMW2004) and the 6th MINT Millimeter-Wave International Symposium (MINT-MIS)*, Feb. 2005, pp. 240–243.

[24] D. Deslandes and K.Wu, “Integrated microstrip and rectangular waveguide in planar form,” *IEEE Microwave Wireless Components Letters*, vol. 11, pp. 68–70, Feb. 2001.

[25] K. Wu, “Integration and interconnect techniques of planar and nonplanar structures for microwave and millimeter-wave circuits-current status and future trend,” in *Proc. Asia-Pacific Microwave Conference (APMC)*, vol. 2, Dec. 2001, pp. 411–416.

[26] F. Xu and K. Wu, “Guided-wave and leakage characteristics of substrate integrated waveguide,” *IEEE Transactions on Microwave Theory and Techniques*, vol. 53, no. 1, pp. 66–73, Jan. 2005.

[27] D. Deslandes and K. Wu, “Accurate modeling, wave mechanisms, and design considerations of a substrate integrated waveguide,” *IEEE Transactions on Microwave Theory and Techniques*, vol. 54, no. 6, pp. 2516–2526, Jun. 2006.

[28] E. R. Brown, “RF-MEMS switches for reconfigurable integrated circuits,” *IEEE Transactions Microwave Theory and Techniques*, vol. 46, no. 11, pp. 1868–1880, Nov. 1998.

[29] C. G. Christodoulou, “RF MEMS and its applications to microwave systems, antennas and wireless communications,” in *Proc. IEEE MTT-S International Microwave Symposium Digest*, Sep. 2003, pp. 525–531.

[30] H. A. Wheeler, “Small antennas,” *IEEE Transactions on Antennas and Propagation*, vol. 23, no. 4, pp. 462–469, July 1975.

[31] H. A. Wheeler, “The radiansphere around a small antenna,” *Proceedings of the IRE*, vol. 47, no. 8, pp. 1325–1331, Aug. 1959.

[32] K. Fujimoto, A. Henderson, K. Hirasawa, and J. R. James, *Small Antennas*. Wiley, 1987.

[33] H. A. Wheeler, “Fundamental limitations of small antennas,” *Proceedings of the IRE*, vol. 35, no.12, pp. 1479–1484, Dec. 1947.

[34] L. J. Chu, “Physical limitations of omni-directional antennas,” *Journal of Applied Physics*, vol. 19, pp. 1163–1174, Dec. 1948.

[35] J. McLean, “A re-examination of the fundamental limits on the radiation Q of electrically small antennas,” *IEEE Transactions on Antennas and Propagation*, vol. 44, no. 5, pp. 672–676, May 1996.

[36] R. F. Harrington, “Effect of antenna size on gain, bandwidth, and efficiency,” *Journal of Research of the National Bureau of Standards – D. Radio Propagation*, vol. 64-D, no. 1, pp. 1–12, Jan.-Feb. 1960.

[37] H. W. Bode, *Network Analysis and Feedback Amplifier Design*. Van Nostrand, 1945.

[38] R. M. Fano, “Theoretical limitations on the broadband matching of arbitrary impedances,” *Technical Report*, no. 41, Jan. 1948.

[39] Z. D. Liu, P. S. Hall, and D. Wake, “Dual-Frequency planar inverted-F antenna,” *IEEE Transactions on Antennas and Propagation*, vol. 45, no. 10, pp. 1451–1458, Oct. 1997.

[40] Y. X. Guo, M. Y. W. Chia, and Z. N. Chen, “Miniature built-in quad-band antennas for mobile handsets,” *IEEE Antennas and Wireless Propagation Letters*, vol. 2, no. 1, pp. 30–32, 2003.

[41] Z. N. Chen, M. J. Ammann, X. Qing, X. H. Wu, T. S. P. See, and A. Cai, "Planar antennas: Promising solutions for microwave UWB applications," *IEEE Microwave Magazine*, vol. 7, no. 6, pp. 63–73, Dec. 2006.

[42] Z. N. Chen, T. S. P. See, and X. Qing, "Small printed ultrawideband antenna with reduced ground-plane effect," *IEEE Transactions on Antennas and Propagation*, vol. 55, no. 2, pp. 383–388, Feb. 2007.

[43] X. Qing and Z. N. Chen, "Compact coplanar waveguide-fed ultrawideband monopole-like slot antenna," *IEE Proceedings IET Microwave, Antennas and Propagation*, vol. 3, no. 5, pp. 889–898, Aug. 2009.

[44] S.-Y. Suh, "A comprehensive investigation of new planar wideband antennas," *PhD Thesis*, Virginia Polytechnic Institute and State University, Blacksburg, VA, Jul. 2002.

[45] S.-Y. Suh, W. L. Stutzman, and W. A. Davis, "A new ultrawideband printed monopole antenna: The planar inverted cone antenna (PICA)," *IEEE Transactions on Antennas and Propagation*, vol. 52, pp. 1361–1365, May 2004.

[46] e-CUBES Project IST-026461 [Online]. Available: http://www.ecubes.org.

[47] S. Saario, D. V. Thiel, J. W. Lu, and S. G. O'Keefe, "An assessment of cable radiation effects on mobile communications antenna measurements," in *Proc. IEEE Antennas and Propagation Society International Symposium*, vol. 1, Jul. 1997, pp. 550–553

[48] C. Icheln, J. Ollikainen, and P. Vainikainen, "Reducing the influence of feed cables on small antenna measurements," *Electronics Letters*, vol. 35, no. 15, pp. 1212–1214, Jul. 1999.

[49] L. Gatzoulis and I. Iakovidis, "Wearable and portable eHealth systems," *IEEE Engineering Medicine and Biology Magazine*, vol. 26, no. 5, pp. 51–56, Sep. 2005.

[50] S. Brebels, S. Sanders, C. Winters, T. Webers, K. Vaesen, G. Carchon, B. Gyselinckx, and W. De Raedt, "3D SoP integration of a BAN sensor node," in *Proc. Electronic Components and Technology Conference*, vol. 2, May/Jun. 2005, pp. 1602–1606.

[51] K. F. Navarro, E. Lawrence, and B. Lim, “Medical MoteCare: a distributed personal healthcare monitoring system,” in *Proc. International Conference on eHealth, Telemedicine, and Social Medicine (eTELEMED)*, Feb. 2009, pp. 25–30.

[52] P. S. Hall and Y. Hao, *Antennas and propagation for bodycentric wireless communications*, 1st ed. Artech House, 2006.

[53] Z. N. Chen, A. L. Cai, T. S. P. See, X. M. Qing, and M. Y. W. Chia, “Small planar UWB antennas in proximity of the human head,” *IEEE Transactions on Microwave Theory and Techniques*, vol. 54, no. 4, pp. 1846–1857, Apr. 2006.

[54] R. Hansen, “Folded and T-matched dipole transformation ratio,” *IEEE Transactions on Antennas and Propagation*, vol. 30, no. 1, pp. 161–162, Jan. 1982.

[55] C. A. Balanis, *Antenna Theory*, 2nd ed. Wiley, 1997.

[56] S. P. Lacour, J. Jones, S. Wagner, T. Li, and Z. G. Suo, “Stretchable interconnects for elastic electronic surfaces,” *Proceedings of the IEEE*, vol. 93, pp. 1459–1467, Aug. 2005.

[57] S. P. Lacour, C. Tsay, and S. Wagner, “An elastically stretchable TFT circuit,” *IEEE Electron Device Letters*, vol. 25, pp. 792–794, Dec. 2004.

[58] S. P. Lacour, J. Jones, Z. Suo, and S.Wagner, “Design and performance of thin metal film interconnects for skin-like electronic circuits,” *IEEE Electron Device Letters*, vol. 25, pp. 179–181, Apr. 2004.

[59] D. Brosteaux, F. Axisa, M. Gonzalez, and J. Vanfleteren, “Design and fabrication of elastic interconnections for stretchable electronic circuits,” *IEEE Electron Device Letters*, vol. 28, pp. 552–554, Jul. 2007.

[60] B. Huyghe, H. Rogier, J. Vanfleteren, and F. Axisa, “Design and manufacturing of stretchable high-frequency interconnects,” *IEEE Transactions on Advanced Packaging*, vol. 31, no. 4, pp. 802–808, Nov. 2008.

[61] Y. N. Xia and G. M. Whitesides, “Soft lithography,” *Annual Review of Materials Science*, vol. 28, pp. 153–184, 1998.

[62] M. Andersson, B. Göransson, I. Skarin, K. From, S. Cheng, E. Öjefors, P. Hallbjörner, L.Manholm, and A. Rydberg, "Antennas with fast beam steering for high spectral efficiency in broadband cellular systems," in *Proc. 9th European Conference on Wireless Technology*, Sep. 2006, pp. 12–15.

[63] G. M. Rebeiz, *RF MEMS: Theory, Design and Technology*. New York: Wiley, 2003.

[64] J. T. Aberle, M. Chu, and C. R. Birtcher, "Scattering and radiation properties of varactor-tuned microstrip antennas," in *Proc. IEEE Antenna Propagation Society International Symposium*, vol. 4, Jul. 1992, pp. 2229–2232.

[65] R. N. Hardin, E. J. Downey, and J. Munushian, "Electrically variable phase shifter utilizing variable capacitance diodes," *Proceedings of the IRE*, vol. 48, pp. 944–945, May 1960.

[66] C. Toker, M. Saglam, M. Ozme, and N. Gunalp, "Branch-line coupler using unequal line lengths," *IEEE Transactions on Microwave Theory and Techniques*, vol. 49, no. 4, pp. 718–721 Apr. 2001.

[67] P. M. Zavracky and R. H. Morrison, "Electrically actuated micromechanical switches with hysteresis," in *Proc. IEEE Solid-State Sensor Conference*, Jun. 1984, pp. 50–51.

[68] C. L. Goldsmith, Z. Yao, S. Eshelman, and D. Denniston, "Performance of low-loss RF MEMS capacitive switches," *IEEE Microwave Guided Wave Letters*, vol. 8, no. 8, pp. 269–271, Aug. 1998.

[69] J. B. Muldavin and G. M. Rebeiz, "High-isolation CPW MEMS shunt switches—Part 1: Modeling," *IEEE Transactions on Microwave Theory and Techniques*, vol. 48, no. 6, pp. 1045–1052, Jun. 2000.

[70] ———, "High-isolation CPW MEMS shunt switches—Part 2: Design," *IEEE Transactions on Microwave Theory and Techniques*, vol. 48, no. 6, pp. 1053–1056, Jun. 2000.

[71] J. B. Rizk, G.-L. Tang, J. B. Muldavin, and G. M. Rebeiz, "High-isolation W-band MEMS switches," *IEEE Microwave and Wireless Components Letters*, vol. 11, no. 1, pp. 10–12, Jan. 2001.

[72] G. L. Tan and G. M. Rebeiz, "A DC-contact MEMS shunt switch," *IEEE Microwave Wireless Components Letters*, vol. 12, no. 6, pp. 212–214, June 2002.

[73] B. Pillans, E. Eshelman, A. Malczewski, J. Emhke, and C. Goldsmith, "Ka-band RF MEMS phase shifter," *IEEE Microwave Guided Wave Letters*, vol. 9, no. 12, pp. 520–523, Dec. 1999.

[74] G. M. Rebeiz and J. B. Muldavin, "RF MEMS switches and switch circuits," *IEEE Microwave Magazine*, vol. 2, no. 4, pp. 59–71, Dec. 2001.

[75] G. M. Rebeiz, G.-L. Tan, and J. S. Hayden, "RF-MEMS phase shifters: Design and applications," *IEEE Microwave Magazine*, vol. 3, no. 2, pp. 72–81, Jun. 2002.

[76] H.-T. Kim, J.-H. Park, Y.-K. Kim, and Y. Kwon, "Low-loss and compact V-band MEMS-based analog tunable bandpass filters," *IEEE Microwave and Wireless Components Letters*, vol. 12, no. 11, pp. 432–434, Nov. 2002.

[77] B. Schoenlinner, A. Abbaspour-Tamijani, L. C. Kempel, and G. M. Rebeiz, "Switchable low-loss RF MEMS Ka-band frequency-selective surface," *IEEE Transactions on Microwave Theory and Techniques*, vol. 52, no. 11, pp. 2474–2481, Nov. 2004.

[78] J. B. Rizk and G. M. Rebeiz, "W-band CPW RF MEMS circuits on quartz substrates," *IEEE Transactions on Microwave Theory and Techniques*, vol. 51, no. 7, pp. 1857–1862, Jul. 2003.

[79] T. Vähä-Heikkilä, J. Varis, J. Tuovinen, G. M. Rebeiz, "Reconfigurable RF MEMS impedance tuners and matching networks," in *Proc. 34th European Microwave Conference*, Oct. 2004, pp. 123–136.

[80] W. H. Weedon, W. J. Payne, and G. M. Rebeiz, "MEMS-switched reconfigurable antennas," in *Proc. IEEE Antenna Propagation Society International Symposium*, vol. 3, Jul. 2001, pp. 654–657.

[81] K. R. Boyle and P. G. Steenenken, "A five-band reconfigurable PIFA for mobile phones," *IEEE Transactions on Antennas and Propagation*, vol. 55, no. 11, pp. 3300–3309, Nov. 2006.

[82] C. Jung, M. Lee, G. P. Li, and F. D. Flaviis, "Reconfigurable scan-beam single-arm spiral antenna integrated with RF MEMS

switches," *IEEE Transactions on Antennas and Propagatio*n, vol. 54, no. 2, pp. 455–463, Feb. 2006.

[83] N. Kingsley, G. E. Ponchak, and J. Papapolymerou, "Reconfigurable RF MEMS phased array antenna integrated within a liquid crystal polymer (LCP) system-on-package," *IEEE Transactions on Antennas and Propagation*, vol. 56, no. 1, pp. 108–118, Jan. 2008.

[84] J. J. Maciel, J. F. Slocum, J. K. Smith, and J. Turtle, "MEMS electronically steerable antennas for fire control radars," *IEEE Aerospace Electronic Systems Magazine*, vol. 22, no. 11, pp. 17–20, Nov. 2007.

[85] K. Topalli, Ö. A. Civi, S. Demir, S. Koc, and T. Akin, "A monolithic phased array using 3-bit distributed RF MEMS phase shifters," *IEEE Transactions on Microwave Theory and Techniques*, vol. 56, no. 2, pp. 270–277, Feb. 2008.

[86] K. M. K. H. Leong, Y. Qian, and T. Itoh, "First demonstration of a conductor backed coplanar waveguide fed quasi-Yagi antenna," in *Proc. IEEE Antenna Propagation Society International Symposium*, vol. 3, Jul. 2000, pp. 1432–1435.

[87] J. Sor, Y. Qian, and T. Itoh, "Coplanar waveguide fed quasi-Yagi antenna," *Electronics Letters*, vol. 36, pp. 1–2, Jan. 2000.

[88] P. Hallbjörner, M. Bergstrom, M. Boman, P. Lindberg, E. Öjefors, and A. Rydberg, "Millimetre-wave switched beam antenna using multiple travelling-wave patch arrays," *IEE Proceedings Microwave, Antennas and Propagation*, vol. 152, no. 6, pp. 551–555, Dec. 2005.

[89] E. W. Strid and K. R. Gleason, "A DC-12 GHz monolithic GaAs-FET distributed amplifier," *IEEE Transactions on Microwave Theory and Techniques*, vol. 82, no. 7, pp. 969–975, Jul. 1982.

[90] ———, "Calibration methods for microwave wafer probing," *Microwave and Millimeter-Wave Monolithic Circuits*, vol. 84, no. 1, pp. 78–82, May 1984.

[91] M. Matloubian, S. E. Rosenbaum, H. R. Fetterman, and P. T. Greiling, "Wide-band millimeter wave characterization of sub-0.2 micrometer gatelength AlInAs/GaInAs HEMTs," *IEEE Microwave and Guided Wave Letters*, vol. 1, no. 2, pp. 32–34, Feb. 1991.

[92] R. Y. Yu, J. Pusl, Y. Konishi, M. Case, M. Kamegawa, and M. Rodwell, "8–96 GHz on-wafer network analysis," in *Proc. Technical Digest of 14th Annual Gallium Arsenide Integrated Circuit (GaAs IC) Symposium*, Oct. 1992, pp. 75–77.

[93] R. Anholt, J. Pence, and E. Godshalk, "On-wafer HEMT characterization to 110 GHz," in *Proc. Technical Digest of the 16th Annual Gallium Arsenide Integrated Circuit (GaAs IC) Symposium*, Oct. 1994, pp. 108–111.

[94] R. Lai, M. Barsky, T. Huang, M. Sholley, H. Wang, Y. L. Kok, D. C. Streit, T. Block, and P. H. Liu, "An InP HEMT MMIC LNA with 7.2-dB gain at 190 GHz," *IEEE Microwave and Guided Wave Letters*, vol. 8, no. 11, pp. 393–395, Jun. 1998.

[95] C. W. Pobanz, M. Matloubian, M. Lui, H.-C. Sun, M. Case, C. M. Ngo, P. Janke, T. Gaier, and L. Samoska, "A high-gain monolithic D-band InP HEMT amplifier," *IEEE Journal of Solid-State Circuits*, vol. 34, no. 9, pp. 1219–1224, Nov. 1999.

[96] A. Tessmann, O. Wohlgemuth, R. Reuter, W. Haydl, H. Massler, and A. Hulsmann, "A coplanar 148 GHz cascode amplifier MMIC using 0.15 µm GaAs PHEMTs," in *Proc. IEEE MTT-S International Microwave Symposium Digest*, vol. 2, 2000, pp. 991–994.

[97] A. K. Fung, D. Dawson, L. Samoska, K. Lee, C. Oleson, and G. Boll, "On-Wafer Vector Network Analyzer Measurements in the 220-325 GHz Frequency Band," in *Proc. IEEE MTT-S International Microwave Symposium Digest*, Jun. 2006, pp. 1931–1934.

[98] A. K. Fung, D. Dawson, L. Samoska, K. Lee, T. Gaier, P. Kangaslahti, C. Oleson, A. Denning, Y. Lau, and G. Boll, "Two-Port Vector Network Analyzer Measurements in the 218–344 and 356–500 GHz Frequency Bands," *IEEE Transactions on Microwave Theory and Techniques*, vol. 54, no. 12, pp. 4507–4512, Dec. 2006.

[99] J. W. Digby, C. E.McIntosh, G. M. Parkhurst, J. W. Hadjiloucas, J. M. Chamberlain, R. D. Pollard, R. E. Miles, D. P. Steenson, N. J. Cronin, and S. R. Davies, "Fabrication and characterization of micromachined rectangular waveguide components for use at millimeter-wave and terahertz frequencies," *IEEE Transactions on Microwave Theory and Techniques*, vol. 48, no. 8, pp. 1293–1302, Aug. 2000.

[100] W. R. McGrath, C. Walker, M. Yap, and Y. Tai, "Silicon micromachined waveguides for millimeter-wave and submillimeter-wave frequencies," *IEEE Microwave Guided Wave Letters*, vol. 3, no. 3, pp. 61–63, Mar. 1993.

[101] L. Yan, W. Hong, G. Hua, J. Chen, K. Wu, and T. J. Cui, "Simulation and experiment on SIW slot array antennas," *IEEE Microwave Wireless Components Letters*, vol. 14, no. 9, pp. 446–448, Sep. 2004.

[102] X. Chen, W. Hong, T. Cui, Z. Hao, and K. Wu, "Symmetric dual-mode filter based on substrate integrated waveguide (SIW)," *Electrical Engineering*, vol. 89, no. 1, pp. 67–70, Oct. 2006.

[103] Z. C. Hao, W. Hong, X. P. Chen, J. X. Chen, and K. Wu, "A single-layer folded substrate integrated waveguide (SIW) filter," in *Proc. Asia-Pacific Microwave Conference (APMC)*, Dec. 2005, pp. 411–413.

[104] Z. C. Hao, W. Hong, J. X. Chen, H. X. Zhou, and K. Wu, "Single layer substrate integrated waveguide directional couplers," *IEE Proceedings Microwave, Antennas and Propagation*, vol. 153, no. 5, pp. 426–431, Oct. 2006.

[105] T. Djerafi and K. Wu, "Super-compact substrate integrated waveguide cruciform directional coupler," *IEEE Microwave Wireless Components Letters*, vol. 17, no. 11, pp. 757–759, Nov. 2007.

[106] W. D'Orazio, K. Wu, and J. Helszajn, "A substrate integrated waveguide degree-2 circulator," *IEEE Microwave Wireless Components Letters*, vol. 14, no. 5, pp. 207–209, May 2004.

[107] W. D'Orazio and K. Wu, "Substrate-integrated-waveguide circulators suitable for millimeter-wave integration," *IEEE Transactions on Microwave Theory and Techniques*, vol. 54, no. 10, pp. 3675–3680, Oct. 2006.

[108] D. M. Pozar, *Microwave Engineering*, 3rd ed. Wiley, 2004.

[109] G. P. Gauthier, A. Courtay, and G. M. Rebeiz, "Microstrip antennas on synthesized low dielectric-constant substrates," *IEEE Transactions on Antennas and Propagation*, vol. 45, no. 8, pp. 1310–1314, Aug. 1997.

[110] I. Papapolymerou, R. F. Drayton, and L. P. Katehi, "Micromachined patch antennas," *IEEE Transactions on Antennas and Propagation*, vol. 46, no. 2, pp. 295–306, Feb. 1998.

[111] M. Zheng, Q. Chen, P. Hall, and V. Fusco, "Broadband microstrip patch antenna on micromachined silicon substrates," *Electronics Letters*, vol. 34, no. 1, pp. 3–4, January 1998.

[112] Q. Chen, V. Fusco, M. Zheng, and P. Hall, "Micromachined silicon antennas," in *Proc. International Conference on Microwave and Millimeter Wave Technology (ICMMT)*, Aug. 1998, pp. 289–292.

[113] D. Neculoiu, A. Muller, P. Pons, L. Bary, M. Saadaoui, C. Buiculescu, O. Andrei, R. Enachescu, D. Dubuc, K. Grenier, D. Vasilache, I. Petrini, and R. Plana, "The design of membrane-supported millimeter-wave antennas," in *Proc. International Semiconductor Conference (CAS)*, vol. 1, Sept.-Oct. 2003, pp. 65–68.

[114] P. Caudrillier, A. Takacs, O. Pascal, H. Aubert, P. Pons, and R. Plana, "Compact circularly polarized radiating element for Ka-band satellite communications," in *Proc. IEEE Antennas and Propagation Society International Symposium*, vol. 1, Jun. 2002, pp. 16–21.

[115] D. Neculoiu, P. Pons, M. Saadaoui, L. Bary, D. Vasilache, K. Grenier, D. Dubuc, A. Muller, and R. Plana, "Membrane supported yagi-uda antennae for millimetre-wave applications," *IEE Proceedings Microwave, Antennas and Propagation*, vol. 151, no. 4, pp. 311–314, Aug. 2004.

[116] E. Ojefors, H. Kratz, K. Grenier, R. Plana, and A. Rydberg, "Micromachined loop antennas on low resistivity silicon substrates," *IEEE Transactions on Antennas and Propagation*, vol. 54, no. 12, pp. 3593–3601, Dec. 2006.

[117] A. Bessemoulin, C. Gaessler, J. Gruenenpuett, and B. Reig, "Hot-via interconnects: a step toward surface mount chip scale packaged MMICs up to 110 GHz," in *Proc. IEEE Compound Semiconductor Integrated Circuit Symposium (CSICS)*, Oct. 2004, pp. 237–240.

[118] A. Bessemoulin, "Design data for hot-via interconnects in chip scale packaged MMICs up to 110 GHz," in *Proc. 34th European Microwave Conference*, vol. 1, Oct. 2004, pp. 97–100.

[119] W.-C. Wu, L.-H. Hsu, E. Y. Chang, C. Karnfelt, H. Zirath, J. P. Starski, and Y.-C. Wu, "60 GHz broadband MS-to-CPW hot-via flip chip interconnects," *IEEE Microwave and Wireless Components Letters*, vol. 17, no. 11, pp. 784–786, Nov. 2007.

[120] E. Beyne, "The rise of the 3rd dimension for system integration," in *Proc. International Interconnect Technology Conference (IITC)*, Oct. 2006, pp. 1–5.

[121] E. Beyne, "3D system integration technologies," in *Proc. International Symposium on VLSI Technology, Systems, and Applications*, Apr. 2006, pp. 1–9.

[122] Annual Statistical Report 2007, *SafetyNet Project Report*, Deliverable D 1.16, Feb. 2008.

[123] V. Viikari, T. Varpula, and M. Kantanen, "Automotive radar technology for detecting road conditions. Backscattering properties of dry, wet, and icy asphalt," in *Proc. 5th European Radar Conference*, Oct. 2008, pp. 276–279.

[124] H. Staras and J. Shefer, "Harmonic Radar Detecting and Ranging System for Automotive Vehicles," *US Patent* 3781879, Dec. 1972.

[125] E. T. Cant, A. D. Smith, D.R. Reynold, and J. L. Osborne, "Tracing butterfly flight paths across the landscape with harmonic radar," *Proceedings of the Royal Society B: Biological Sciences*, vol. 272, no. 1565, pp. 785–790, Apr. 2005.

[126] B. G. Colpitts and G. Boiteau, "Harmonic radar transceiver design: Miniature tags for insect tracking," *IEEE Transactions on Antennas and Propagation*, vol. 52, no. 11, pp. 2825–2832, Nov. 2004.

[127] ADOSE Project ICT- 216049 [Online]. Available: http://www.adose-eu.org/.

[128] L. C. Van Atta, "Electromagnetic Reflector," *US Patent* 2908002, no. 514040, Oct. 1959.

[129] E. Sharp and M. Diab, "Van Atta reflector array," *IRE Transaction on Antennas and Propagation*, vol. 8, no. 4, pp. 436–438, Jul. 1960.

[130] Rogers Corporation, *Ultralam@3000 Series Liquid Crystalline Polymer* [online]: www.rogerscorporation.com.

[131] G. Zou, H. Gronqvist, J. P. Starski, and J. Liu, “Characterization of liquid crystal polymer for high frequency system-in-a-package applications,” *IEEE Transactions on Advanced Packaging*, vol. 25, no. 4, pp. 503–508, Nov. 2002.

Acta Universitatis Upsaliensis

*Digital Comprehensive Summaries of Uppsala Dissertations from the Faculty of Science and Technology* 698

Editor: The Dean of the Faculty of Science and Technology

A doctoral dissertation from the Faculty of Science and Technology, Uppsala University, is usually a summary of a number of papers. A few copies of the complete dissertation are kept at major Swedish research libraries, while the summary alone is distributed internationally through the series Digital Comprehensive Summaries of Uppsala Dissertations from the Faculty of Science and Technology. (Prior to January, 2005, the series was published under the title "Comprehensive Summaries of Uppsala Dissertations from the Faculty of Science and Technology".)

Distribution: publications.uu.se
urn:nbn:se:uu:diva-111197

ACTA
UNIVERSITATIS
UPSALIENSIS
UPPSALA
2009